POLITECNICO DI MILANO

Facoltà di Ingegneria Industriale

Corso di Laurea in
Ingegneria Aerospaziale

Preliminary design of a transonic wind tunnel

Progetto preliminare di una galleria del vento transonica

Relatore: Prof. Alberto GUARDONE
Politecnico di Milano, Italia

Co-relatore: Prof. Emmanuel BENARD
University of Gaslgow, UK

Tesi di Laurea di:

Michea GIUNI Matr. 707997

Anno Accademico 2008 - 2009

Ai miei genitori

Acknowledgments

In everything give thanks:
for this is the will of God
in Christ Jesus concerning you.

Un primo grazie a Dio, principio di ogni cosa. E non solo in senso generale ma anche della scienza e della vita.

Grazie ai miei genitori, che mi hanno dato la possibilità, le capacità, il supporto necessari per godere di questi studi. Grazie ai miei fratelli, Gioia ed Emmanuel, che son stati dei bravi ed utili fratelli nonstante la distanza. Grazie agli "zii di Milano", che mi son stati un prezioso e gradito appoggio.

Grazie a Rugiada, che ha reso felici e leggeri questi ultimi anni con il suo sorriso.

Grazie agli amici con i quali ho condiviso il collegio, la mensa ISU ed innumerevoli partite a PES. Grazie a Nico, il Roby, il Goro, Luca e Doctor Kumalo.

Grazie ai vari ed eventuali compagni di studi (o di partite a biliardino), al Gianlu ed il simbolo di Batman, a Billy ed Effe che parlano solo ad alta voce, a Simone che penso ringrazierò ancora fra non molto tempo.

Grazie a Glasgow ed alla sua università, che mi hanno accolto con entusiasmo. Grazie a Tony ed il suo "I don't see any problems".

Un ultimo grazie a Dio, fine di ogni cosa. E non solo in senso generale ma anche della scienza e della vita.

Contents

List of Figures

List of Tables

Preliminary design of a transonic wind tunnel

Abstract: in collaboration with the University of Glasgow, a small intermittent transonic wind tunnel has been preliminarily designed. The study has been focused on an innovative Mach number regulation system based on a combined use of a test section shaped wall and a wedge before the diffuser. A numerical model has been then validated with reference to experimental results obtained in a similar facility. The efficiency of the new chocking system, compared to the existing ones, has been demonstrated by the simulations.

Keywords: transonic, wind tunnel, design, chocking system.

Progetto preliminare di una galleria del vento transonica

Sommario: da un progetto di collaborazione con l'università di Glasgow, è stato sviluppato il progetto preliminare di una galleria del vento transonica ad intermittenza di piccole dimensioni. Lo studio si è concentrato su un innovativo sistema di regolazione del numero di Mach basato su un uso combinato di pareti sagomate nella camera di prova e un'ala posta prima del diffusore. E' stato quindi validato un modello numerico confrontandosi con risultati sperimentali ottenuti in una simile galleria del vento. Le simulazioni hanno dimostrato l'efficienza del nuovo sistema di bloccaggio confrontato con i sistemi già esistenti.

Keywords: transonico, galleria del vento, progetto, sistema di bloccaggio.

Chapter 1

Introduction

Contents

Transonic flows study represents one of the most difficult problems in compressible fluid dynamic [1]. In a stationary transonic flow, subsonic and supersonic regions live at the same time which are governed respectively by elliptical equations and hyperbolic equations. Since these two types of equation require completely different solution methods, in general it is not possible to obtain solutions valid for the entire region.

Furthermore, even when it is possible to introduce small perturbation hypotheses, in transonic flow, the equation remains not linear and it is then not possible to find a solution by superimposition of elementary solutions like as in subsonic and supersonic cases.

For this reason, transonic wind tunnel tests still play a big role in the research on this field.

Transonic flows can be divided into two categories: internal flows in which transition from subsonic to supersonic flows is observed (e.g. supersonic nozzles) and external flows where a high subsonic flow encounters a body.

Transonic regime leads to important flow behaviours such as supersonic bubbles, shock waves and expansion waves interaction, shock waves and boundary layer interactions, shocks unsteadiness and it is therefore widely studied.

Very important applications of these studies are in commercial airplanes working at transonic regime. Most modern jet powered aircrafts are engineered to operate with as high a subsonic air speed as possible. The limit is

set before their airfoils experience the onset of transonic wave drag, which becomes prevalent. The importance of transonic wave drag lies in the fact that it is a non-linear phenomenon and leads to very strong contributes on the total drag.

Subcritical or supercritical airfoil is generally adopted in these aircrafts. The first is designed to keep the flow velocity over the airfoil never reaching sonic conditions. The latter is an airfoil designed, primarily, to delay the onset of the wave drag in the transonic speed range. This profile controls the supersonic bubble which is isentropically re-compressed avoiding the shock that is the cause of the fall of lift and the increase of drag.

Furthermore, severe instability can occur at transonic speed because of the oscillation of the shock waves position. This topic in particular is an important research field whether the disturbances come from a boundary layer separation interaction or from the upstream turbulence.

Transonic speeds can also occur at the tips of rotor blades of helicopters and aircraft. However, as this puts severe, unequal stresses on the rotor blade, it is avoided and may lead to dangerous accidents if it occurs. This is one of the limiting factors to the size of rotors, and also to the forward speeds of helicopters (as this speed is added to the forward-sweeping side of the rotor, thus possibly causing localized transonic flows).

In this thesis, a preliminary design of a transonic wind tunnel has been carried out. The two main purposes were to create a basic and working wind tunnel to be further improved with more specifics studies and to establish a satisfactory CFD model to be used for further analysis and future preliminary comparisons with experimental data.

An appropriate scale of the wind tunnel has been found in a $4''$ by $4''$ test section[1]. A small facility gives an intrinsic simplicity in the design and it allows a low cost of the associated visual measurements equipment and the models. Furthermore, referring to other wind tunnels already working, these dimensions have been found allowing high level studies.

The innovative concept in this design lies on an improved Mach regulation system and a chapter of this thesis will particularly focus on this part.

A rigorous procedure to validate a CFD model on Fluent[2] has been carried out comparing the numerical simulation results with the experimental results obtained in an equivalent wind tunnel. A study on the grid has also been accomplished to ensure grid independence results.

Several numerical tests on the wind tunnel and on the chocking system have then been performed. The advantages of the new Mach regulation

[1] Along this work imperial units will sometime occur. Just to remind:
$1'' = 0.0254\,\mathrm{m}$
$1\,foot = 12'' = 0.3048\,\mathrm{m}$

system have been presented along with a detailed description of the working concept.

The main philosophy of the design can be seen in a high modularity that gives to the wind tunnel the possibility to be easily improved and the possibility to set up easily a wide range of different tests. For this reason the simplicity of each module is an important aspect. For example, there will be the possibility to carry on tests both on internal and external flows by changing part of the contraction or the walls of the test section.

1.1 General overview of transonic wind tunnels

A classical [3] definition of transonic wind tunnels is that they operate at speeds varying from the speed at which compressibility effects become important (considered at about Mach number equal to 0.5)[2], through the speed of sound and to a maximum Mach number of about 1.4. A further sub class of wind tunnel are the so called nearsonic wind tunnels that cover the lower portion of this speed range up to just below the speed of sound.

The typical *nearsonic wind tunnel* is basically a high powered subsonic wind tunnel. It is normally a closed circuit, fan driven tunnel with continuous operation capability where the test section has the minimum cross section of the tunnel circuit. The air speed in the test section is increased simply by changing the fan speed or changing the pitch of the fan blades. The walls of the test section are solid, and herein lies the major difference between the nearsonic and transonic tunnels. Unlike the nearsonic type tunnel, the *transonic wind tunnels* usually have walls vented with slots or perforations in a way that minimizes the walls effects on the shapes of the streamlines in the vicinity of the model. At subsonic speeds the solid tunnel walls do not allow the spread of the streamlines around the model which would occur in flight, and consequently there is a distorted flow field. Nowadays, with the important and accurate role of the CFD, it is possible to consider another idea that consists in shaping solid walls in such a way that the the streamlines can behave more similar to the flight conditions.

As previously mentioned the test section of the nearsonic tunnel has the minimum cross sectional area and hence the highest velocity of the circuit. When a model is placed in the test section, the minimum cross section occurs at the model. What happens at this point is that the tunnel becomes "choked" in the vicinity of the model as conditions for Mach number equal to 1 are approached, with the result that the model is no longer in a uniform flow field. In choked conditions the wind tunnel works with a fixed mass flow rate imposed by the minimum area and the upstream conditions no matter

[2]It is very possible to meet other ranges as definition of transonic regime (such as from 0.7 to 1.3). Anyway the important thing is that transonic range is across the speed of sound (Mach number equal to 1).

the downstream pressure. In other words, there is no communication across the sonic line between the upstream and downstream regions. Hence, the size of a model that can be tested in a classical nearsonic tunnel without choking becomes vanishingly small as Mach 1.0 is approached.

Regarding energy cost, the power to drive a low-speed wind tunnel varies as the cube of the velocity in the wind tunnel. Although his rule does not hold into the high speed regime, the implication that test speed increase rapidly increases power requirements is correct. Because of the power requirements, high speed wind tunnels are often *intermittent wind tunnels*, in which energy is stored in the form of pressure or a vacuum, or both, and is allowed to drive the tunnel only few seconds for each pumping hour.

The major characteristic of intermittent tunnels is the fact that they can only run for a limited period of time[3] because the capacity system used for the air supply. There are several different types of intermittent tunnels and the two basic concepts are blow-down and indraft tunnels. In the blow-down wind tunnel, the air is stored in containers at high pressure and discharged across the tunnel to the atmosphere. In the indraft tunnel (or suction tunnel), atmospheric air is sucked across the tunnel into a container brought to a pressure below atmospheric before the test.

Other tunnels commonly used at high Mach numbers combine the two systems and use air which is discharged from a high pressure container, through the tunnel, to a low pressure container.

The running time can vary from fractions of a second to many minutes. It depends on the pressure level and capacity of the container and on the weight flow per second crossing the test section. After each run the tank is brought back to the conditions existing before the run by means of compressors or vacuum pumps. These require very little power in comparison with the power required by a continuous tunnel having the same test section dimensions and aerodynamic characteristics. As a result, the time between runs is considerably longer than actual running time.

1.2 Use of a new chocking technique to control the Mach number

The main features of this project are the merging of wind tunnel nearsonic range and design concepts, intermittence facilities, walls as active role in the design and supersonic ideas on test Mach number control.

The regulation system of the air speed in the test sections of indraft wind tunnels can vary in many differing ways and involve a wide range of concepts. In such wind tunnels there are no fans or turbines to be regulated as in continuous wind tunnels, and the control of the velocity (i.e. the

[3]That leads to the "panic of rapid testing" as called by Pope [3]

pressure jump for the maintaining of the flow) is usually achieved through geometrical devices. The limited run time also forces adjustments to be over a very small time frame and often the Mach number is fixed before the test.

The types of throats or working sections wherein the model is placed for testing are a very distinguishing characteristic. The section F about transonic wind tunnels of the comprehensive book by Goddard et al. [4] gives an overview of different test section arrangement: closed throat, open throat, closed throat with flexible wall, close throat with wall liners, closed throat with submerged jet, ventilated throat, slotted throat and perforated throat are only some of the systems adopted in the wind tunnels. This "variety" of arrangements highlights the difficulty of the design of a transonic wind tunnel and the challenge of the transonic regime.

Since the facility will be transonic and in particular a nearsonic wind tunnel, the solutions to the speed regulation are not well established because this range is usually covered by continuous high power wind tunnels. Therefore this feature positions the wind tunnel presented in this thesis in a particular class where the pressure jump is given by an usually supersonic wind tunnel system (high and low pressure tanks[4] that bring to an intermittent facility) but the mean flow is still subsonic and the velocity regulation systems are very different (because the flow is very different) from the supersonic ones.

The control can not be achieved through modifications on the convergent line as in the interesting flexible convergent-divergent nozzles case well described by Kenney and Webb [5] and shown in fig. 1.1) or through plug type nozzle as sketched in fig. 1.2) because these nozzles bring to a supersonic outlet modifying the ratio between the exit section and the throat.

As it will be described later, for a sufficient low pressure ratio between the outlet and the inlet, the flow in the minimum section that corresponds to the throat will be sonic, in the convergent/upstream part subsonic and in the divergent/downstream part supersonic. It can hence be concluded that the nozzle has to be a solely convergent one where the exit is subsonic or, at the maximum, sonic.

The idea in these kinds of wind tunnels (not very common) is to have a sort of valve at the end of the test section before the diffuser that modifies the section area. This area will be the minimum section in the entire channel, so called throat or choke, where the Mach number is 1. For this reason the walls in the test section can play an important role increasing the section area. With these systems the flow is subsonic everywhere except for the choke section where it is sonic. The Mach number in the test section is therefore a function of the choke section area. Of course, for the presence of a model in the test section, other supersonic flow regions or shock waves can appear due to supervelocity effects. This, once more, shows the complexity

[4]The high pressure tank in this case is the atmosphere.

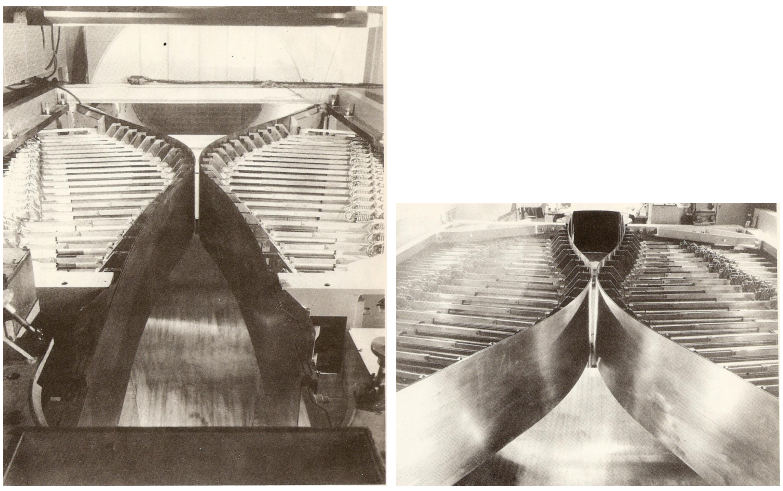

Figure 1.1: A typical symmetric flexible-wall design from Jet Propulsion Laboratory in California Institute of technology. [5]

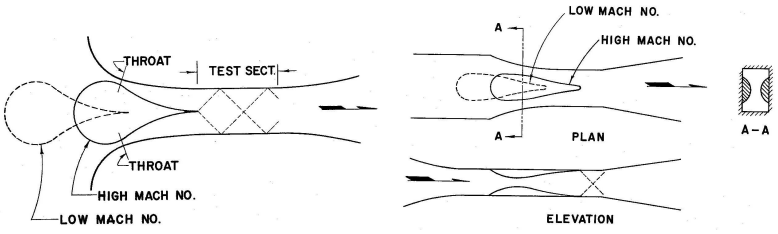

Figure 1.2: Centered and sidewall plug-type nozzle design. [5]

of the transonic regime where the different behaviours of both subsonic and supersonic regimes live together.

An adjustable/countoured test section wall needs then to be added to improve the functionality of such type of choke. This feature aims firstly to keep the choke area the minimum one and then to reduce the walls effects on pressure waves (or shock waves), to reduce the shrinkage of the effective test section area by the growth of the boundary layer, to take into account the blockage of the model and to have a different range of Mach numbers for the same wedge choke.

The Mach number is therefore controlled by a combination of effects of the position of the wedge after the test section and the shape of the walls in the test section. The shape of the walls has to be attentively designed in relation to the particular test and model in the test section. As mentioned later, this step can be done by iterative methods and the use of a Computational Fluid Dynamic (CFD) code. In this facility, as it will be primarily compared to some experimental data, the test section upper wall has been

shaped as it was in those experiments and the choice has been made in the direction of an easily changeable shaped wall instead of a continuous controlled and flexible wall.

This system can be conceptually compared to the adjustable supersonic nozzle where the test section is just before the throat. The divergent part of the nozzle is therefore linked to the diffuser of the wind tunnel where the flow will be supersonic. The design of the diffuser on wind tunnels of the kind described here has to take into account the presence of the vacuum tank downstream in order to avoid, or keep very low, the total pressure losses that diminish the run time.

A wedge choking system will be described that is conceptually very easy, practical in terms of manufacturing and technology and very suitable for short run time in nearsonic wind tunnels. All these advantages fit well with the philosophy of this project in terms of simplicity, economy, brevity and modularity.

1.3 Design philosophy

The main concepts which have led the design of the wind tunnel can be summarized as follows:

- *Safety*: the wind tunnel is inherently safe as being based on vacuum (only an implosion risk). Therefore it can be used for and by undergraduates students.
- *Simplicity*: the operation relies on a quick opening of a valve.
- *Maintenance*: at the exception of the vacuum pump, it is a very low maintenance facility.
- *Polyvalent*: because the design is modular, and not based on fixed geometry/set up of a manufacturer, it can be modified to fit any vacuum based specific requirement.
- *Low Cost Materials*: the choice of technology allows manufacturing with low cost materials. As the use of the vacuum is not constant (at peak times: 10 runs a day), also a more economical choice can be done regarding the pump.
- *Appropriate Scale*: although bigger is better in terms of aerodynamical scaling, a small facility allows a low cost of the associated visual system and this decreases the cost of models. It is thought that a $4''$ x $4''$ size, for a 3 second run, is probably fine for teaching purposes (using recent high speed cameras) and a good starting point for applied and fundamental research. It also means that the facility could be easily moved if necessary.

1.4 Structure of the thesis

Chapter 2 describes the procedure and the choices adopted in designing the wind tunnel as well as some theoretical background. The design of the wind tunnel has been split into subparts, where each one has been separately analyzed. Some of the sketches on Solid Edge of the different modules components are reported at the end of the chapter.

Chapter 3 validates the CFD methodology comparing the numerical results with experimental results obtained in the very similar wind tunnel of Queen's University of Belfast. The CFD model is based on bidimensional simulations on Fluent [2] and the experimental results concern a bump (circular arc) mounted on the wall at a high subsonic flow.

Chapter 4 goes into more detail on the design of the velocity regulation system and simulates the flow on the choke using the CFD model validated in the previous chapter. The choke is the very delicate part of this wind tunnel as well as innovative and the advantages of the solution introduced in this thesis will be presented.

The Conclusion summarizes the obtained results and discusses the topics which were unable to be included in this project. The steps to conclude the design of the wind tunnel will be proposed as well as some inklings on first experimental tests.

Appendixes A and B show further sketches of the components and some picture of the wind tunnel.

Chapter 2

Overview of the experimental facility and design procedure

Contents

2.1 Schematics and brief description of the wind tunnel

The main parts or modules of this wind tunnel and their set-up are shown in fig. 2.1 in a very simplified scheme that helps to split the design into its subparts.

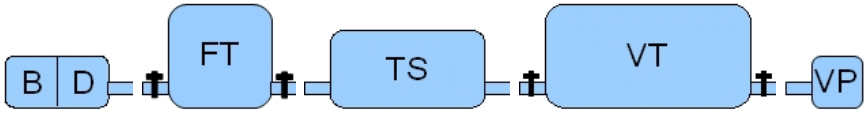

Figure 2.1: Layout of the wind tunnel.

The different components of this simple scheme are:

- *BD*, the blower and dryer module that is used to remove humidity from the air to avoid condensation in the test section and to pressurize the feeding tank before each run. Due to the small dimensions of the entire system it is possible to feed the whole volume of the test section before the run. This is true if the pressure will not be too high considering the need of an airtight design;

- *FT*, the feeding tank where the dry and pressurized air is stored before the run. Here it is possible here to control and change the initial conditions as well as controlling the temperature of the air;

- *TS*, the test section that is the main part of the wind tunnel and includes the settling chamber before the contraction, the contraction itself, the test chamber where the model is mounted, the apparatus for the regulation of the Mach number, the diffuser and the main valve. This section in particular will be discussed in greater detail later;

- *VT*, the vacuum tank downstream of the test section. Time available for each run depends on tank volume and pressure (as close as possible to vacuum) and for this reason it is a very important module of the wind tunnel. Another vital component is the valve between the test section and the vacuum tank, which acts as the main switch of the wind tunnel and it should therefore be as quick as possible to maximize the run time;

- *VP*, the vacuum pump, which is used to suck out air from the vacuum tank. Two characteristic of the pump are very important: the minimum pressure the pump can create that determines the initial pressure of the tank (and therefore the run time) and the velocity that affects

the time needed to suck the air, which determines and so the minimum time between two subsequent runs.

This modularity allows various changing of layouts. For example, it is possible to use more than one tank to increase the run time or have a test without the feeding tank to simplify the layout and using the atmospheric conditions as initial conditions. These two different configurations are shown in fig. 2.2 and 2.3.

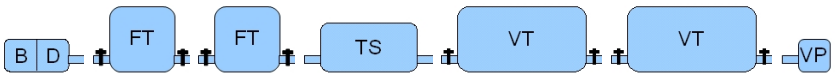

Figure 2.2: Configuration 1: extravolume.

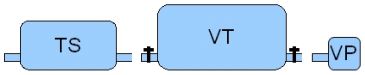

Figure 2.3: Configuration 2: simple.

The *BD* and the *FT* modules are not essential in this initial stage of the design and in the following chapters only the vacuum tank and the test section are studied. The feeding tank could also be thought of as a balloon deflating during the tests, with the pump chosen by considering the final pressure, and the speed required, to empty the tank.

The block *TS* can be divided further into other different and independent submodules shown in fig. 2.4.

Figure 2.4: Layout of the test section.

The parts that compose this section are:

- *SC*, the settling chamber composed in different units where each one has got a grid, or screen, to reduce the turbulence with the aim to increase the quality of the flow. Leaving the flow from either the clear atmosphere or the feeding tank that are in rest condition, the turbulence to reduce is small and due mainly to inflow effects. A funnel-shaped settling chamber is therefore preferable. The area of the settling chamber is determined by the range of admissible velocity;

- *C*, the convergent. The contraction in this wind tunnel is composed by two different twodimensional contractions because both the initial section and the test section are square;
- *TC* is the proper test chamber of the wind tunnel. It has an uniform and square section with the possibility to easily change the upper and lower walls. In this way it will be possible to change and test different configurations[1];
- *Ch*, the choke or the wind tunnel that is the smallest cross area. The possibility to modify this area is used to regulate the velocity of the flow (the Mach number) in the test section;
- *D* is the diffuser aims to recover the pressure and to reduce the speed principally in order to reduce losses of pressure. As it is a supersonic diffuser[2], the decrease of speed is usually through shock waves and it requires particular attention;
- *Vv* is the main valve of the wind tunnel and it is the valve that starts the runs and for this reason it has to be very quick.

The choke will be extensively described in chapter 4 while a presentation of the calculations and choices taken for the other parts follow at the end of this chapter.

2.2 Governing equations and math modeling

2.2.1 Introduction of phenomenological and behavioural models

A given physical phenomenon can be studied through mathematical models of different degrees of complexity and closeness to reality. Therefore, the choice of the model is a very important task before each design.

The choice of a structure for the mathematical model is called *model-structure selection* or more concisely *characterization*. A typical example of model is a first-order linear differential equation or, simpler, an algebraic equation.

Also characterization is critical, because intuition plays an important role. It is of paramount importance, since it defines the choice available for the selection of the "best model".

In general the choice between the different models is usually done taking into account the following points:

[1] The walls can be perforated or shaped to create particular geometries, minimize blockage effects, minimize shock waves reflections and/or control the Mach number.

[2] As the choke is the minimum section and when choked it is at Mach number equal to 1, an increase of area brings the flow to be supersonic.

- the aim of the modeling;
- the conditions under which the model is going to be employed (operation ranges, nature of inputs, communication with other elements of a control system...);
- the cost of building the model;
- the information available (there is no point in conceiving a very complex model with many parameters if data is scarce and imprecise).

A first and important distinction is between phenomenological and behavioural models [6] that brings out two types of modeling that translate into differing requirements.

Phenomenological (or *knowledge-based*) *models* are the typical ones used, for instance, in physics or chemistry courses. They are built from basic principles by writing down conservation or balance equations (for mass, momentum, energy...). The fact that this type of model is built from physical considerations facilitates incorporation of prior information and *a posteriori* checking of order of magnitude of the estimated parameters.

A significative example are the well known Navier-Stokes (NS) equations based on conservation of mass and momentum. The starting point of these equations are considerations on the kinetic theory that bring to the definitions of continuum fluid, pressure, temperature and density. All the variables and parameters have a precise and concrete meaning.

Such models may thus consist of many equations, often non linear (e.g. the NS equation case). The simulation of these complex models generally takes a lot of time on powerful computers and they are therefore seldom used directly to compute a control law. On the other hand, they are well suited to detailed simulation for the prediction of long-term behaviour or for gaining further insight into the internal working of the process. One must then resort to simplified models.

At the other end of the spectrum, one finds *behavioural models*, which merely approximate observed behaviour without requiring any prior knowledge of the process that generates data. It is not even know what the inputs and outputs stand for or in what units they are expressed. The model structure does not claim to correspond in any more fundamental way to that of the process, and the parameters have non physical meaning.

If, for example, an experimental curve is described by the polynomial

$$y_m(t, \mathbf{p}) = p_1 + p_2 t + p_3 t^2 + p_4 t^3 + ...$$

it is possible to reproduce with arbitrary precision any finite set of experimental data $y(t_i)$, $i = 1, ..., n_t$, provided that the degree of the polynomial is large enough. This is a particularly simplistic example of a behavioural

model, with a very poor predictive capability. There are, of course, more sophisticated methods of building models, the aim of which is still to reproduce input-output behaviour independently of any knowledge of the underlying process. The sensitivity of such solution to variation of these parameters could, of course, be extreme.

Behavioural models are in general easier to simulate and more suited to the computation of controls than phenomenological models because they are built by the user but their validity domain is more restricted.

The choice between phenomenological and behavioural models is not always as simple as the previous discussion shows. Estimating for example the few parameters of a phenomenological model (that could be a suitably discretized partial differential equation) may turn out to be simpler than estimating that many parameters of a multi-input multi-output behavioural model which would not exploit the physical laws governing the process studied.

Models adopted during the design will be described passing from gasdynamic of isentropic flows to the use of the CFD, from semi empirical methods in shaping the contraction to "expert experience".

2.2.2 Isentropic flows

The equations that fully govern the flows are the Navier-Stokes equations accompanied with an energy equation and an equation of state of the fluid. The diffulty in solving such complex equations is well known. Therefore in almost all the cases, the study is aimed at finding approximations that result in produce a "good" solution simplifying the problem.

Here follows the equations governing *stationary*, *one-dimensional*, *inviscid*, *adiabatic*, *isentropic* flows of gases. Equations are very useful at an early stage of the wind tunnel design because they are very simple and describe the mean flow accurately enough.

- At any point in a flow field the pressure P expressed in Pascal, the density ρ in $\mathrm{Kg/m^3}$ and the temperature T in K are related by the *equation of state*:
$$P = \rho R T \tag{2.1}$$
where R is the specific gas constant expressed in $\frac{\mathrm{J}}{\mathrm{Kg \cdot K}}$.

- For continuous flow in a duct or stream tube, the conservation of mass flow at any two stations (1 and 2) is specified by the *continuity equation*:
$$\rho_1 A_1 U_1 = \rho_2 A_2 U_2 \tag{2.2}$$
where A is the cross-sectional area of the duct at a given station in $\mathrm{m^2}$ and U is the flow velocity in m/s.

- From the summation of forces between two stations in a constant area stream tube, or duct with no friction, the following *momentum equation* is obtained:
$$P_1 + \rho_1 {U_1}^2 = P_2 + \rho_2 {U_2}^2 \tag{2.3}$$

- If no energy is added or lost during the flow of a sample of fluid between two stations in a duct (that is if the flow is *adiabatic*), the following *energy equation* is valid:
$$c_p T_1 + \frac{{U_1}^2}{2} = c_p T_2 + \frac{{U_2}^2}{2} = c_p T^t \tag{2.4}$$
where c_p is the specific heat at constant pressure expressed in $\frac{\mathrm{m}^2}{\mathrm{sec}^2\mathrm{K}}$ and the superscript t denotes conditions at zero velocity or, identically, stagnation conditions.

- If the change of state of a fluid during its flow from one station to another is *isentropic*, the following thermodynamic relation is applicable:
$$\frac{T_1}{P_1^{(\gamma-1)/\gamma}} = \frac{T_2}{P_2^{(\gamma-1)/\gamma}} \tag{2.5}$$
where γ is the ratio of specific heat at constant pressure c_p to specific heat at constant volume c_v.

In addition to the above equations, the following definitions are needed in the next section:
$$M = \frac{U}{c} \tag{2.6}$$
$$c = \sqrt{\gamma R T} \tag{2.7}$$
$$c_p = \frac{\gamma R}{\gamma - 1} \tag{2.8}$$
where c is the speed of sound expressed in m/sec and M is the Mach number that is dimensionless.

From the energy equation (2.4) and the definitions of eqs. (2.6), (2.7) and (2.8) it can get:
$$\frac{T_1}{T_2} = \frac{1 + [(\gamma-1)/2]{M_2}^2}{1 + [(\gamma-1)/2]{M_1}^2} \tag{2.9}$$
Combining eq. (2.9) with the equation for isentropic flow (eq. (2.5)) yields:
$$\frac{P_1}{P_2} = \left\{ \frac{1 + [(\gamma-1)/2]{M_2}^2}{1 + [(\gamma-1)/2]{M_1}^2} \right\}^{\frac{\gamma}{(\gamma-1)}} \tag{2.10}$$
Combining eqs. (2.9) and (2.10) with the equation of state (eq. (2.1)) yields:
$$\frac{\rho_1}{\rho_2} = \left\{ \frac{1 + [(\gamma-1)/2]{M_2}^2}{1 + [(\gamma-1)/2]{M_1}^2} \right\}^{\frac{1}{(\gamma-1)}} \tag{2.11}$$

Adding in the continuity equation (eq. (2.2)) it obtains

$$\frac{A_1}{A_2} = \frac{M_2}{M_1}\left\{\frac{1+[(\gamma-1)/2]{M_2}^2}{1+[(\gamma-1)/2]{M_1}^2}\right\}^{-\frac{(\gamma+1)}{2(\gamma-1)}} \tag{2.12}$$

From the definitions of eqs. (2.6), (2.7) and (2.8), the following equation for dynamic pressure ($\rho U^2/2$) is obtained:

$$q = \frac{\gamma}{2}PM^2 \tag{2.13}$$

From the proceeding equations, together with the knowledge that stagnation conditions will exist at $M = 0$, the following isentropic flow relations are obtained:

$$\frac{P}{P^t} = \left(1+\frac{\gamma-1}{2}M^2\right)^{-\frac{\gamma}{(\gamma-1)}} \tag{2.14}$$

$$\frac{\rho}{\rho^t} = \left(1+\frac{\gamma-1}{2}M^2\right)^{-\frac{1}{(\gamma-1)}} \tag{2.15}$$

$$\frac{T}{T^t} = \left(1+\frac{\gamma-1}{2}M^2\right)^{-1} \tag{2.16}$$

$$\frac{q}{P^t} = \frac{\gamma}{2}M^2\left(1+\frac{\gamma-1}{2}M^2\right)^{-\frac{\gamma}{(\gamma-1)}} \tag{2.17}$$

Using an area at $M = 1$ (A^* corresponding to the throat of a supersonic nozzle or the choke section in the wind tunnel studied here) as a reference, the eq. (2.12) becomes

$$\frac{A}{A^*} = \frac{1}{M}\left\{\frac{1+[(\gamma-1)/2]M^2}{[(\gamma+1)/2]}\right\}^{\frac{(\gamma+1)}{2(\gamma-1)}} \tag{2.18}$$

A simple example on the model dimension

In order to demonstrate the order of eq. (2.18), it is considered a model in a nearsonic wind tunnel that causes choking condition being the minimum section area.

For a model frontal area of 0.9 percent of the test section area so that

$$\frac{A_{TS}}{A^*} = \frac{A_{TS}}{A_{TS}-A_m} = \frac{A_{TS}}{A_{TS}(1-0.009)}$$

the upstream Mach number is equal to 0.9 where to have a nominal test Mach number of 0.95 the model frontal area should be $A_m = 0.2\%\, A_{TS}$.

The importance of the use of ventilated, slotted or contoured walls to test at high subsonic ranges without have choking conditions on the model is now clearer.

For these problems it is also common practice [3] to consider data from a nearsonic tunnel erroneous if the reference test Mach number is less than 0.02 below the choking Mach number.

2.2.3 Nozzle theory

The area-Mach number relation in eq. (2.18), see fig. 2.5, is very important in one-dimensional study of compressible flow through nozzles.

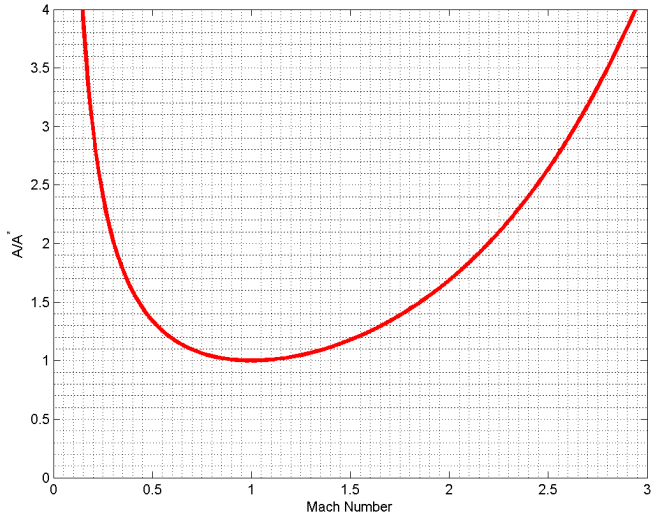

Figure 2.5: Relation between area ratio and Mach number.

This equation tells that $M = f(A/A^*)$: Mach number at any location in the duct is a function of the ratio of the local duct area to the sonic throat area (or the choked area). Therefore A must be greater than or at least equal to A^*: the case where $A < A^*$ is physically not possible in an isentropic flow. Equation (2.18) yields two solutions for M at a given area ratio: a subsonic value and a supersonic value. Which of the two values of M is the real one, depends on the pressures at the inlet and exit of the duct and on the shape of the nozzle.

With reference to fig. 2.5: for subsonic values of M, as M increases, A/A^* decreases (i.e. the duct converges); at $M = 1$, $A/A^* = 1$; finally, for supersonic values of M, as M increases, A/A^* increases (i.e. the duct diverges).

It is possible now to discuss the *choke condition* considering a convergent-divergent nozzle as sketched in fig. 2.6 taken from the fundamental book of Anderson [7].

If the exit pressure P_e is equal to the total/initial pressure P_0, no pressure difference exists and no flow occurs inside the nozzle. By slightly reducing P_e, the small pressure difference will produce a very low subsonic flow inside the nozzle. The local Mach number will increase slightly through the conver-

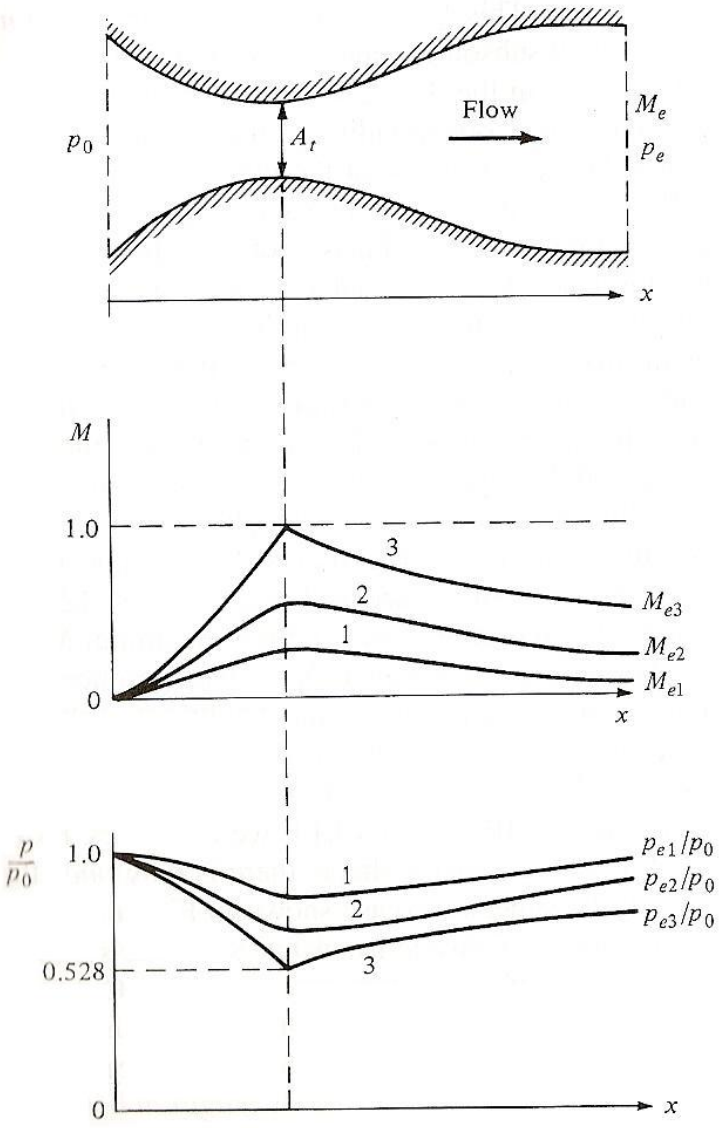

Figure 2.6: Isentropic subsonic convergent-divergent nozzle flow. [7]

gent portion, reaching a maximum value at the throat. This Mach number at the throat will not be sonic but it will be some subsonic value. Downstream of the throat, the local Mach number will decrease in the divergent section, reaching a very small but finite value $M_{e,1}$ at the exit. Correspondingly, the pressure in the convergent section will gradually decrease from P_0 at the inlet to a minimum value at the throat, and gradually increase to the value $P_{e,1}$ at the exit. It is important to note that because the flow is not sonic at

the throat in this case, the throat area A_t is not equal to the sonic throat area A^*. In the case of purely subsonic flow through a convergent-divergent nozzle, A^* takes on the character of a reference area: it is the area the flow would have if it were somehow accelerated to sonic velocity.

If exit pressure $P = P_{e,2}$ is further decreased, the flow moves faster through the nozzle and the maximum Mach number at the throat increases but remains less than 1. Reducing the pressure to $P = P_{e,3}$, the flow just reaches sonic conditions at the throat. The throat Mach number is therefore 1 and the throat pressure is $0.528\,P_0$ from eq. (2.14) for $M = 1$ applied to air. The flow downstream is again subsonic.

From now on, decreasing the exit pressure leads to a supersonic flow just downstream of the throat and the same subsonic flow as before for the convergent part. So, for a given nozzle shape, there is only one allowable isentropic flow solution for the supersonic case[3]. In contrast, there are an infinite number of possible isentropic subsonic solutions, each one corresponding to some value of P_e, where $P_0 \geq P_e \geq P_{e,3}$. Only three solutions of this infinite set of solutions has been sketched in fig. 2.6. Hence it has been shown that the key factors for the analysis of purely subsonic flow in a convergent-divergent nozzle are A/A^* and P_e/P_0.

Considering now the mass flow through the convergent-divergent nozzle in fig. 2.6, as the exit pressure is decreased, the flow velocity in the throat increases; hence, the mass flow increases. The mass flow can be evaluated at the throat:

$$\dot{m} = \rho_t U_t A_t$$

As P_e decreases, U_t increases and ρ_t decreases. However, the percentage increase in u_t is much greater than the decrease in ρ_t. As a result, $\dot{m}$ increases, as sketched in fig. 2.7 where an increase in pressure corresponds on a movement toward left. When $P_e = P_{e,3}$, sonic flow is achieved at the throat and

$$\dot{m} = \rho^* U^* A^* = \rho^* U^* A_t$$

Now, if P_e is further reduced below $P_{e,3}$, the conditions at the throat take on a new behaviour: they remain constant. Because the Mach number at the throat cannot exceed 1, if P_e is further reduced, M will remain equal to 1 at the throat. Consequently, the mass flow will remain constant as P_e in reduced. In a sense, the flow at the throat, as well as upstream of the throat, becomes "frozen". This corresponds to a very important and useful observation: once the flow becomes sonic at the throat, disturbances cannot

[3]An adapted convergent-divergent nozzle is considered here, where the exit pressure is equal to the external pressure. It is not considered therefore the presence of shock waves or expansion waves in the supersonic portion.

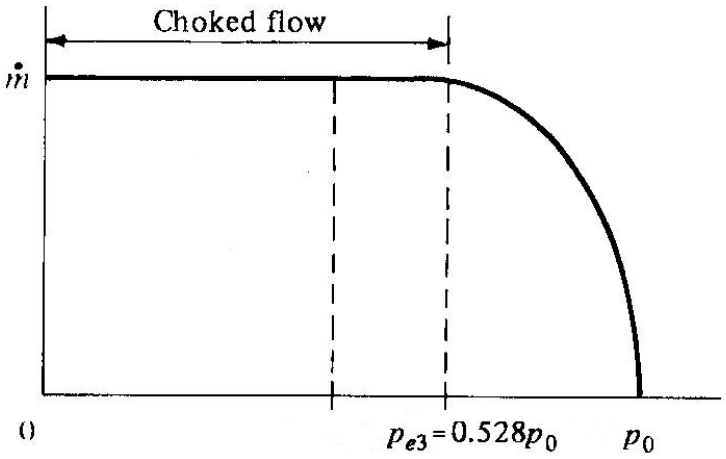

Figure 2.7: Variation of mass flow with exit pressure; illustration of choked flow. [7]

work their way upstream of the throat. Hence, the flow in the convergent section of the nozzle no longer communicates with the exit pressure and has no way of knowing that the exit pressure is continuing to decrease. This situation (when the flow goes sonic at the throat and the mass flow remains constant no matter how low P_e is reduced to) is called *choked flow.*

This last behaviour of the flow in reaching the sonic conditions is the theoretical starting concept in the choke design. If the test section is considered as the extension of the convergent nozzle, the choking system downstream the test section is considered as the throat, the diffuser as the divergent part of the nozzle and the exit pressure as the vacuum tank pressure, the above conclusions can be applied on the present wind tunnel.

While the inlet end exit pressure ratio is less than 52.8 percent , the mass flow is choked (constant) and it is function of the ratio A/A^* imposed with the choke system. The disturbances of the choke or whatever downstream the choke do not influence the flow in the test section that remains frozen.

2.2.4 Air flow rate

The rate of air flow through the tunnel is calculated as already metioned:

$$\dot{m} = \rho U A \tag{2.19}$$

It is possible to express the density and the velocity of the air using the previous equations. From the equation on the variation of ρ with Mach

number (eq. (2.15)) and the equation of state (eq. (2.1)) one gets

$$\rho = \left(\frac{P^t}{RT^t}\right)\left(1+\frac{\gamma-1}{2}M^2\right)^{-\frac{1}{\gamma-1}} \tag{2.20}$$

Now eqs. (2.6) and (2.7) combined with eq. (2.16) yield the following equation for the velocity:

$$U = M\left[\gamma RT^t\left(1+\frac{\gamma-1}{2}M^2\right)^{-1}\right]^{\frac{1}{2}} \tag{2.21}$$

Eq. (2.19) then becomes

$$\dot{m} = P^t AM\left(\frac{\gamma}{RT^t}\right)^{\frac{1}{2}}\left(1+\frac{\gamma-1}{2}M^2\right)^{-\frac{(\gamma+1)}{2(\gamma-1)}} \tag{2.22}$$

It is convenient to make the calculation at the nozzle throat, where Mach number equals 1. For this case eq. (2.22) becomes:

$$\dot{m} = P^t A^*\left(\frac{\gamma}{RT^t}\right)^{\frac{1}{2}}\left(1+\frac{\gamma-1}{2}\right)^{-\frac{(\gamma+1)}{2(\gamma-1)}} \tag{2.23}$$

Since γ and R are constant the previous equation (2.23) can be re-written in the following way:

$$\dot{m} = \left[\left(\frac{\gamma}{R}\right)^{\frac{1}{2}}\left(1+\frac{\gamma-1}{2}\right)^{-\frac{(\gamma+1)}{2(\gamma-1)}}\right]\frac{P^t A^*}{\sqrt{T^t}} \tag{2.24}$$

where the term within square brackets is constant[4]. It is now possible to evaluate the flow rate in the wind tunnel knowing the geometry and the characteristic of the air entering in the nozzle. The ratio of test section area to throat area is given by eq. (2.18) and already plotted in fig. 2.5.

2.2.5 Run time

The run time of an indraft wind tunnel is the key design parameter because it is considerably affected by the size of the test section, the size of the vacuum tank, the need of a storage tank, the Mach number of the test and the kind of tests to be carried out considerably affect this value.

The run time is limited by the rising pressure in the vacuum tank. When the vacuum tank pressure rises to the point where the pressure ratio across the tunnel is not sufficient to sustain the tunnel at the desired Mach number

[4]Using dry air with $\gamma = 1.4$ (isentropic process) and a gas constant $R = 287.05\frac{\mathrm{J}}{\mathrm{Kg{\cdot}K}}$, the constant C is equal to $0.04041\frac{\mathrm{s}\sqrt{\mathrm{K}}}{\mathrm{m}}$.

(i.e. losing of the choke condition), the run comes to an end. If the total pressure of the tunnel, the operating Mach number and the corresponding pressure ratio required are known, the conditions in the vacuum tank at the end of the run will be known.

The process to obtain the formula of the run time t suggested by Pope and Goin [3] originates from the mass conservation law: the mass flow of air through the tunnel during the runtime is equated to the change of mass of air in the vacuum tank. Hence

$$\dot{m}t = V(\rho_e - \rho_i) \tag{2.25}$$

where V_v is the vacuum tank volume in m^3; the subscript e denotes end of run and i denotes beginning of run (initial condition). Rearranging the formula (2.25):

$$t = \frac{V\rho_e}{\dot{m}}\left(1 - \frac{\rho_i}{\rho_e}\right) \tag{2.26}$$

The condition in the tank during a run can be represented by a polytropic compression process, so that

$$\frac{\rho_i}{\rho_e} = \left(\frac{P_i}{P_e}\right)^{1/n} \tag{2.27}$$

where n is the polytropic coefficient[5]. Redefining ρ_e using the gas law (eq. (2.1)) and combining equations (2.26) and (2.27) yields

$$t = \frac{VP_e}{\dot{m}RT_e}\left[1 - \left(\frac{P_i}{P_e}\right)^{1/n}\right] \tag{2.28}$$

where T_e is the temperature in the tank at the end of the run. All the air entering the tank will have a temperature approximately equal to the total temperature of the air entering the nozzle, T^t. The flow of air into the tank causes a compression of the air already in the tank with a consequent temperature rise. This has a relatively small overall effect and a final tank temperature $T_e = T^t$ is assumed. With this assumption, the rate flow from eq. (2.23) and the area ratio from eq. (2.18), eq. (2.28) becomes

$$t = \frac{V}{AM}\frac{P_e}{P^t}\frac{1}{\sqrt{\gamma RT^t}}\left(1 + \frac{\gamma - 1}{2}M^2\right)^{\frac{(\gamma+1)}{2(\gamma-1)}}\left[1 - \left(\frac{P_i}{P_e}\right)^{\frac{1}{n}}\right] \tag{2.29}$$

[5]The polytropic coefficient n can only be estimated before the tunnel is operated. The possible variation of this coefficient for an air wind tunnel is from 1.0 for an isothermal process to 1.4 for an adiabatic process. The larger the vacuum tank and the shorter the run time, the nearest this coefficient should approach 1.4. A value of 1.15 is suggested [3] for computations involving a new tunnel; moreover experiments on small vacuum tanks [**?**] show a compression very close to be isothermal.

Mach number and area are those of the test section; values of total temperature and total pressure to be used in solving should be the values downstream of the drier, since the drier cause a pressure drop and a temperature rise. In absence of the dryer/blower section this pressure can be taken as the atmospheric conditions.

The value of the exit pressure should be the value at the end of the diffuser or, still better, its value in the vacuum tank with the wind tunnel still choked. This value depends on the behaviour of the flow in the diffuser and on the discharge into the tank and so it needs to take into account the related shock waves, expansion waves and reflections. P_e can be roughly and initially estimated from the nominal Mach number in the test section and using, for example, the isentropic formula in eq. (2.14).

2.2.6 Viscosity effects

As presented, all the above considerations lie on the strict assumption of inviscid flow. Although this discussion is useful in analytically describing the mechanism of the flow, the correlation with actual flow could be quite poor unless viscous effects are included.

The first important difference between ideal and real flows is the presence of the boundary layer that is the thin region where the flow increase from the necessary zero value on the wall to the freestream velocity. Detailed introductions on viscosity effects (Reynolds number), boundary layers, characterization of laminar and turbulent boundary layer, development and separations can be found in many books; a good reference is the evergreen book by Anderson [7].

Regarding this particular case as a high speed pipe flow, the Reynolds number could be estimated of the order of 10^6 based on the hydraulic diameter and rough estimation of velocity (nearsonic) and viscosity. It is therefore possible to assert that the boundary layer in the test section of this wind tunnel will be turbulent and compressible (due also the high Mach number).

Without conducting a thorough theoretical discussion about this topic, it is possible to give a few basic considerations which are very important in the design and in the understanding of the results.

First of all, boundary layers represent a loss of total pressure generated by the skin friction due the presence of the wall that imposes zero velocity on the first layer of the fluid. It will be discussed again later the importance in keeping the pressure losses as low as possible for the maintenance of a choked flow.

Secondly, the presence of the boundary layer is often taken into account as an effective shift of the walls, corresponding to the boundary layer thickness. This means that the actual section area will be decreased by the boundary layer effect and, for example, the fundamental equation (2.18) will be affected.

Furthermore, characteristic of the boundary layer is to grow along the surface, with the growing function strongly dependent on the Reynolds number. This effectively results in a continuous decreasing of the cross section area in the test section if the walls are straight, with the consequence of a positive velocity gradient. The test section, so designed, with the presence of the boundary layer will work as having low convergent walls.

The flow will also be significatively changed at corners where boundary layers from the two perpendicular walls collapse.

Lastly, separations of boundary layers for strong adverse pressure gradients can occur and should be avoided for the sake of limited losses in pressure. This can occur particularly in the diffuser where the walls are usually divergent.

As already mentioned, particular devices on the tunnel walls are adopted to alleviate the boundary layer effects: slotted or perforated walls can give different wall conditions (in terms of velocity, pressure and permeability) and movable and shaped walls can do the same job maintaining a constant velocity gradient along the test section.

2.3 Design of the wind tunnel

As discussed in the introduction, the size of the test chamber has been taken $4''$ by $4''$ (square section of 101.6 mm) of 800 mm length. These dimensions are the starting point of the design and they match with the Queen's University of Belfast which results will be used as reference for the validation of this wind tunnel.

The design of each single component of the test section is described below with special attention on the contraction. If a square cross section gives more problems on the contraction, it provides easier optical access because of the straight walls (i.e. windows).

2.3.1 Drying system and feeding tank

The dryer can be designed to dry the air at the rate at which the air is used and for a length of time equal to the run time. The air is therefore dried continuously during the time required for the filling of the vacuum tank. In this case the air can be taken directly from the atmosphere but the dryer must be quite large.

The dryer can also be of the capacity type: dry air is stored at atmospheric pressure in a container placed upstream of the tunnel (the feeding tank). In this case, the dryer required is much smaller than the dryer of the type considered above.

Depending on the pressure, it can be adopted a balloon or a proper pressure tank, the dry air can be stored at a higher pressure than the atmo-

spheric one with the benefits of lengthening the runs and having the total pressure as a supplement parameter to be set.

As shown before, these parts are not essentials for the functioning of the wind tunnel and the design will be carried on without considering them anymore.

2.3.2 Settling chamber

The section area of the settling chamber is designed by evaluating the flow velocity in it in order to avoid big losses of pressure through the screens, honeycombs and grids[6]. This prevents convection currents from non-uniform temperature distributions that would persist from the settling chamber through the test section[7].

The settling chamber is therefore usually designed [3] for a velocity no greater than 80 to 100 feet per second (24 to 30 m/s) and no less than 10 feet per second (3 m/s). Using the equation of the flow rate (2.22) evaluated in the test section (at Mach equal to 1) and in the settling chamber and knowing that the flow rate in both these sections is the same, it is possible to calculate the velocity of the flow in the settling chamber.

In this case the calculation is:

$$\begin{aligned} \dot{m}_{SC} &= \dot{m}_{TS} \\ P^t A_{SC} M \left(\frac{\gamma}{RT^t}\right)^{\frac{1}{2}} \left(1+\frac{\gamma-1}{2}M^2\right)^{-\frac{(\gamma+1)}{2(\gamma-1)}} &= P^t A^* \left(\frac{\gamma}{RT^t}\right)^{\frac{1}{2}} \left(\frac{\gamma+1}{2}\right)^{-\frac{(\gamma+1)}{2(\gamma-1)}} \end{aligned}$$

using typical atmospheric values for total pressure, total temperature, density and using $A_{SC} = 366.4\,\text{mm}$ by $366.4\,\text{mm}$ and $A^* = 4''\text{x}4''$, results in a value of the flow velocity in the settling chamber equal to 15.3 m/s, which lies perfectly in the range of speed discussed. The areas so defined correspond to a contraction ratio of 13.

Regarding the spacing between the screens (and so the width of the independent modules constituting the whole settling chamber) there are two important properties to consider:

- for the pressure drops through the screens to be completely independent, the spacing should be such that the static pressure has fully recovered from the perturbation before reaching the next screen (i.e. $dp/dy = 0$);

[6]The loss of pressure through screens or grids is proportional to the dynamic pressure that is a quadratic function of the velocity of the flow.

[7]This problem is unusual in blowdown or indraft tunnels like this one because the differences between the air temperature in the settling chamber and the walls of the settling chamber are insignificant.

- for full benefits from the turbulence reduction point of view, the minimum spacing should be of the order of the large energy containing eddies.

It had been found by Bradshaw [8] that a screen combination with a spacing equivalent to about $0.2 \times d_{SC}$, where d_{SC} is the settling chamber diameter, performs successfully. The optimum distance between the last screen and the contraction entry has also been found to be about $0.2 \times d_{SC}$. If this distance is much shorter, significant distortion of the flow through the last screen may be expected. On the other hand, if the distance, or for that matter the overall length of the settling chamber, is too long then unnecessary boundary layer growth occurs.

The diameter of the settling chamber d_{SC} is, in the case of non-circular section, the equivalent diameter which is defined as:

$$d_{SC} = \sqrt{\frac{4A}{\pi}} = \sqrt{\frac{4 \cdot 366.4^2}{\pi}} = 413.4\,\text{mm} \tag{2.30}$$

and the spacing is then:

$$L_{SC} = 0.2d = 82.7\,\text{mm} \quad \Rightarrow \quad 101.6\,\text{mm}\,(4'')$$

The over-rate of the length has been done considering the additional turbulence created by the corners.

2.3.3 Contraction

The contraction is one of the most important parts of the entire wind tunnel because from a good design of the contraction a good quality of the flow is achieved and clearly the good quality of the flow is one of the very important characteristic of a wind tunnel.

The initial section is the square section of the settling chamber (366.4 mm by 366.4 mm) whereas the final section is the test section area ($4''$ by $4''$). Both sections are square and the contraction is chosen to be composed by 2 distinct twodimensional convergents. This solution gives a further modularity to the design and simplifies the design without a big loss of quality considering. Furthermore, where it intends to have transonic flow tests (high subsonic speed of the air), the contraction is solely convergent. To modify the Mach numbers of the air going into the low supersonic range, it can be done "easily" by changing the second part of the contraction with a convergent-divergent twodimensional nozzle. At this stage of the project, an only convergent nozzle is designed.

Each part can then be designed differently and there will be the possibility to change each part separately (both for new, better designs and to change the range of Mach number).

The design of the two parts of the contraction now consists of finding the two functions $y = f(x)$ that give particular characteristic of the flow, indices of goodness. Furhermore, there are two main aspects to concentrate on in designing the contraction: maintenance of good *exit flow uniformity* (regarding both exit-flow uniformity and exit boundary layer thickness) and avoidance of *flow separation*. This said, the contraction design is basically a search for the optimum wall shape leading to the minimum nozzle length required for a given purpose. The design usually aims to limit the nozzle length in order to minimize its size and cost but, on the other hand, it must avoid making it too short. Nozzles that are too short produce an exit flow with inherent unsteadiness and thick boundary layers.

The first part of the contraction can be considered incompressible (the Mach number is less than 0.3) and it is easy to find analytical, empirical or semi-empirical methods for this kind of design where the flow is essentially twodimensional and there are no effects of compressibility. The optimum contraction lies between a good exit-flow uniformity, the control of separations and the minimum total length. See for example the works by Jordinson [9] for an overview of the problem, Mikhail [10] for the concept of optimum design of contractions and Libby et al. [11] for a two-dimensional design. The reference paper by Morel [12] describes the calculation of an analytical function composed of two cubics where the parameters are derived by considerating on the pressure coefficients and wall velocity.

The second part of the contraction leads to a compressible behavior of the flow and so the cited papers are not useful anymore (or at least can not give the solution like as it was for the first part directly).

Therefore the design of this part relies on conclusions and experience by Pope [3]:

`[...] The entrance section for a transonic nozzle is usually designed to give a smooth variation of Mach number with distance between the settling chamber and the minimum section of the nozzle. [...]`

supported by comparison and observation of other similar facilities and on the conclusions and comments on the paper, by Morel [12].

Beckwith I. E.[8] discussed the latter paper and has written:

`"[...] Hence we conclude that Morel's design procedures to avoid inlet separation are important in the design of wind tunnels over the entire Mach number range when low noise levels and minimum flow unsteadiness are required."`

[8]Head of Gasdynamics section, NASA Langley research center, Hampton, Va.

and in the author's closure (citing a study on contractions for incompressible turbulent flows by Hussain et al. [13]):

"[...] As Hussain and Ramjee pointed out, their results showed clearly that the cubic gave a better exit flow with a thinner boundary layer, with only a small penalty in velocity non-uniformity. Their statement that any of these nozzle is adequate, was meant for applications utilizing only the central core of the exiting stream and not for wind tunnels. [...]"

For all these reasons, like as in the first part of the contraction, the shape of this second part is composed by two cubic functions where the length and the match point (the connection point between the two functions) are in this case decided *a priori* in order to create a similar shape to the ones already working in other wind tunnels.

The choosing of the coefficients of the cubic functions, their discussion and the comparison with other facilities are in the next section.

2.3.4 Contraction design

The design of the contraction for this high subsonic configuration is composed of two different twodimensional, only convergent stages. The first one is essentially incompressible and the design is done following the paper of Morel [12] *Design of two-dimensional wind tunnel contractions*. The second stage presents of course compressible effects (it leads to a Mach number of up to 1) and the same paper is used, but more as a guideline to achieve a contraction similar to other facilities.

The paper is based on the construction of a shape function composed by two cubic functions matched in a middle point (the slope at the beginning and at the end is zero). In order to evaluate the coefficients of these functions, tables, empirical functions, theoretical assumptions are available and they are also presented in the following section. Regarding the second part, there are some sketches and photographs of other contractions of transonic wind tunnels.

First stage of the contraction

The schematic wall contour with the two cubic functions and the relative match point is shown in fig. 2.8. The nomenclature adopted in this section is as reported by Morel [12] and it is specified here when needed.

The initial and final heights are the dimensions of the settling chamber and the test section and the velocity in the in the inlet plane U_1 is the exiting velocity of the flow from the settling chamber.

$$H_1 = \frac{0.3664}{2} = 0.1832\,\mathrm{m}; \qquad H_2 = \frac{4 \cdot 25.4}{2} = 50.8\,\mathrm{m}; \qquad U_1 = 15.3\,\mathrm{m/s}$$

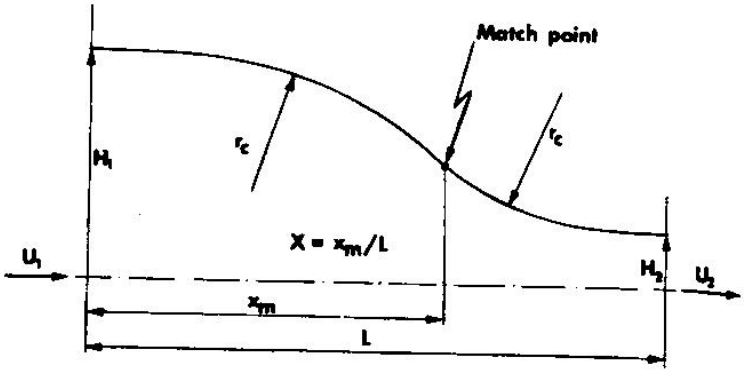

Figure 2.8: Wall contour made of two cubic arcs. [12]

The parameter m, defined as the ratio of the heights is:

$$m = \frac{H_1}{H_2} = 3.61$$

and the contraction area ratio CR is

$$CR = \frac{(H_1 \cdot H_1)}{(H_2 \cdot H_1)} = m = 3.61$$

As mentioned before, the primary criterions of the contraction design are:

1. some prescribed level of exit-flow uniformity,
2. avoidance of separation.

In addition it is usually desired to satisfy two other criteria:

3 minimum nozzle length,

4 minimum exit boundary layer thickness.

The only parameters available are the nozzle shape parameter $X = x_m/L$ and the length L because the values and the zero-slopes at the beginning and at the end of the nozzle are imposed.

The two primary criteria may always be satisfied by an increase in L for any (reasonable) wall shape. The boundary layer thickness, however, increases with increasing L due to the increased length of its development, and due to the decrease in favorable pressure gradients within the nozzle. Thus, it may be argued that to satisfy all four criteria one should probably aim at a design where separation is just avoided and the exit nonuniformity is equal to the maximum level of tolerable in the given application.

In order to assess whether the flow will separate, the wall pressure distribution has to be analysed. Thus the only flow-related information needed are the values of two wall pressure coefficients, defined as

$$C_{pe} = 1 - \left(\frac{U_{2,\infty}}{V_e}\right)^2$$
$$C_{pi} = 1 - \left(\frac{V_i}{U_{1,\infty}}\right)^2$$

where the subscripts e and i refer to the point of maximum and minimum wall velocity and U and V refer to the mean velocity and wall velocity.

The design problem is thus reduced to *a priori* determination (choice) of C_{pi} and C_{pe} to be used in the design charts to produce the nozzle length and shape. The choice of these coefficients will be made using Stratford's separation criteria [14]. Defining $\tilde{u}_2$ as

$$\tilde{u}_2 = \frac{V - U_c}{U_{2,\infty}}$$

it is left up to the investigator to be set the maximum value that can be tolerated, taking into account the rapid decay of the downstream non-uniformity.

A simple working form of the cited Stratford's separation criteria was derived by Morel [15] for the almost similar pressure distributions found in cubic nozzles:

$$C_{pi} = 0.7 \left(\frac{x_0 + 0.9x_i}{s}\right)^{-\frac{1}{3}} (10^{-6} Re_x)^{\frac{1}{15}}$$

where $Re_x = U_{1,\infty}(x_0{+}0.9x_i)/\nu = O(10^6)$, x_0 is the distance from the virtual origin of the boundary layer to the beginning of the nozzle, the length x_i is the distance from the nozzle beginning to the wall pressure maximum (that is the wall velocity minimum) and can be found with reference to fig. 2.9 and where s is defined as in fig. 2.10

The criterion at the narrow end is either the non-uniformity (relations found and discussed in the paper yields to $C_{pe} = 5.3\tilde{u}_2$) or separation. It is also stated that for the requirement of $\tilde{u}_2$ to be less than 2 percent, separation is not the decisive criterion for C_{pe}[9].

The iterative solution is now defined by the following operative steps:

1. choose the values of CR, C_{pi} and C_{pe};
2. read the values of F_e and F_i from fig. 2.11

[9] Some additional comments concerning the separation criterion at the narrow end are given in reference [16].

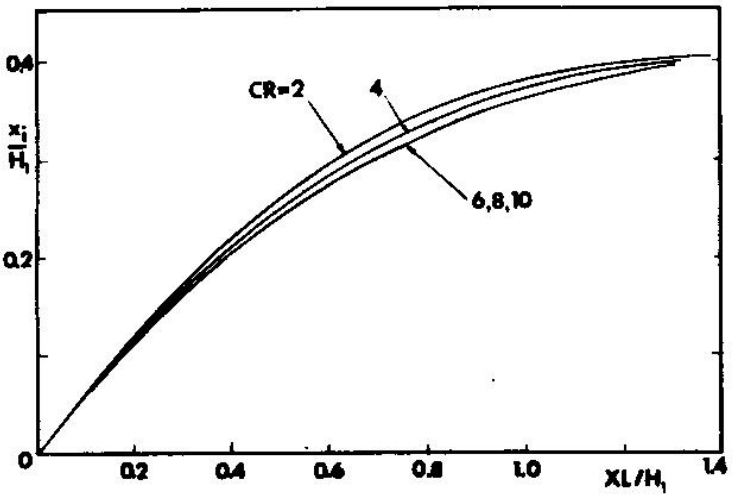

Figure 2.9: Distance from the nozzle beginning to the wall pressure maximum versus distance from the nozzle beginning to the cubic match point. [12]

3. solve for X from the equation

$$X = \left[1 + \frac{1}{m}\left(\frac{F_i}{F_e}\right)^{\frac{1}{2}}\right]^{-1}$$

4. calculate the value of L from one of the equations

$$\begin{aligned} F_i &= \frac{m-1}{m} X^{-2} \left(\frac{L}{H_1}\right)^{-3} \\ F_e &= \frac{m-1}{m^3} (1-X)^{-2} \left(\frac{L}{H_1}\right)^{-3} \end{aligned}$$

obtained by Morel in [15];

5. obtain the contour coordinates from

$$\begin{aligned} \frac{H-H_2}{H_1-H_2} &= 1 - \frac{1}{X^2}\frac{x^3}{L^3} && x/L \le X \\ &= \frac{1}{(1-X)^2}\left(1-\frac{x}{L}\right)^3 && x/L > X \end{aligned}$$

Data and choices used to find the shape are:

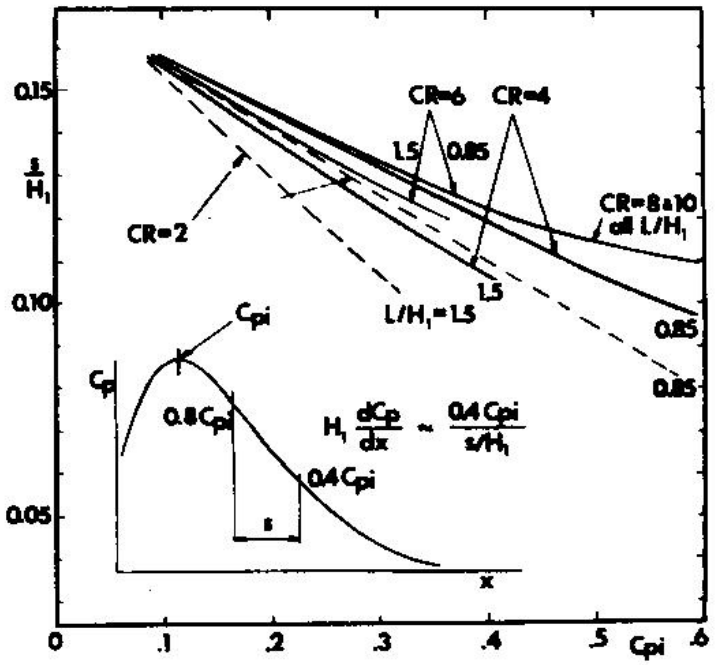

Figure 2.10: Wall pressure gradient at the inlet. [12]

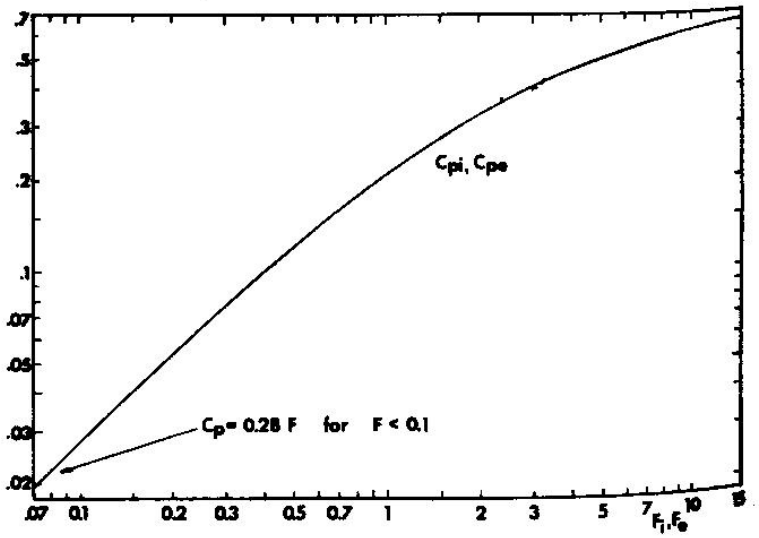

Figure 2.11: Dependence of C_{pi} and C_{pe} on the dimensionless parameters F_i and F_e, respectively. [12]

x_0	=	$101.6 + 16.1\,\text{mm}$	from the length of the module of the settling chamber added to the length of the contraction part before the beginning of the shape
x_i	=	$0.05\,\text{mm}$	from fig. 2.9
s	=	$0.13 \cdot H_1\,\text{mm}$	from fig. 2.10
$\tilde{u}_2$	=	2	

and the values at the end of the iterative process are:

$$\begin{aligned} C_{pi} &= 0.328 \\ C_{pe} &= 0.106 \\ F_i &= 2.3 \\ F_e &= 0.41 \\ X &= 0.5714 \\ L &= 0.1655\,\text{mm} \end{aligned}$$

The sketch of the contraction obtained from the iterative process is shown in fig. 2.12

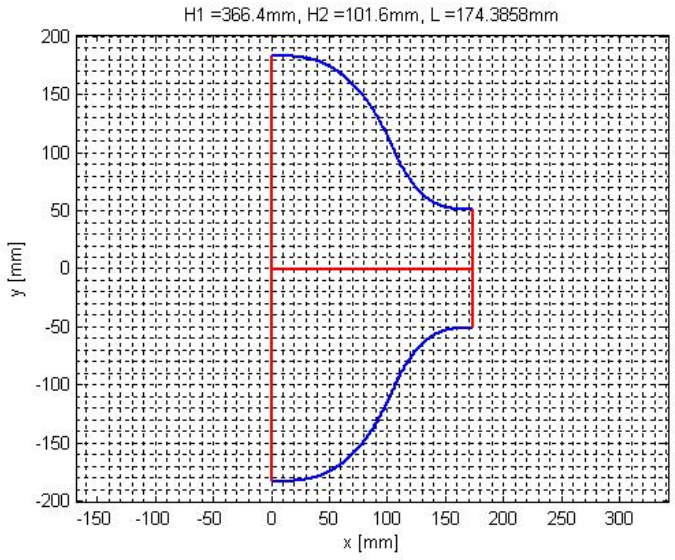

Figure 2.12: First contraction function.

CFD simulation of the first stage of the contraction

Preliminary twodimensional CFD simulations of the first stage of the contraction have been carried out using Fluent. To ensure a developed boundary

layer and to avoid exit condition influence, straight tubes have been added upstream and downstream the contraction.

A grid of 116337 cells has been adopted (see the zoom in fig. 2.13) and the turbulent nondimensional wall coordinate y^+ at the first points of the grid has acceptably been found in the range suggested in the manual of Fluent [2] of 30-60 when wall functions are used.

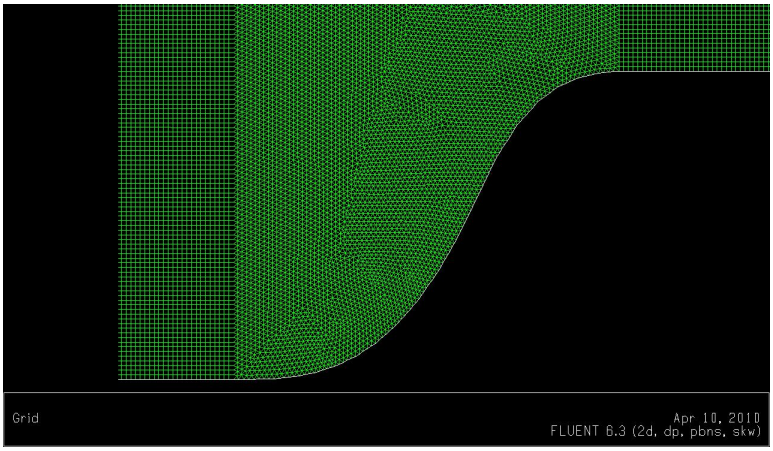

Figure 2.13: Zoom of the first contraction grid.

A $k\omega$ turbulent model on incompressible viscous flow was used with inlet condition of constant velocity of 15.6 m/s.

The velocity so obtained is shown in fig. 2.14. Figure 2.14(a) shows the horizontal velocity component at the inlet and the outlet of the contraction; the third profile is at about 1 exit diameter downstream the outlet of the contraction. Figure 2.14(b) shows the velocity contour on the whole computed domain.

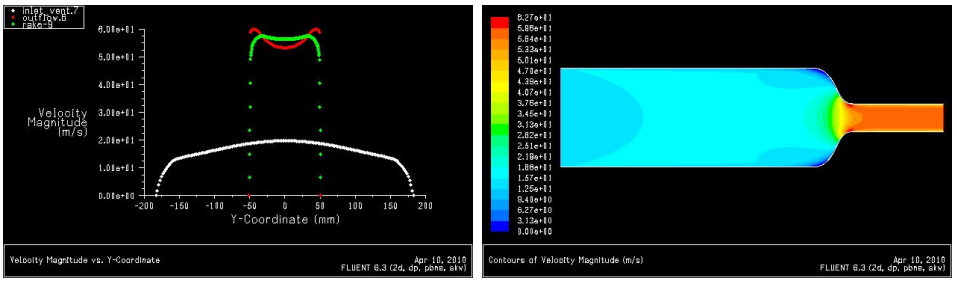

(a) Horizontal velocity component V_x. (b) Velocity magnitude contour.

Figure 2.14: Velocity on the first contraction.

It can be observed that the outflow velocity has a constant x component

at already one diameter after the outflow at the exception of the boundary layer.

Second contraction

The next figures (figs. 2.15 -2.22) are the geometry descriptions or photographs of some of the wind tunnels and numerical tests used in the European project UFAST[10] (a series of studies on unsteady effects of shock wave induced separation). All these wind tunnels work for transonic and low supersonic Mach numbers; some of them have contractions divided in two twodimensional parts and some others have threedimensional contractions.

In the convergent-divergent type nozzles the noteworthy point is the convergent part before the throat (minimum section).

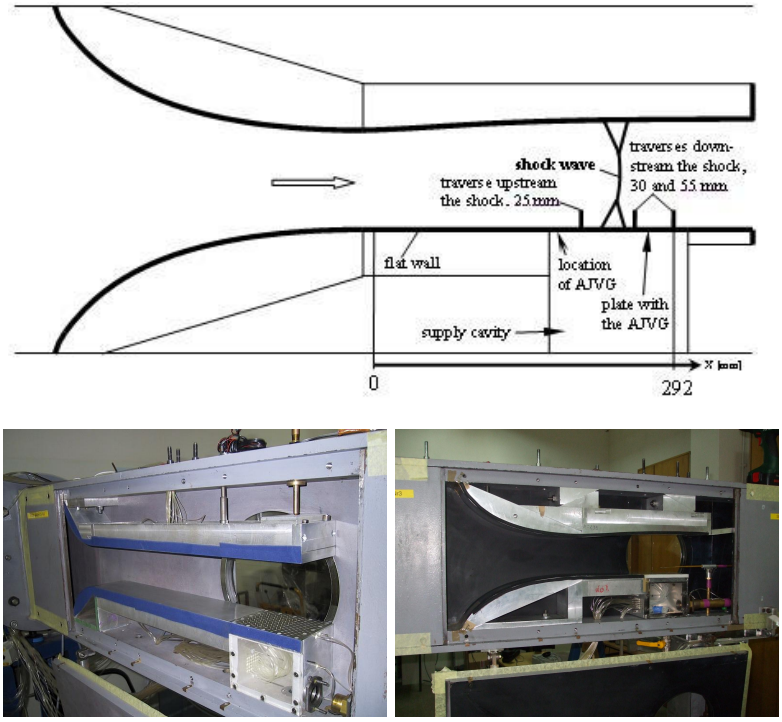

Figure 2.15: IMP test section.

Firstly, it is noted that the shapes of the contractions shown are quite different from each other. Therefore, the design (choose) of the contraction of this wind tunnel is done in a preliminary and simple way remembering also that the extreme modularity, the modest dimensions and costs allow the wind tunnel to be easily modified in its different parts.

[10]Project where Prof. Benard participates.

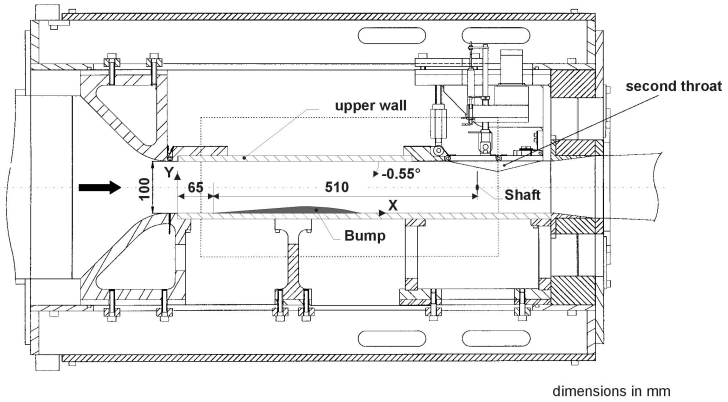

Figure 2.16: ONERA test section.

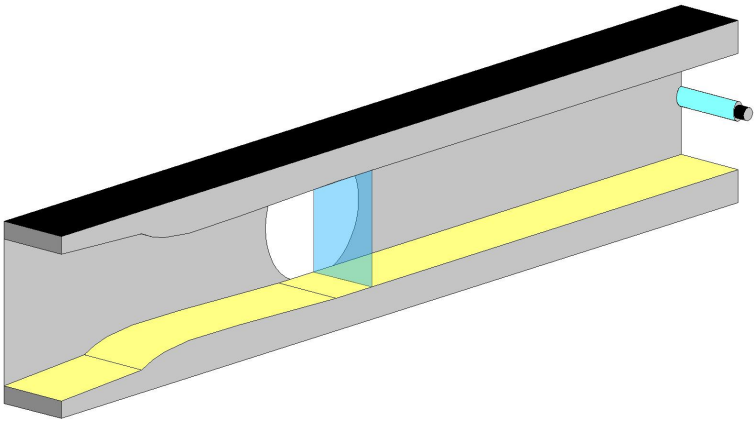

Figure 2.17: UCAM-DENG test section.

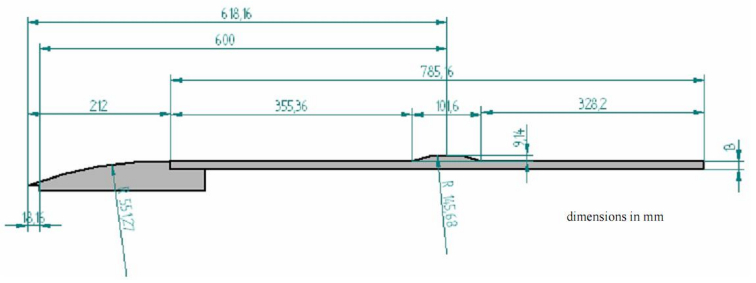

Figure 2.18: QUB test section bottom wall.

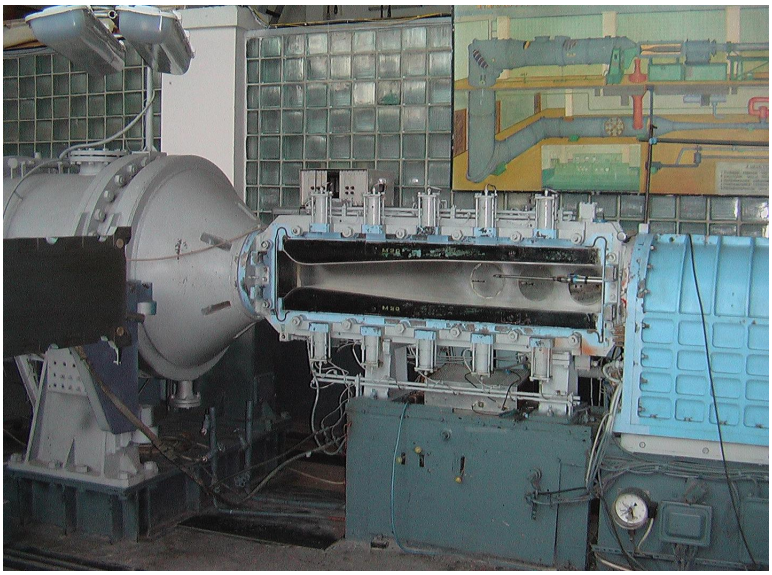

Figure 2.19: ITAM test section.

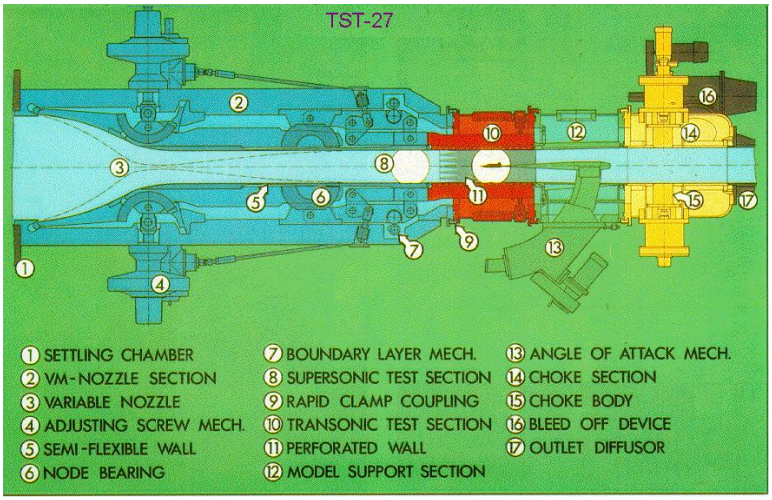

Figure 2.20: TUD test section.

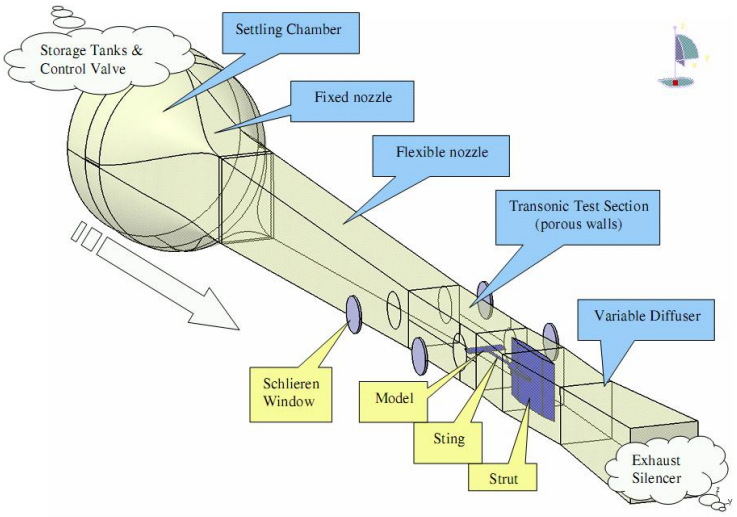

Figure 2.21: INCAS test section.

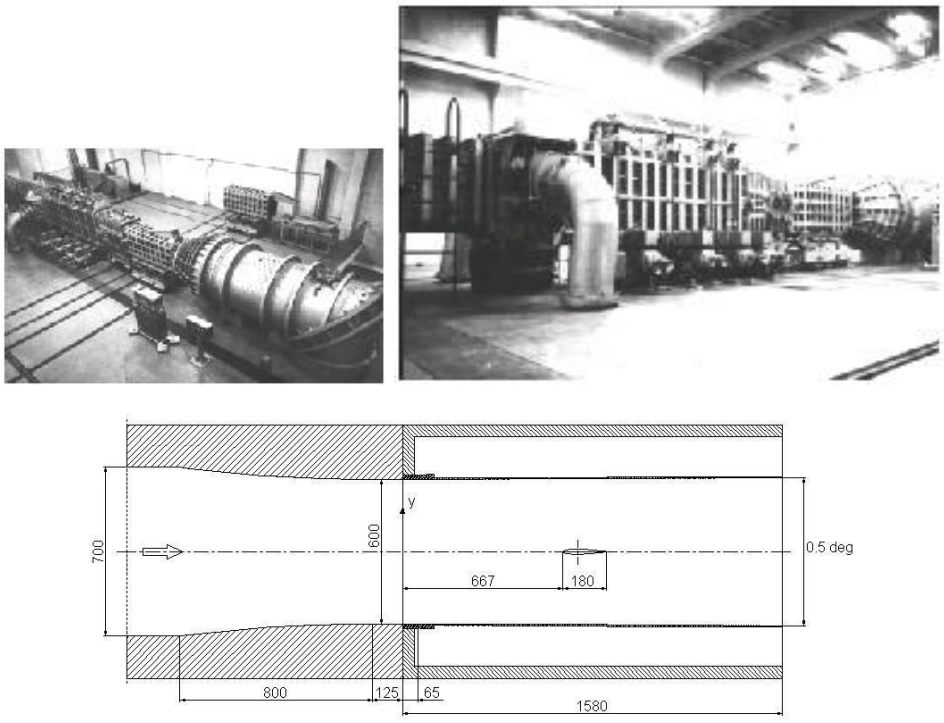

Figure 2.22: IoA test section.

Furthermore it is noted that the last part of the contractions of the previous facilities is quite different from the first part (which is in fact similar to the one achieved with the methods in section 2.3.4). In particular, the slope of the last part is very small compared to the first part.

The same type of contraction was used for the second part as was used in the first (two cubic functions) because of the good quality of the exit flow [13]. Given the initial and final heights, the only variable is the dimensionless X (defined by the length of the contraction L and the abscissa of the match point x_m).

The length of the second contraction block was chosen to be 1 foot. This length is in the range of 2-3 times the height of the test section that can be found in the other nozzles.

With the length defined, the variable left is the position of the match point. This position has only been chosen comparing the shape of the other nozzles with this one varying the value of x_m. The variation in the shape of the nozzle with the value of x_m is shown in fig. 2.23.

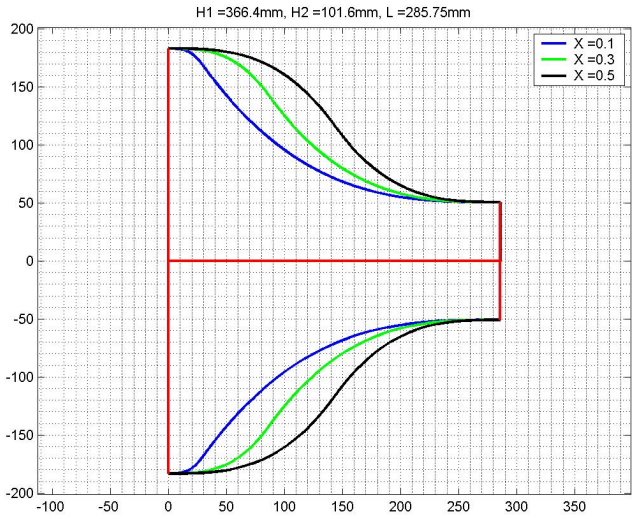

Figure 2.23: Comparison of different shapes varying x_m.

The value of x_m used for the contraction was set at 0.1 as this resulted in a contraction whose shape was inline with those previously designed elsewhere. The big difference in shape between this contraction and the first one previously shown is also clear.

CFD simulations on the second stage of the contraction have been integrated with test chamber and choke simulations (for details on the model see chapter 3). In fig. 2.24 an example of distributions of the two velocity

components are shown, where a good uniformity is noted.

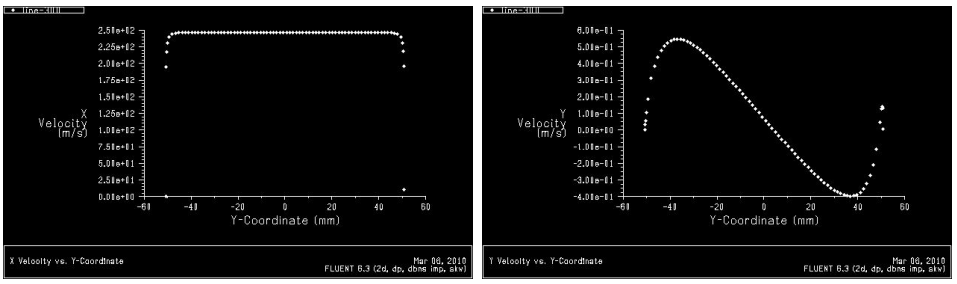

(a) V_x. (b) V_y.

Figure 2.24: Velocity components at the second contraction exit.

2.3.5 Test section

The comparison with other wind tunnels and the requirement of a small facility have led to a choice of a cross sectional area of $4''$ by $4''$ and a test section length of 750 mm. All the other choices concerning the design are related to the comfort in doing the tests.

From this point of view, the sides of the test section were designed to be easily removed in order to be accessed more readily. The windows were chosen to be as wide as possible to enable easier visual measurement (i.e. Schlieren measurements) and to see the whole test section. In this sense it is clearer the choice for a square section instead of a circular test section. The relatively small dimensions makes the problem of the strength of the glass not too limitative: 1 cm thick optic glass was used[11]. Moreover the windows are made so that it is possible to have visual access $2''$ below the proper test section channel as this could be useful, for example, in cavity flow tests. The test section was design to have two chambers above and below where all the measurement devices can be cabled or some pressurization and ventilation system can be mounted. As also mentioned in the introduction, this configuration easily allows the installation of perforated or slotted walls on the test section.

All the walls of the test section can be removed easily and quickly. This is also to reduce the time of the operations between two tests with different configurations. In particular the lower wall is composed by 3 different parts where the central one is a square $4''$x$4''$ where can be shaped into different profiles to be studied.

Both the upper and lower walls can be supplied with instrumentations like pressure tapings or hot films.

[11]Remembering that the during the test the pressure in the test section can easily drop below half atmosphere because the high Mach number.

In particular, the upper wall can be shaped in order to avoid the reflection of the shock wave generated from the bump mounted on the lower wall and to increase the area. In fig. 2.25 the example of the contour of the upper wall is reported. This wall is the one found using CFD in Queen's University of Belfast for an experiment on a bump [17] (this experiment will be described in chapter 3)[12].

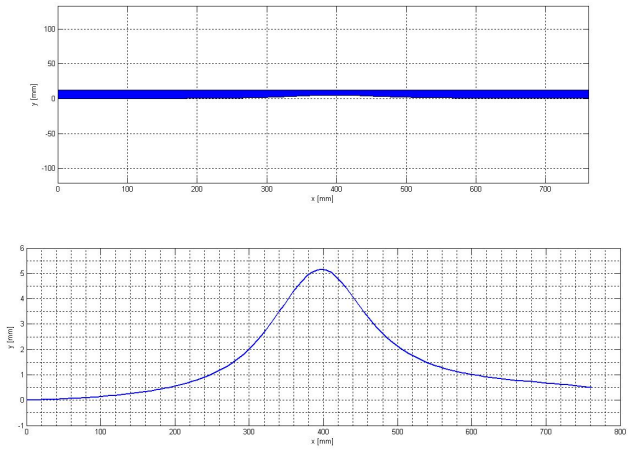

Figure 2.25: Top wall contour.

The changing of the shape of the wall can also let the model be bigger and keep the minimum section at the choke.

The necessary sealing for all the test section is achieved by rubber in grooves along the top and bottom walls, and all the support of the side frame where the windows is mounted.

Another problem to be taken into account is the stress due to the difference of pressure between the test section and the rooms underneath and overlying it during the tests. It can be easily estimated using the isentropic equation (2.14) a difference of pressure of around 35000 Pa for a value of $M = 0.8$ that there will be. A common way to avoid this stress is to provide slots in the test section (typically at the end) or to equalize the pressure of the external chambers with a certain section of the diffuser with a pipe or a hole. Therefore, holes to have access, in terms of pressure regulations, to those two chambers have been made through the choke blocks.

[12]Note that the length is slightly modified in order to fit with this facility.

2.3.6 Choke

The choke has got the smallest area of all the sections of the wind tunnel and as long as the pressure ratio between the vacuum tank and the initial condition[13] is less than the critical value ($P_e/P_i = 0.528$), the Mach number in this section is equal to 1.

Modifying the value of this area, hence the ratio between the choke and the test section area, the air speed of the latter one changes from the theoretical maximum value of 1 (if the areas are the same) to a minimum corresponding to the minimum section area that the choke can supply.

In this facility the choke is composed of a wedge on the lower wall and a slight divergent top wall. When the wedge slides into a different position it changes the corresponding section area. A more detailed discussion of the choke design is found in chapter 4.

It is worth to note that a small change in the choke section area can change significantly the Mach number in the test section. Therefore the choke is a very critical component and needs an accurate design.

2.3.7 Diffuser

The role of the diffuser is to connect the test section (actually in this case the end of the choke) with the vacuum tank where there are static conditions. The need of slowing down the air has to be done with the minimum dissipation of energy. In fact, the actual difference of pressure that guarantees the choking of the wind tunnel is affected by the loss of total pressure in the diffuser.

The shock wave is the mechanism by which most supersonic flows, including those in a wind tunnel, are slowed down[14]. In general, a continuous deceleration from supersonic velocity to subsonic velocity is not possible. When a supersonic flow passes through a shock wave, a loss in total pressure occurs. It is important to note that the losses through the shock wave represent a large portion of the total losses (equivalent to the power requirements) for higher Mach number supersonic tunnel operation. For continuous type, it may represent 90 per cent of the total energy loss [18].

The above considerations have led to the design of different diffusers. From [4] they can be classified in three main geometries. The sketches that follow are for supersonic wind tunnel with convergent-divergent nozzles but again it can be said that the throat corresponds to the choke of the studied wind tunnel and therefore the conclusions can be the same.

- *Simple normal shock diffuser*

[13] This is a very rough approximation because should be taken in account all the losses of pressure (i.e. the settling chamber for the screens and grids, the losses in the test section and in the divergent).

[14] They may also be slowed by friction or cooling.

The simplest practical supersonic diffuser is one in which the test section is followed immediately by a diverging subsonic diffuser as shown in fig. 2.26 and the transition from supersonic to subsonic flow takes place through normal shock waves standing just at the entrance to the subsonic diffuser.

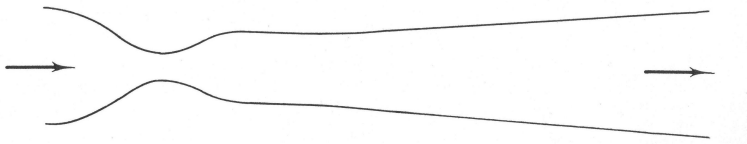

Figure 2.26: Simple normal shock diffuser. [4]

The subsonic flow downstream of the normal shock may, in principle, be decelerated isentropically to the tank pressure.

Experiments show that the flow picture is not as simple as this. The compression occurs through several shocks which extend down into the subsonic diffuser and reacts with the tunnel boundary layer. As a result, a considerably less than normal shock pressure recovery is realized. Furthermore, the angle of the walls plays a very important role in the design.

Transonic diffusers of such a kind could show a multiple shocklets behaviour instead of a weak shock wave as studied in [19].

- *Constant area entry diffuser*

  A considerable improvement in the pressure recovery is obtained with the arrangement in fig. 2.27. Here a long constant area duct is placed between the end of the nozzle and the entry into the subsonic diffuser. In this case the compression occurs through a system of several normal and oblique shock waves in the parallel duct. In such ducts there exists in the subsonic flow, downstream of the shock compression area, a positive velocity gradient which tends to stabilize the boundary layer and reduce separation at the duct walls.

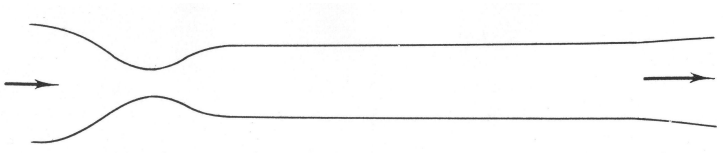

Figure 2.27: Constant area entry diffuser. [4]

As a result the shock wave compression is improved and the performance of the subsonic diffuser also improves. If the parallel duct is long enough (ten times its height or more [4]) this diffuser gives almost normal shock pressure recovery. This diffuser arrangement is useful for Mach numbers up to 2.5.

- *Double throat diffusers*

  At higher Mach numbers than 2.5, more efficient diffusers may be obtained by contracting the duct to form a second throat as shown in fig. 2.28. Diffusers of this kind have a convergent entry section in which appreciable compression is achieved at supersonic speeds through an oblique shock wave system. The final compression, to subsonic speed, occurs by means of shock compressions of the type discussed above near the diffuser throat on its downstream side.

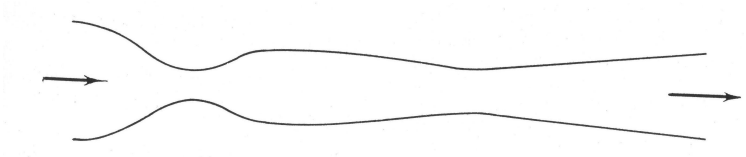

Figure 2.28: Double throat diffuser. [4]

Now, this kind of diffuser with fixed geometry is generally designed in conjunction with a fixed geometry nozzle which produces flow at a single and fixed Mach number.

In starting a tunnel it is found that, as the pressure ratio across the nozzle is increased, the length of supersonic flow downstream of the nozzle throat increases and a normal shock moves towards the test section. Thus it is clear that the diffuser throat must be large enough to pass the test section mass flow, which has gained entropy in compression through the normal shock which occurs at the test section Mach number. When the stationary flow is established then a shock wave on the second throat at a relative low supersonic Mach number occurs.[15]

If now the diffuser is a variable geometry diffuser, a further contraction of the diffuse throat is possible after the tunnel flow has been established, since it has been found that the pressure ratio needed to maintain the tunnel flow is much smaller than then the pressure ratio needed to establish the tunnel flow. A variable geometry nozzle is shown schematically in fig. 2.29.

[15] A more detailed working of such diffusers can be found for example in [3].

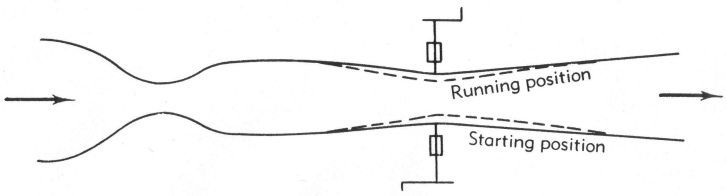

Figure 2.29: Variable double throat diffuser. [4]

> It is clear that the use of a variable geometry diffuser, particularly at high Mach numbers, is highly advantageous. It increases the running time of a blow-down tunnel and decreases the power necessary to run a continuous wind tunnel as compared with a fixed geometry diffuser.

It is important to mention that the considerations above apply only to an empty test section. The interference of a model may have a strong influence on the diffuser and, generally, it may significantly reduce the pressure recovery. Unfortunately models are quite varied in configurations and sizes and the interference effects are very difficult to estimate.

Considering the low supersonic Mach number in this wind tunnel and the relative low shock wave pressure losses, the constant area entry diffuser type was chosen. This arrangement, with a small loss of total pressure, allows a very useful consideration: the constant area duct can infact be slid into the vacuum tank remembering that in this case the length (being ten times of the height and the height $4''$) is slightly greater than one meter. For this arrangement the valve clearly needs to be placed in between the choke chamber and the diffuser.

2.3.8 Valve

Just like the facility described by Munro [20], it could be convenient to use as valve a diaphragm to brake (burn) with a resistance rather than other mechanical or hydraulic valves. This is the typical arrangement of shock tube tunnels or Ludwieg tubes and it is quite easy to design, easy to change, cheap and it has got a simple control system which is very quick (this is very important because for such wind tunnels, the run lasts for only few seconds).

The design could be very elementary: a membrane fixed on a frame that connects the end of the wind tunnel and the vacuum tank. It has been found that a square frame (that fits easier to the end of the diffuser) has big problems of leakages in the corners and a better solution is a round valve with a section comparable to the ending section.

What requires particular attention is the disposition and calibration of the wires and the current that would break the membrane in an optimum

way in terms of quickness, width of the aperture and attention to any release of materials (that would go into the vacuum tank).

2.3.9 Vacuum tank and pump

The volume of vacuum tank is a decisive factor in the run time (see eq. (2.29)). A compromise between the dimensions, the cost and the manageability has lead to the purchase of a cylindrical vacuum tank 3.66 m long, 1.5m in diameter and reinforced with internal rings to avoid implosion; the useable volume is 4.35 m^3.

2.4 Calculation of the run time

With the previous assumptions it is now possible to evaluate the run time. The quantities involved in the formula are:

- $V = 4.35\,\mathrm{m}^3$ volume of the vacuum tank;
- $A = 16\,sq\,\mathrm{in} = 10.32 \times 10^{-3}\,\mathrm{m}^2$ test section area;
- $M = 0.85$ typical test Mach number in the test section;
- $P_i = 1000\,\mathrm{Pa}$ initial pressure in the vacuum tank. Value assumed considering the characteristic of typical vacuum pumps;
- $P^t = 101325\,\mathrm{Pa}$ total pressure of the flow entering in the nozzle. Neglecting the losses in the settling chamber and in the contraction (even if they could be relevant) and not using any feeding tank, the atmospheric pressure is a good approximation;
- $P_e = 0.55 \cdot P^t\,\mathrm{Pa}$ final pressure in the vacuum tank (guessed from theory);
- $\gamma = 1.4$ ratio of specific heats of air;
- $R = 287.05\,\mathrm{J/(Kg \cdot K)}$ specific gas constant;
- $T^t = 293\,\mathrm{K}$ total temperature of the flow (for the same reasons of the total pressure, total temperature could be taken as the atmospheric temperature);
- $n = 1.1$ polytropic coefficient (see note on section 2.2.5);

Hence

$$t = \frac{V}{AM}\frac{P_e}{P^t}\frac{1}{\sqrt{\gamma R T^t}}\left(1+\frac{\gamma-1}{2}M^2\right)^{\frac{(\gamma+1)}{2(\gamma-1)}}\left[1-\left(\frac{P_i}{P_e}\right)^{\frac{1}{n}}\right] = 1.16\,\mathrm{sec}$$

It is now clear that an important aspect in transonic tests with this kind of wind tunnels is the run time, which is very short and so the rest of the system must also be very quick in order to maximize the test (i.e the opening of the valve, the moving mechanism of the choke or other movements in the test section, the data acquisition system etc). It is always possible in this facility to add new tanks and increase therefore way the run time (which is proportional to the tank volume). Note also that the Mach number influence on the run time is very weak; in other terms, as can be seen in eq. (2.24), the flow rate is proportional to the choke area which changes by up to a few percent.

2.5 Overview drafts

The single components were sketched using Solid Edge and in fig. 2.30-2.34 are reported the assemblies of the different modules.

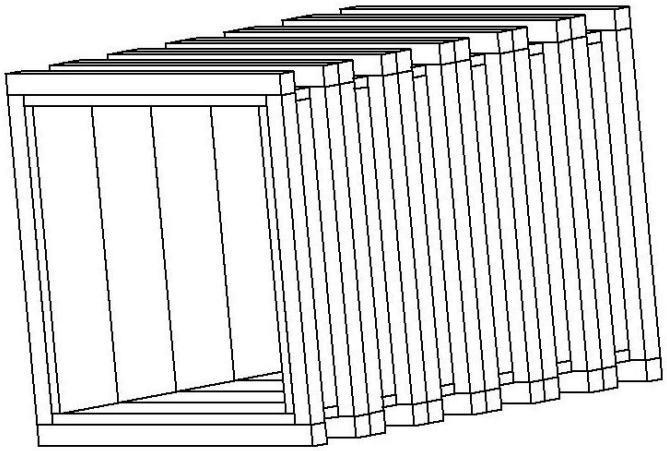

Figure 2.30: Overview of the Settling chamber.

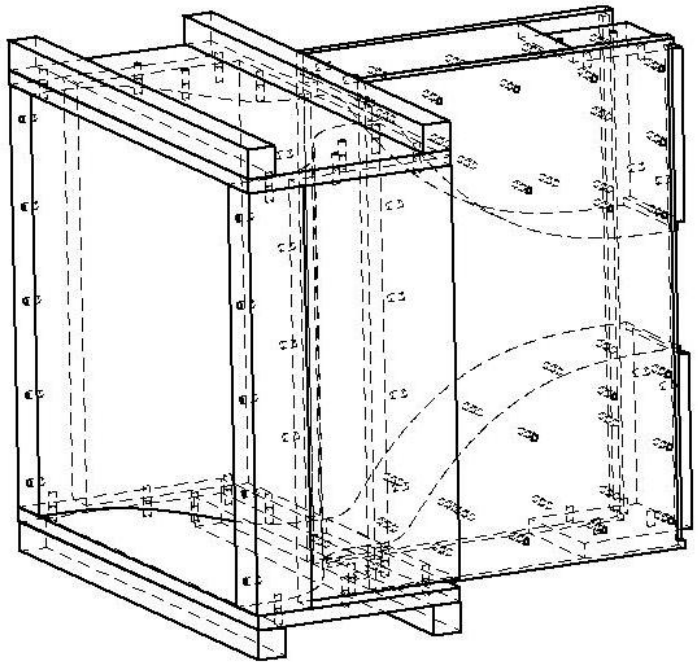

Figure 2.31: Overview of the Contraction.

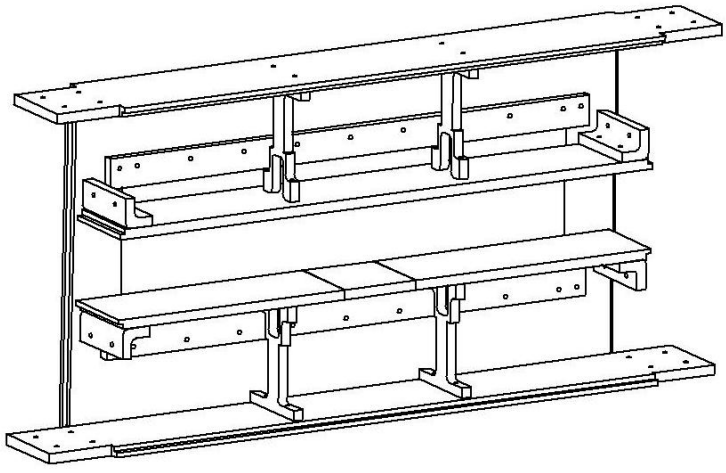

Figure 2.32: Overview of the Test section.

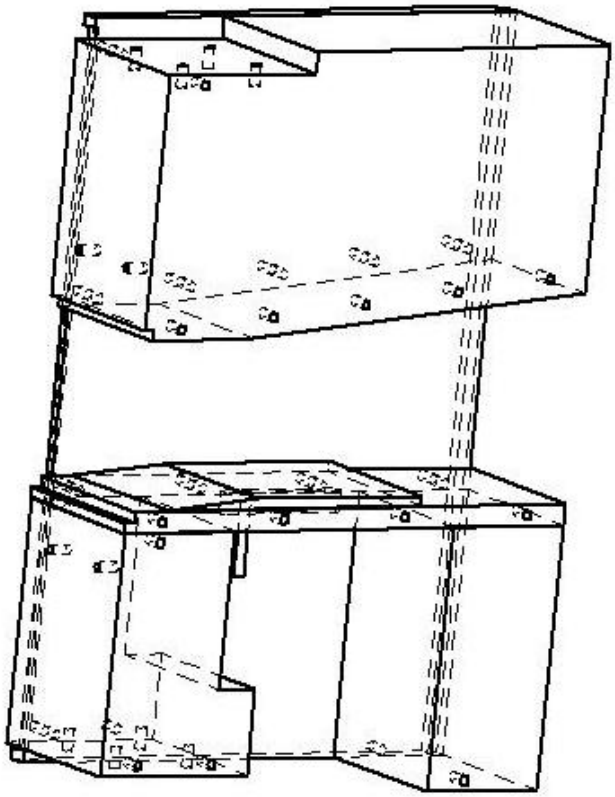

Figure 2.33: Overview of the Choke

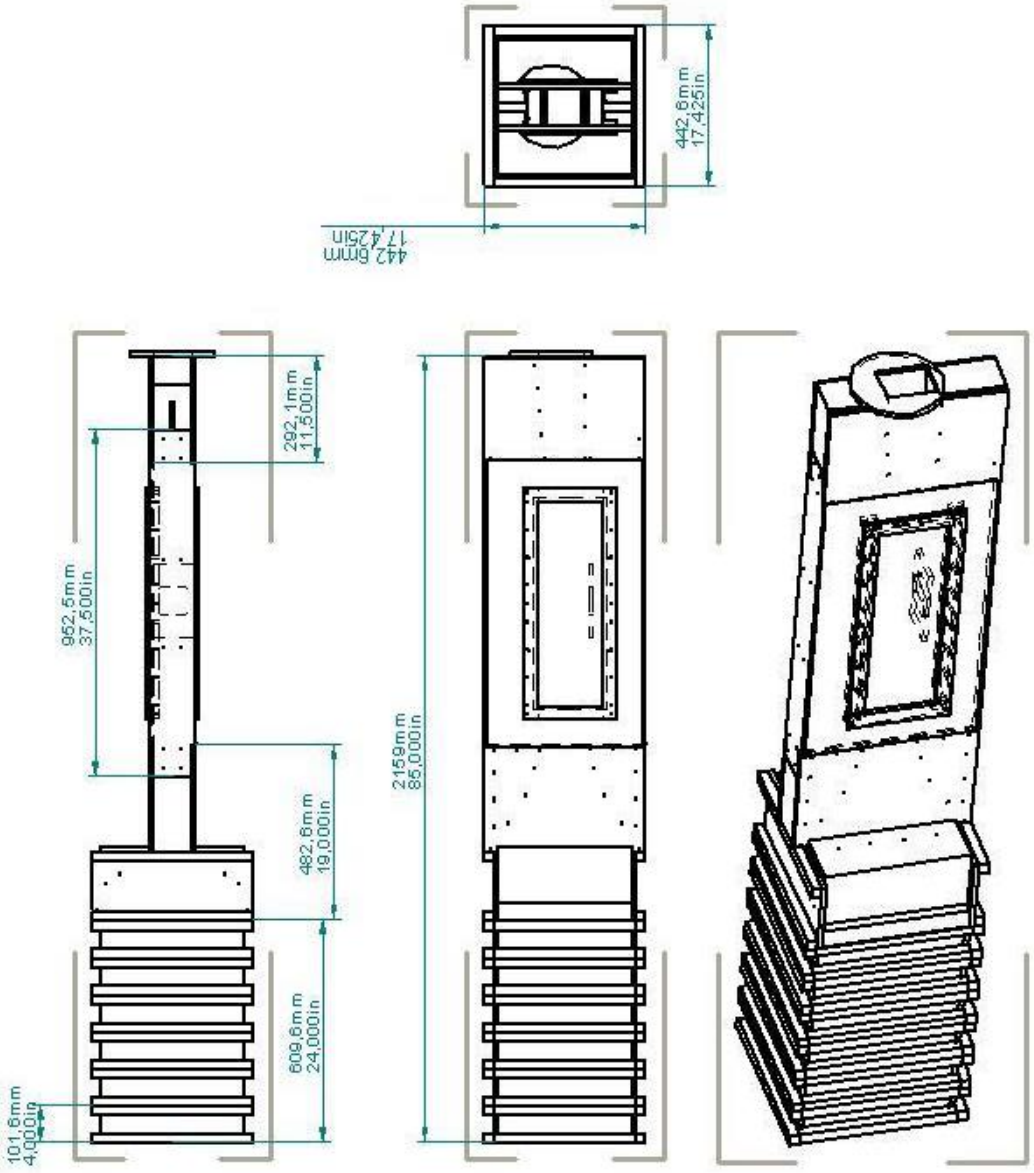

Figure 2.34: Overview of the wind tunnel (Vacuum tank and diffuser omitted; valve only sketched).

Chapter 3

Reference geometry: the bump

Contents

The article *"Investigation of transonic flow over a bump: base flow and control"* [17] describes an experiment over a circular arc bump in the transonic wind tunnel of Queen's University of Belfast. As mentioned earlier, this facility has got the same section area and test chamber length of the wind tunnel designed in this thesis. The article, also supported with numerical simulations, investigates shock wake/boundary layer interactions and proposes a shaped upper wall to achieve a clear transonic interaction.

This easy geometry, which brings to important fluid dynamic features, has been chosen as test case for the CFD validation. Due to the commercial role and the availability, the software used for this study is Fluent. The

simulations have been carried out in a 2D geometry of the designed wind tunnel from the second part of the convergent to the end of the diffuser with the bump and the shaped upper wall. This region is the part that can be described as mainly twodimensional flow; anyway, the not 2D effects will be discussed.

It is also worth to cite a recent article by Konig et al. [21] where similar bumps are used to control the shock position on a transonic airfoil. This study brings to interesting results in terms of reduction of the drag.

This chapter will describe firstly the cited experiments, then a twodimensional CFD model on Fluent will be introduced and validated and next it will present a comparison between the results of the experimental tests and the results obtained by the CFD simulations. The last section will discuss the results in order to test and understand the limits and the trustworthiness of the numerical model adopted.

3.1 Part A: Belfast experiments

3.1.1 Belfast experiment description and experimental technique used

The overview of the Belfast facility is shown in the figure 3.1. It is an indraft wind tunnel with a threedimensional solely convergent contraction (the tank is not shown in the picture). The test Mach number is therefore below the sonic condition and regulated through a translational wedge choke at the end of the test section. The test section (in fig. 3.2) has the same dimensions of

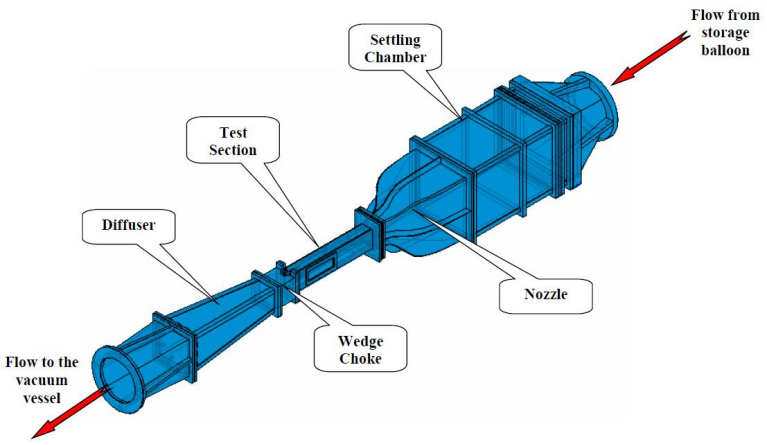

Figure 3.1: QUB Wind tunnel. [17]

the one described in this thesis that is $4''$ by $4''$. A circular arc bump of 9.1 mm high, $4''$ long and $4''$ wide (the whole test section width) is mounted in

the middle of the test section. A contoured top wall, shown earlier in fig. 2.25, is also mounted. Its design is computed with the method of Amecke [22].

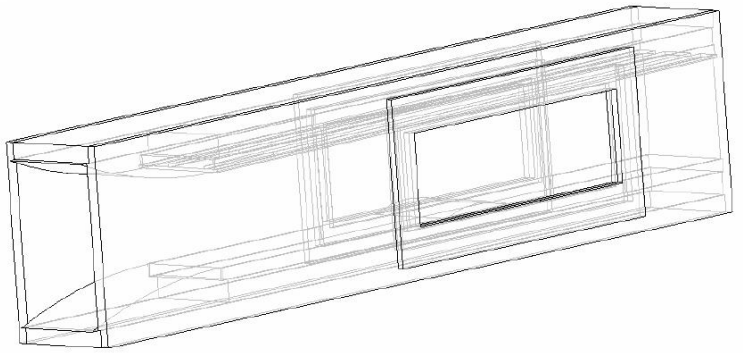

Figure 3.2: QUB Test Section. [17]

In figure 3.3 the main features of this flow are visualized: a supersonic bubble lives on the bump and terminates with a curved shock; in correspondence of the shock the boundary layer detaches and reattaches downstream the bump.

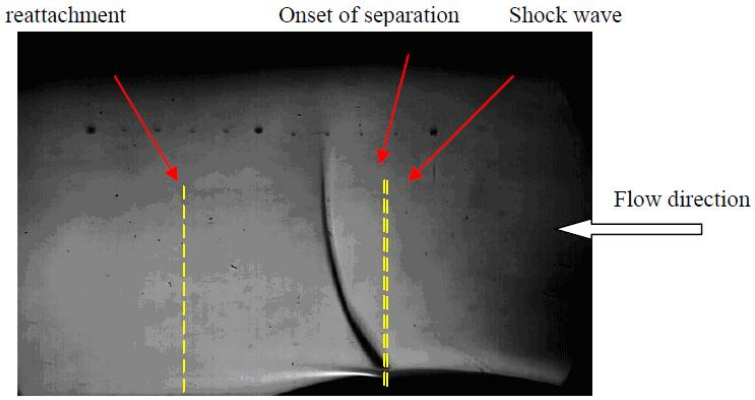

Figure 3.3: Schlieren visualization of the shock. [17]

The study has been carried out using different experimental techniques such as china clay flow visualization, Schlieren flow visualization, wall static pressure tappings and piezoresistive pressure sensors along the centre line. Moreover, results have also been obtained by a CFD solver in 2D geometry using RANS equation and SST $k\omega$ turbulence model. A second numerical step was the 3D configuration solved firstly by RANS equations and then by LES.

3.1.2 Presentation of the experimental results

The main features of this flow can now be presented in a schematic table (tab. 3.1) which highlights the mean values taken in the middle plane of the test section. There are reported the upstream Mach number M_∞, the shock Mach number M_S (the maximum in the test section), the shock wave position x_{shock} (adimensionalized by the chord of the bump) as well as the separation point of the boundary layer $x_{separation}$ and its reattachment $x_{reattachment}$. It is also notable a difference between china and Schlieren visualizations in the measures of the positions.

M_∞	0.783
M_S	1.365
x_{shock}	0.60-0.62
$x_{separation}$	0.63-0.64
$x_{reattachment}$	1.32-1.40

Table 3.1: QUB test main results.

The other important aspect to be mentioned is the effect of the threedimensionality due to the side walls.[1] A china clay flow visualization is shown in figure 3.4 and it clearly points out the shock wave position, the separation and the reattachment of the boundary layer.

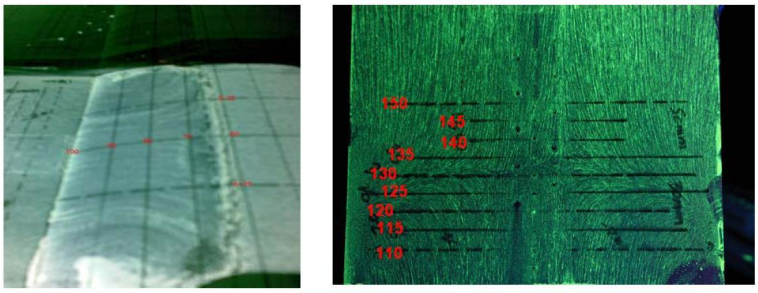

Figure 3.4: China clay visualization on the bump and downstream the bump. [17]

Wall corner vortices are formed behind the shock wave and the size of each vortex is approximately 35% of the bump spanwise length. As a result, a twodimensional flow region is formed around the centerline of the bump covering about ±15% of its span. So, the effect of side tunnel walls is a restriction of the flow that results in a subsequent supervelocity in

[1] The effect of the upper wall, as discussed, is well compensated with the contoured shape.

the middle plane. This extends the separation region downstream and the reattachment is therefore well after the trailing edge of the bump.

Figures 3.5 and 3.6 present plots obtained through the CFD simulations and highlight the mentioned 3D effects.

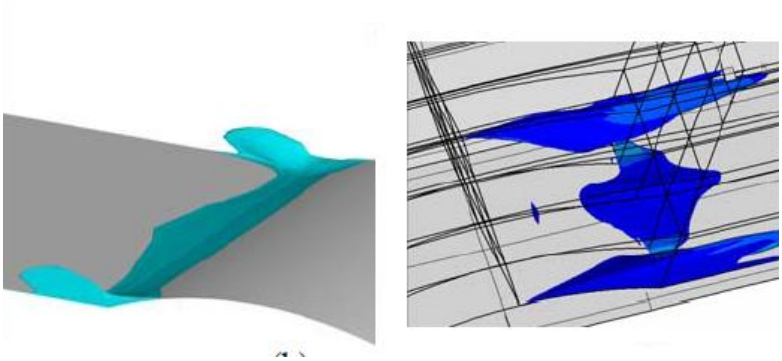

(a) Separated flow. (b) Isosurface of zero velocity.

Figure 3.5: Separation behind the bump. [17]

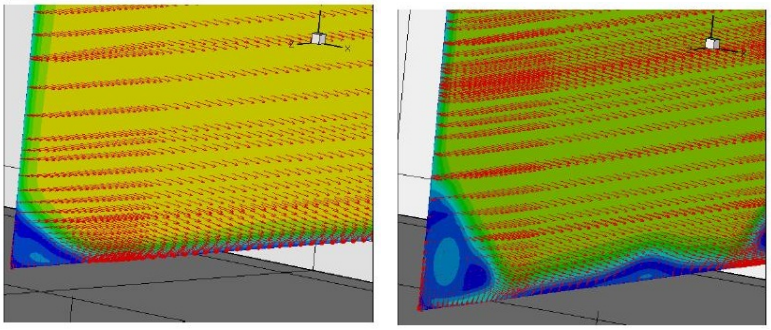

(a) Before the bump. (b) At the beginning of the separated flow region.

Figure 3.6: Development of the separated flow region in the streamwise direction; contours of Mach number. [17]

3.2 Part B: CFD model for tunnel design

3.2.1 Use of the CFD tool to discuss the main flow features

The requiring of panoramic and parametric simulations, the available computational and time resources, the level of representation required at this stage of the design has led to the choice of a twodimensional stationary RANS simulation based on Fluent.

The questions at this point so should be: what kind of data is it possible to obtain with such tools? How much reliable are these solutions?

Even before entering in the discussion of the capability of the software it is obvious to ascertain that, being the flow dominated by threedimensional effects, a twodimensional simulation can not accurately catch the real behaviour. In particular, there will not be that supervelocity due to the corners separation and the 2D code will intuitively bring to a lower upstream Mach number than in the experiments and, again intuitively, the shock wave will retard its formation and will show a lower shock Mach number.

The computed geometry is from the second part of the contraction to the straight diffuser of the designed wind tunnel including the bump and the shaped wall as shown in fig. 3.7.

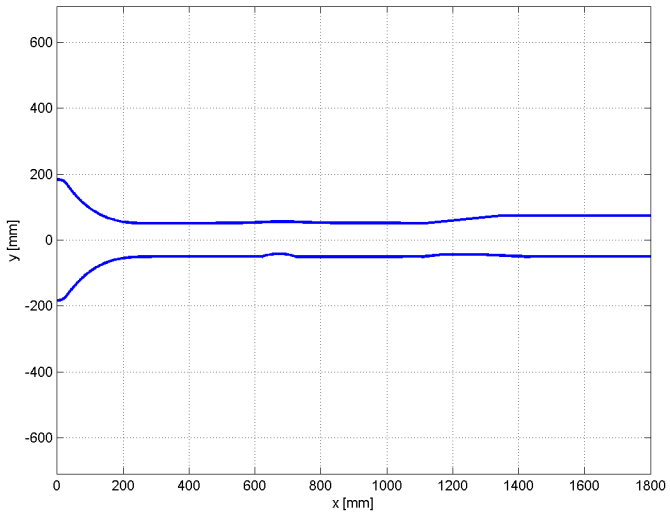

Figure 3.7: Computed wind tunnel geometry.

The same dimensions of the test section with the Belfast experiment, the fact that the choke is far away from the bump and so the contraction, the use of the same environmental conditions allow to say that the use of this geometry for the validation of the CFD model is a sufficiently good choice.

3.2.2 Identification of the models and procedure adopted for the simulations

Looking at the QUB CFD simulations done in parallel with the experimental tests [17], comparing the Fluent manual [2] and Wilcox [23], the turbulence model selected for these simulations is the $k\omega$ in its standard formulation with the incorporation of compressibility effects and shear flow spreading.

This model can predict free shear flow spreading rates that are in close agreement with measurements for far wakes, mixing layers, and plane, round, and radial jets and is thus applicable to wall bounded flows and free shear flows. It predicts also quite well adverse pressure gradient flows, airfoils and transonic shock waves.

In tab. 3.2 are reported the data for the identification of the input parameters required by Fluent where the turbulent intensity is the measured value in the QUB wind tunnel and is defined as the ratio of the root mean square of the velocity fluctuations to the mean flow velocity.

Turbulent model	standard $k\omega$
Turbulent intensity	0.35%
Hydraulic diameter	101.6 mm

Table 3.2: CFD turbulent model.

The final flow simulations residuals are 1e-05 with a discretization method that is *second order upwind*.

The inlet and the outlet pressures are respectively set the atmospheric condition and 0 Pa. Even if this the latter value is not fixed during the test but increases, the flow behaviour in the test section is guaranteed by the choked conditions and the stationary assumption is so valid.

The fluid is described by ideal gas equations with piecewise linear viscosity due the high range of temperature encountered in a flow with shock waves.

3.2.3 Grid convergence

To ensure a gird independent solution, simulations using different meshes have been carried out. Fig. 3.8 shows the subsonic velocity contours using uniform meshes with increasing number of cells[2]. In these plots the convergent and the diffuser have been cut out.

The fig. 3.9(a) shows the influence of the grid with reference to the Mach number in the test section, the position of the shock wave on the bump and the shock Mach number for a wedge choke at a position of $x = 25.4\,\text{mm}$. It is also reported the value of the ratio between the minimum pressure at the wall, corresponding to the maximum velocity position, and the initial total pressure (1 atm).

Besides, fig. 3.9(b) shows the pressure distribution across the shock computed with the different grids. The minimum pressure decreases when the grid cells become smaller. This is also caused by the position of the first point out the surface that, in coarser meshes, is farer from the wall.

[2]The flow, as it will be for all the following figures, is from left to right.

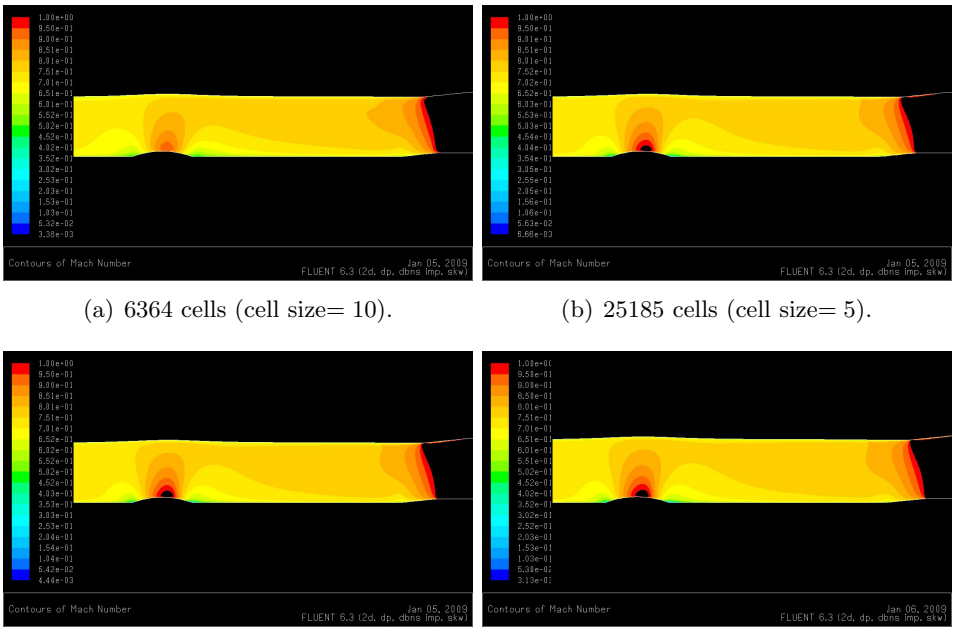

(a) 6364 cells (cell size= 10).

(b) 25185 cells (cell size= 5).

(c) 51975 cells (cell size= 3.5).

(d) 102165 cells (cell size= 2.5).

Figure 3.8: Subsonic velocity contours for different meshes.

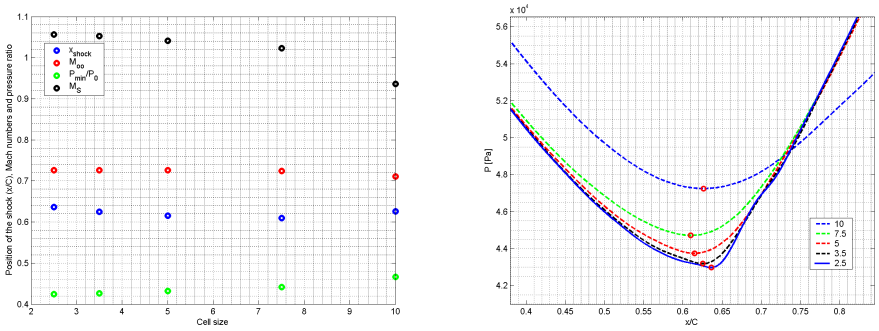

(a) Shock features

(b) Wall static pressure distributions

Figure 3.9: Main flow features using different meshes (choke at 25.4 mm).

3.2.4 Boundary layer treatment

The mesh has been analyzed also in terms of boundary layer treatment. The wall function treatment was chosen and a grid refinement proposed by Fluent was used. This adaptation consists in a succession of halving of the cells close to the walls till an acceptable value of the adimensional wall coordinate y^+ has reached. Fluent manual [2] suggests a value between 30 and 60. The final mesh so obtained is shown in fig. 3.10.

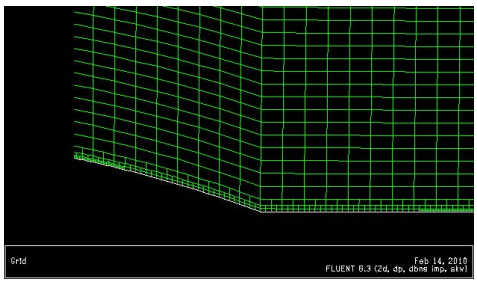

Figure 3.10: Mesh adapted for boundary layer description.

In figure 3.11 the subsonic velocity contours during the different steps of the grid adaptation are shown. In these simulations there was no wedge choke.

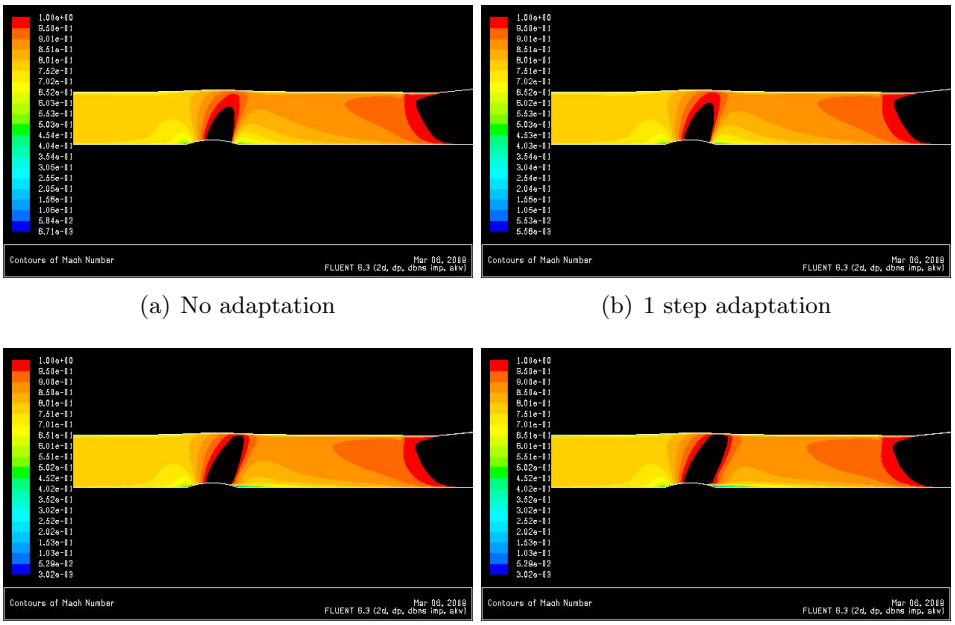

(a) No adaptation (b) 1 step adaptation

(c) 2 step adaptation (d) 3 step adaptation

Figure 3.11: Subsonic velocity contours at different adaptation steps.

The size of the supersonic bubble on the profile increases with the accuracy of the mesh: using the finest mesh the supersonic bubble reaches the upper wall, or better, it reaches the boundary layer of the upper wall. This is a quite interesting effect although fig. 3.12(a) shows that the main flow features do not change so much. Shock position slightly moves upstream and shock Mach number slightly decreases where upstream Mach number and wall pressure remain constant.

Oscillations of pressure in fig. 3.12(b) can be attributed to the very rude

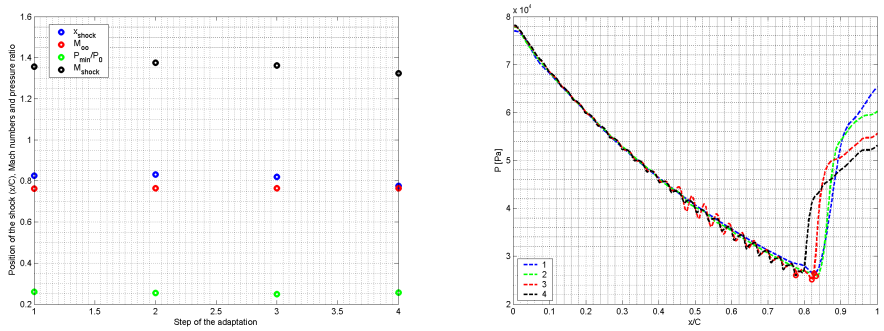

(a) Shock features

(b) Wall static pressure on the bump

Figure 3.12: Main flow featured with reference to the grid adaptation step

boundary layer treatment used; when a finer and graduate change of cells size is used a smoother curve can be expected.

It is also possible to see from the previous analysis that the detachment of the boundary layer caused by the shock, the relative separation region and the reattachment occur and are better described when the mesh on the wall is finer. A zoom on the separation region of the previous figures is shown in fig. 3.13. Better is the resolution on the detached flow, more the separation bubble comes to be longer and more upstream it moves.

Lastly, the velocity vectors of the recirculation on the 3^{rd} adaptation step mesh are shown in fig. 3.14.

3.3 Part C: Presentation of the results

3.3.1 Turbulence intensity

The value of the turbulence intensity used for these simulation is the same used in the described article and calculated in the Belfast wind tunnel. In this section, simulations with different values of turbulence intensity are compared. Figure 3.15 shows the subsonic velocity contours computed with two different turbulence intensities and in fig. 3.16 the main flow features behaviour changing the turbulence are reported. It has been also tested the laminar case that is the limit to no turbulence although it solves different equations (i.e. Euler equations and not the limit to zero viscosity of Navier-Stokes equations).

It is seen that the turbulent intensity does not play a big role at the exception of a slightly higher shock Mach number for the laminar and the high turbulence case. A value of 0.1% has been chosen for the following simulations.

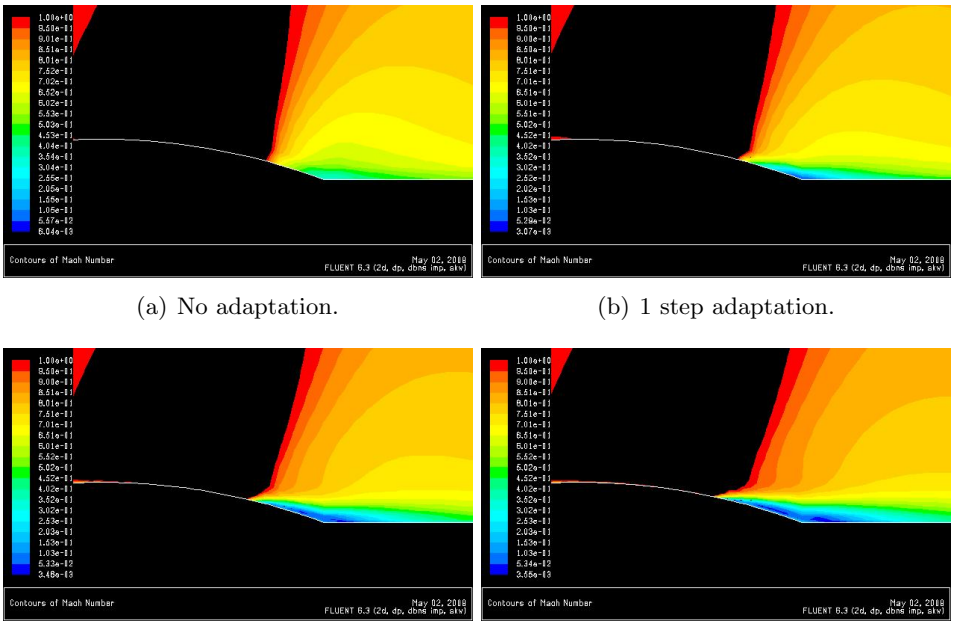

(a) No adaptation.

(b) 1 step adaptation.

(c) 2 step adaptation.

(d) 3 step adaptation.

Figure 3.13: Subsonic velocity contours of the separation region for different adapted meshes.

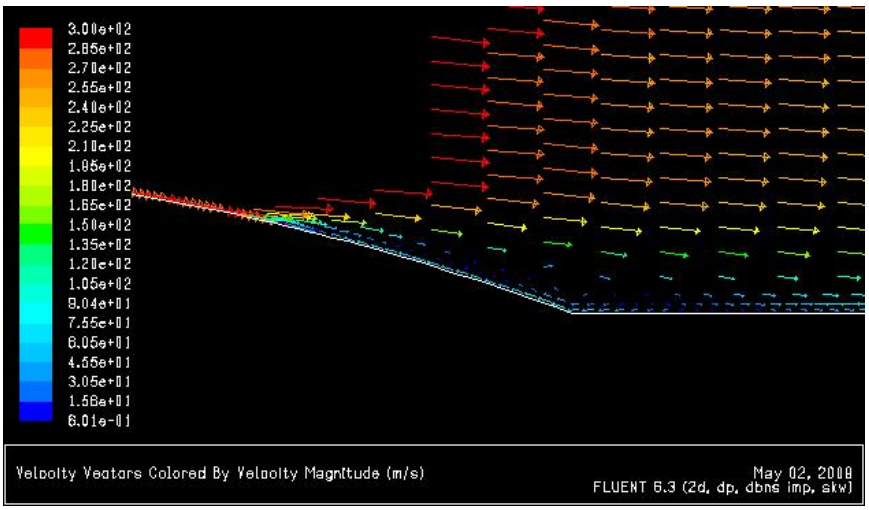

Figure 3.14: Velocity vectors of the separated flow downstream the bump.

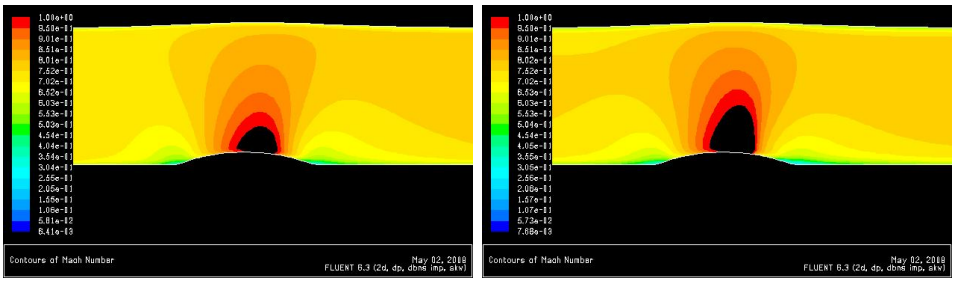

(a) $I = 0.1\%$ (b) $I = 1\%$

Figure 3.15: Subsonic velocity contours for different turbulence intensities

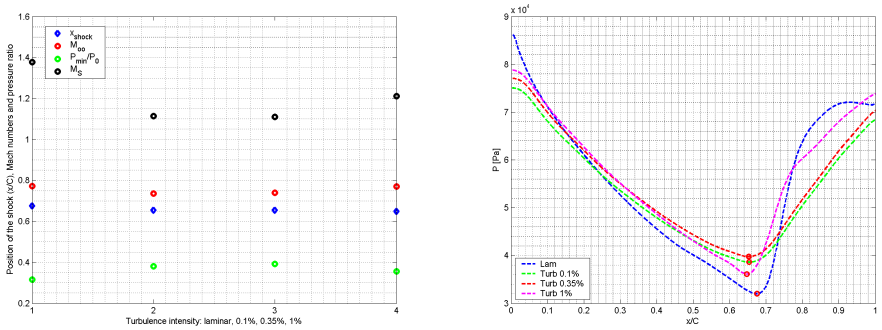

(a) Shock features (b) Wall static pressure distribution

Figure 3.16: Main flow features with reference to turbulence intensities

3.3.2 Position of the choke

It has been chosen as compromise between the time required for the calculations and the goodness of the results, the grid with 25185 cells[3]. The figure 3.17 shows the subsonic velocity contours changing the position of the wedge choke.

In order to find the working point of the choke system that fits better with the Belfast experiments, tests on different position have been carried out. In fig. 3.18(a) is shown the influence of the position of the wedge choke with reference to the Mach number in the test section, the position of the shock wave on the bump and the shock Mach number. It is also reported the value of the ratio between the minimum pressure at the wall and the initial total pressure. Besides, on fig. 3.18(b), the pressure distributions with reference to the position of the wedge choke is plotted. The minimum pressure for each test decreases whit the increment of the position of the

[3]For such solution the total calculation time required for the right convergence and the grid adaptation can be estimated around 10 hours with the available computer.

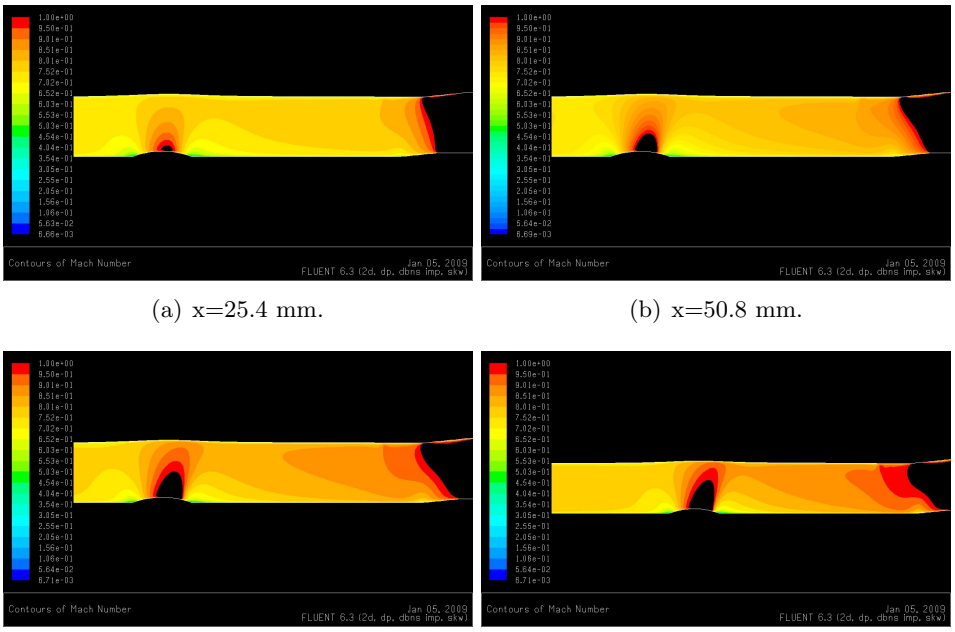

(a) x=25.4 mm. (b) x=50.8 mm.

(c) x=63.5 mm. (d) x=76.2 mm.

Figure 3.17: Subsonic velocity contours for different choke positions.

wedge choke that corresponds to an increment of the nominal Mach number. The simulation plotted in with $x = 87\,\text{mm}$ corresponds to the case without the wedge.

Even if the upstream Mach numbers do not change of big values, the features of the flow sensibly change (i.e. the shock Mach number and the shock position that constantly grow).

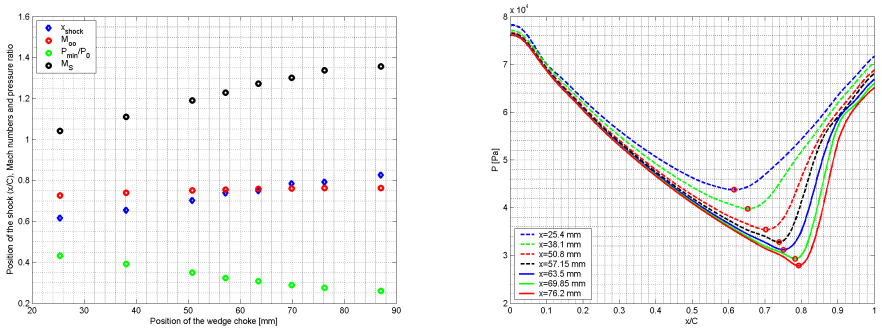

(a) Shock features. (b) Wall pressure distribution.

Figure 3.18: Main flow features with reference to the choke position.

3.4 Part D: Discussion of the results

3.4.1 Performance and reliability of the CFD model

The turbulence intensity does not change drastically the shock features. Except for the shock Mach number in the laminar case, the other values are overall the same among the simulations. As can be noted in fig. 3.15, even the separation bubble size is not so affected by these levels of turbulence.

The results of the described CFD simulations on Fluent are now added to the table 3.1. The two cases selected are at choke positions of $x = 25.4\,\text{mm}$ and $x = 76.2\,\text{mm}$ because they match the most the results obtained in Belfast.

	QUB	CFD	
x[mm]	\	25.4	76.2
M_∞	0.783	0.724	0.761
M_S	1.365	1.041	1.337
x_{shock}	0.60-0.62	0.615	0.792

Table 3.3: Comparison between QUB experiments and Fluent simulations.

As it can also be noted in fig. 3.14 or figs. 3.17, and as discussed in relation to the figures 3.13, the computed separation and reattachment points are very different from the experimented ones. In particular, the computed separated regions start at the feet of the shock and are much smaller then the bubbles observed in the experiments which end farer from the bump.

The first case reported in table 3.3 shows that for, a position of the shock on the bump close to the one in the experiment, the upstream Mach number and the shock Mach number are instead much smaller then the experiments. In reverse, with comparable values of the Mach numbers between the experiments and the CFD simulations (the maximum got in these simulations), the position of the shock in the latter one is more downstream.

These results follow the intuitions got on the behaviour of the shock and the separation region in relation to the threedimensional features observed in the experiments. Because of the separation bubbles formed in the corner, a higher velocity on the bump is observed with a consequent increasing of the shock Mach number and the separation bubble length.

Due the strong threedimensional effects, CFD simulations limited to the two dimensions can not give the same results. The cost in time and computational resources of a higher resolution CFD simulation has been evaluated too high in this design phase. However, CFD simulations as described earlier have been evaluated a good qualitative tool for further considerations on the design, especially on the choke.

Chapter 4

Mach regulation system: the choke

Contents

As already mentioned in section 2.3.6, the choke is a very critical part in designing the wind tunnel and it needs an accurate and precise design itself.

In order to understand better the problem, it is reported again in fig. 4.1 the curve from the eq. (2.18) that relates the sonic section with all the other sections. The use of this figure, knowing the area of the test section, makes possible to relate each Mach number in the test section with a value of area of the choke section.

The problem has now moved therefore in finding a system which allows to modify the choke section area. The control system is an important feature because of the short run time available in this kind of wind tunnels. A quick and accurate control system allows the test to be more efficient in the precision of Mach number tested. Moreover, it gives the possibility to have test with variable Mach numbers.

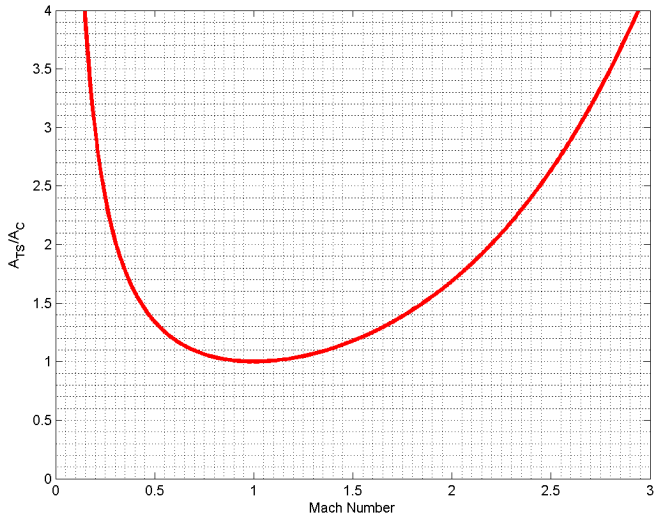

Figure 4.1: Relation between area ratio and Mach number.

4.1 Pro-cons of different choking systems

Firstly, it is important to calculate the amount of the variation of the choke section area. Considering a range of Mach number in the test section of $0.75 < M_{TS} < 1$ (where the minimum corresponds to the minimum choke area and 1 corresponds to a choke area equal to the test section area) it is easy to determine the minimum choke area using the eq. (2.18) where A is the test section area equal to $4'' \times 4'' = 10.32 \times 10^{-3}\,\mathrm{m}^2$:

$$A_C = \frac{A_{TS}}{\frac{1}{M}\left\{\frac{1+[(\gamma-1)/2]M^2}{[(\gamma+1)/2]}\right\}^{\frac{(\gamma+1)}{2(\gamma-1)}}} = 9.72 \times 10^{-3}\,\mathrm{m}^2$$

It is worth to note that the difference between the two areas is small (around 6 percent) that explains itself the delicacy in designing this part of the wind tunnels.

Four different concepts in achieving the described variation of area are here presented and commented.

4.1.1 Wing - rotation (butterfly valve)

A first and elementary system is a wing along the span of the section area which rotates modifying the frontal area that the flow encounters (see fig. 4.2).

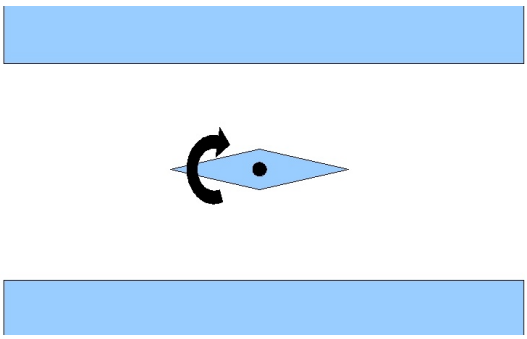

Figure 4.2: Sketch of the rotational wing choking system.

The variation of the Mach number in the test section is so a function of the angle of rotation of the wing (which can be, for example, a simple dihedral wing). The first problem of this solution is the flexibility of the wing due to the necessary small thickness and the use of the wing at an incidence that may conduce to aeroelastic phenomenons. The second problem is the difficulty, also for the previous reason, to have and calibrate an accurate control system.

4.1.2 Wing - translation (plug type valve)

Starting from the problems that occur in the rotational wing choking system, a second solution (conceptual similar to the plug-type variable Mach number nozzle in fig. 1.2) is to use the same wing but with a translational movement system which gradually moves the wing into the proper choke area from a divergent section, as sketched in fig. 4.3.

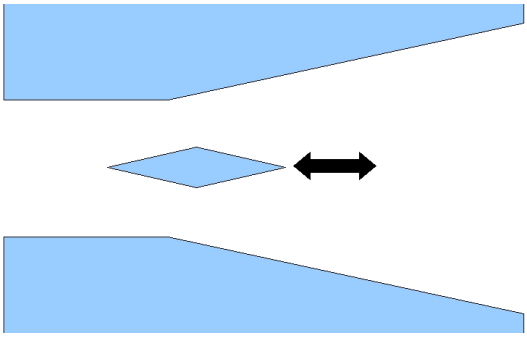

Figure 4.3: Sketch of the translational wing chocking system.

The angle of the wing and the angle of the divergent part are, at the limit, the same in order to maintain the same area after the choked one. The

accuracy of the system is both on the angle (smaller is the angle, higher is the accuracy) and on the accuracy of the moving system (e.g. stepper motor). In this way it is easier to find a compromise between the thickness of the wing and the avoidance of aeroelastic problems (note that, in this system, the wing is at zero incidence).

In order to clarify about the thickness of the wing, the maximum thickness (which brings the minimum Mach number) could be calculated from the choke area in eq. (4.1) and knowing that the wing spans for the whole choke section width:

$$\Delta A = (A_{TS} - A_C) = 0.6 \times 10^{-3}\,\mathrm{m}^2$$
$$\frac{\Delta A}{4''} = 5.9\,\mathrm{mm}$$

That is a thin wing!

4.1.3 Bars

A different concept to decrease the area in the choke section is to have some external "body" which can slide into the choke section (fig. 4.4). This body can be a wing where the movement is now not parallel to the flow but transversal.

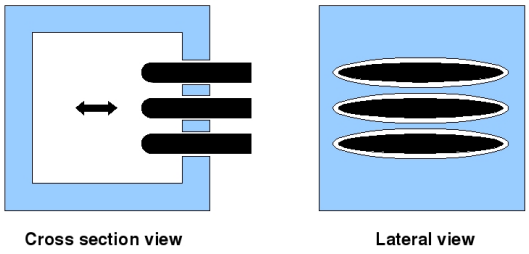

Figure 4.4: Sketch of the bars choking system.

The section of the wing could be a subcritic profile and the use of more than one bar could be also an option. For this case it appears the problems in avoid leakages through the slots.

4.1.4 Membrane

Figure 4.5 shows a different system that consists in a membrane where the shape is function of the difference of pressure between the two faces. The pressure in the choke section can be estimated, as first approximation, from

the critical ratio $P_C = 0.528 \cdot P_i$ so that the choke can be governed as function of the pressure in the external part of the membrane.

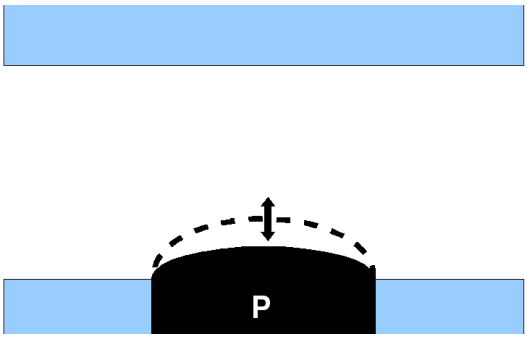

Figure 4.5: Sketch of the membrane choking system

This system is a as innovative as complicated to study. The calibration of this chocking system is a very difficult and demanding task and the variability of the elastic behaviour of the membrane is not negligibly. In fact it changes for oldness and it is also function of the temperature.

Furthermore the pressure on the choke area is affected by what happens in the test section (i.e. loss of pressure by friction and shock waves). To show how the losses can affect, in fig. 4.6 sonic line and the $P = 0.528 \cdot P_i$ line are reported for a simulation using the wedge choke proposed in this thesis and a shock wave generated by the bump in the test section.

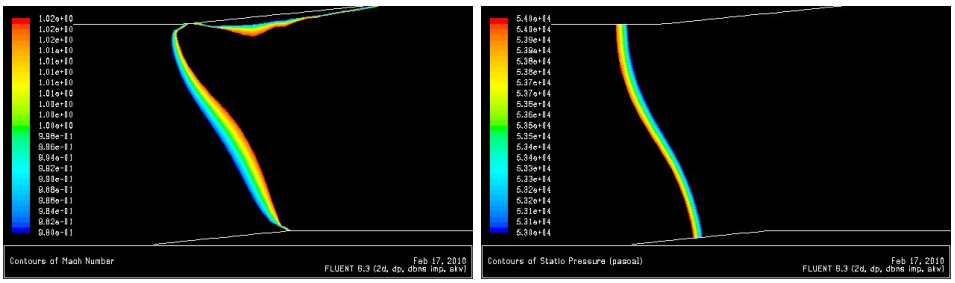

(a) Sonic line. (b) $P = 0.528 \cdot P_i$ line.

Figure 4.6: Test section losses effect on the choke.

The sonic line is, as expected, where the section area is minimum that is at the choke whereas the losses by friction and by the shock wave moves the pressure line upstream. The pressure at the choke section will be therefore lower than the value estimated with the theoretical equation.

4.2 Choke system design procedure

An innovative, but still very simple, compromise of the methods presented earlier is shown in figure 4.7 where the width of the device is the same of the test section that is $4''$. This solution can be seen either as a modified translational wing system (obtained cutting half of the system) or as a modified membrane system where the geometry modification is on the wall. It takes the advantages of both of them without the disadvantages: aeroelastic problems are avoided and high durability is achieved. It is then possible to adopt a wide range of wings of different thicknesses to change the choke functionality (e.g. sensitivity and test section Mach number range). Furthermore, the translational movement, combined with the angles of wing and upper wall, allows to achieve higher accuracy in the control of the Mach number as well as a high repeatability of chocking conditions. The asymmetry of the control system will be seen to do not affect the test section flow.

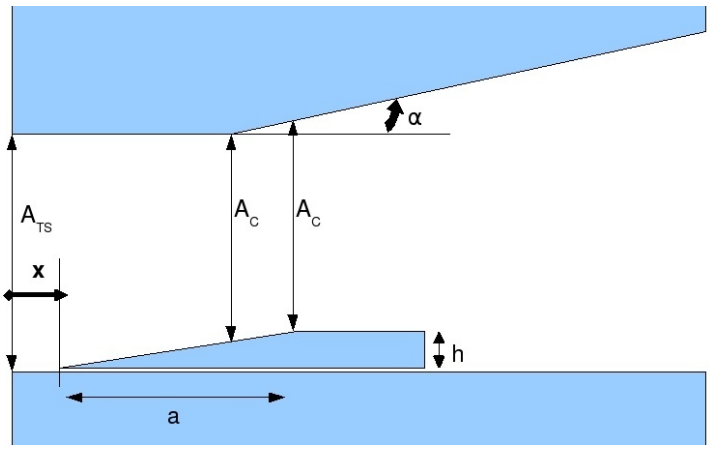

Figure 4.7: Sketch of the choke system

The motor is below the floor of the choke and the slot from where it leads the wing is always covered by the wing itself.

The choke system separates the flow into three regions that are the one that starts from test section area to choke area, the region with constant section (choke area) and the one after the choke section with increasing area which leads then to the diffuser.

The main variables to consider with this configuration of choke are therefore the height h, the length a and the angle α (that is function of the other two variables and is the same for the wing and the upper block). The variable x is the one that regulates the Mach number and with reference to the fig. 4.7, increasing x the test section Mach number increases. For $x = 0$

the nominal Mach number is the minimum one and it is fixed by the choke height h and the volume where the area is equal to A_C is reduced to a single plane. For $x > a$ the interference of the wedge is minimal and the test section Mach number is maximum (in theory equals to 1).

The height fixes the range of Mach number in test section. The sensitivity of the system is dependent to the length and the angle is the one limited by technological, manufacture and stiffness problems. For the latter problem the material of the movable part has been decided to be in steel.

Another aspect to be taken into account regarding the angle is the boundary layer separation. The angle of the upper block, which works as a short divergent, has to be small enough to avoid separations and pressure losses. Some basic experiment from the 50's about the angle influence in convergent-divergent nozzles can be found on the Research Memorandum by Steffes et al. [24]; for conical nozzles, the maximum admissible angles were found around 30^o. Other experiments by the same group [25] show that an excessive high divergent angle cause to unchoke the nozzle at a lower pressure then theoretically expected. Anyway, the requirement of keeping the angle as low as possible ensures the avoiding of separation problems.

For same problems of flow separation and to avoid strong expansion waves, the "trailing edge" of the wedge has been cut at an angle of 45^o, differently from what shown in fig. 4.7. More details on this aspect will be presented in section 4.3.4.

Choosing as compromise of the mentioned reasons a length of $2.5''$, a height of $1/4''$ and a corresponding angle of 5.7^o, the relation between the variable x and the Mach number in the test section is plotted in figure 4.8.

As already mentioned, in order to move the choke the lower part will have a runner and the choke will be linked through a bar to a motor or some other device used to regulate the position x. Hence, other considerations will regard the total length of the movable part to avoid leakages through this hole.

Lastly, it has to be noted that all the previous considerations and plots come from theoretical considerations. A finer calibration and testing of this system has to be carefully accomplished remembering also the intrinsic not linear relation between the choke position and the test section Mach number.

4.3 Results of the CFD simulation

It is interesting now to see how actually the choke works and how far from the theoretical solution it behaves.

CFD simulations using the twodimensional model validated in chapter 3 have been carried out. The simulations have been focused on the sonic lines which determine the choked conditions. Firstly, the same tests with the

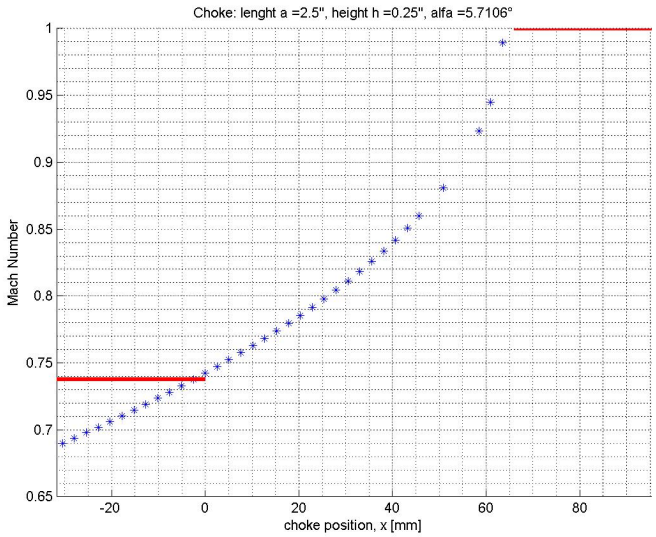

Figure 4.8: Choke variable and Mach number relation.

bump and the shaped upper wall as in chapter 3 are reported here paying attention on the Mach regulation system. Secondly, sonic line results for clean test section (i.e. with straight walls in the test section) are presented.

A comparison between twodimensional CFD simulations and the theoretical description has been also reported along with a discussion on the choke trailing edge.

Lastly, the combination of effects of chocking system and shaped walls in the test section is analyzed showing how the choking system is actually constituted of both the wedge and the test section walls.

4.3.1 Sonic line

In fig. 4.9 are reported the same solutions as in fig. 3.17 with emphasis on the choke and the shapes of the sonic line can particularly be observed. As can be noted from the legend, the contours are for Mach numbers between 0.9 and 1.1 where the green shades are the Mach numbers equal to 1 regions.

The quasi 1D theory used for the eq. (2.18) is based on the fact that at fixed streamwise position the flow conditions are the same that is like to say that the sonic lines are straight and perpendicular to the flow.

What is obvious in these contours is that the sonic lines are not straight but are affected by the boundary layers, the sharp corners and the disuniformity generated by the bump (along with what happens in the test section). In particular it notes that the green region (approximately the sonic line) tends always to born at the sharp corner of the wedge and to end at the

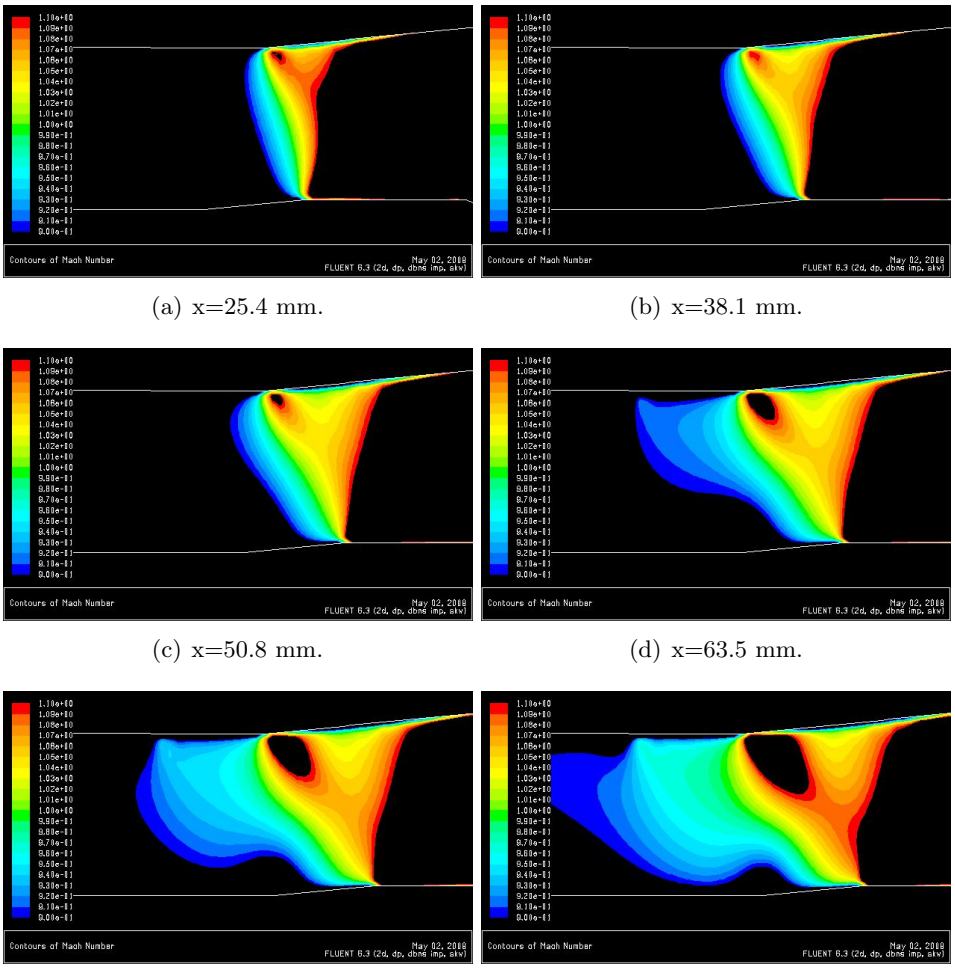

(a) x=25.4 mm. (b) x=38.1 mm.

(c) x=50.8 mm. (d) x=63.5 mm.

(e) x=69.85 mm. (f) x=76.2 mm.

Figure 4.9: Subsonic velocity contours on the choke for different positions.

sharp corner of the top wall and that the trajectory of the sonic line is not straight especially for the last positions.

The imposition of the sonic line vertices on the sharp corners gives a good repeatability and robustness on unsteadiness from the test section.

Furthermore, supersonic bubbles (bigger as the choke slides downstream) are noted; they are generated by the expansion of the flow close to the top wall and they end with a weak shock wave.

Where the downstream flow does not feel so much all these features keeping indeed a quite uniform behaviour, the upstream part, that is what comes from the test section, changes radically moving the choke. This is exactly what the choke is for, to change the flow conditions in the test section. Even if differently from the theoretical quasi 1D behaviour, it appears that the

Mach number upstream the choke increases as the choke slides.

4.3.2 Sonic line in clean test section

The irregular lines created upstream the sonic lines in the previous data are mainly caused by what happens in the test section (shock wave, flow separations, expansion waves). Therefore, it is comprehensible that also the calibration of the choke is different changing the type of test.

To analyze more in detail this aspect, in fig. 4.10 are reported the sonic lines obtained with an empty test section that is without any bump or shaped wall.

The change in computed domain geometry is small enough to ensure that the conclusions on the model presented in chapter 3 are still valid. In fact, the maximum difference between the shaped wall and the straight wall is less then 6 mm (see fig. 2.25) where the maximum height of the bump is 9.1 mm.

Note that the position of the wedge are not the same as the fig. 4.9. Here it has been tested also a forward choke position ($x = -25.4\,mm$), the $0\,mm$ position and a very far position ($x = 101.6\,\text{mm}$).

It appears also in these simulations that the sonic line (again the green region) vertices are at the sharp corners of the choke. This is a good point as noted also in fig. 4.9 for the repeatability of the test where little changes in the ambient conditions can not affect this fundamental feature which reflects the test section conditions.

The difference between the loaded and the unloaded test section case can be seen, for example, in the $x = 76.2\,\text{mm}$ case where the latter one maintains a good symmetry of the flow in the test section. It is important to note that the asymmetry of the choke geometry does not influence the flow upstream farer then a wedge length.

It is in some way encouraging to see the sonic line shape for the $x = 0\,\text{mm}$ case fully reflecting the theory in terms of shape and boundary layer interaction that can be found, for example, in the book by Sabetta [1].

4.3.3 Comparison with theoretical description

An important step is now to compare the theoretical behavior of the choke shown in fig. 4.8 with the computed one. To do so, the test section has been described by straight walls without bump and contoured ceiling.

The Mach number in the test section, at a location where the bump was mounted, with reference to the position of the choke is shown in fig. 4.11 and the relative Mach number on the mean line of the test section is in fig. 4.12.

Comparing the test section Mach number between the bump case (fig. 3.18) and the clean case (fig. 4.11) it is clear the big difference in the working

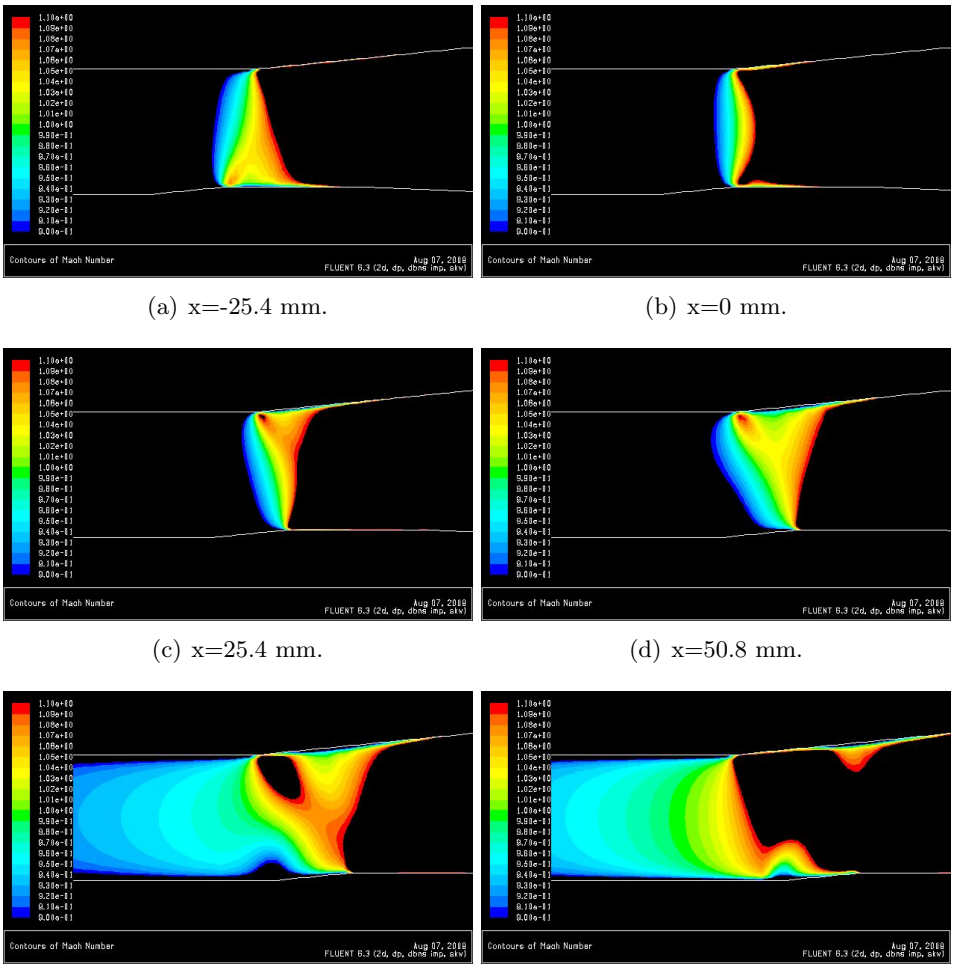

(a) x=-25.4 mm. (b) x=0 mm.

(c) x=25.4 mm. (d) x=50.8 mm.

(e) x=76.2 mm. (f) x=101.6 mm.

Figure 4.10: Subsonic velocity contours on the choke for different positions in empty test section.

of the choke between different load conditions. Where in the bump case the upstream Mach number changed by few percent, the clean case gets closer to the not linear quasi 1D function changing between 0.75 and almost 0.9 the test section Mach number.

The mean line Mach number trends in fig. 4.12 show a positive gradient in the test section that becomes stronger with the increase of the nominal Mach number (i.e. the position of the choke). The main reason for this undesirable behaviour is the growth of the boundary layer on both the walls which operates as a slightly convergent pipe.

With these results, it is more comprehensible the potential request of some mentioned devices like slotted or perforated walls, shaped or inclinable

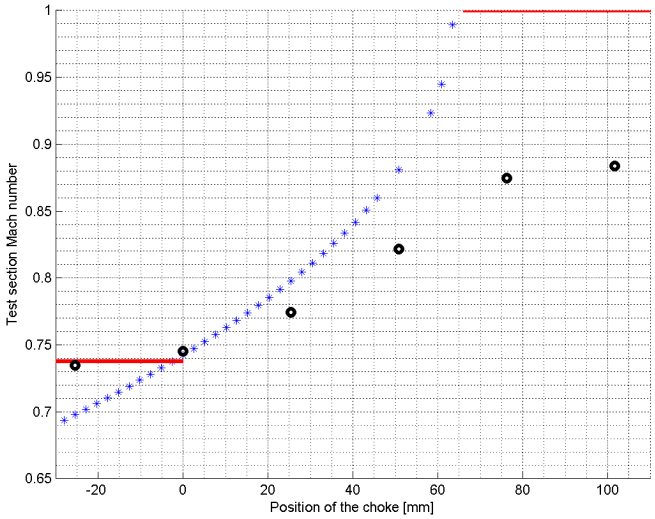

Figure 4.11: Comparison between the theoretical function and the computed solutions.

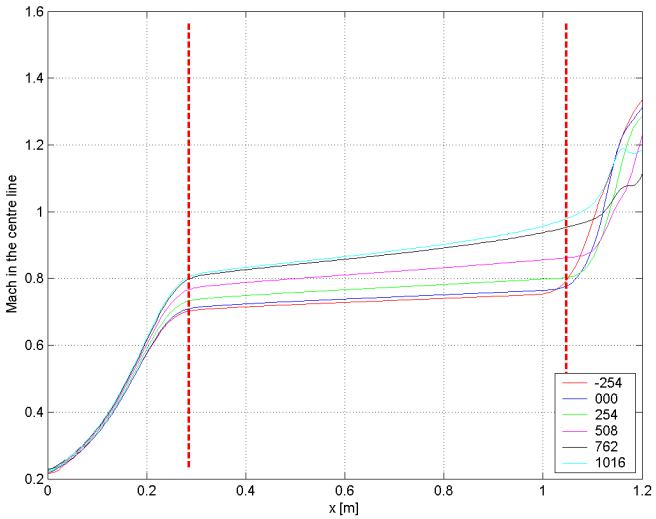

Figure 4.12: Mach number distribution in the test section changing the position of the wedge choke.

walls or even ventilated walls in order to be able to control also this effect.

CFD simulations of these devices are big efforts. Books that give use-

ful qualitative and experimental advices are for example [27] and [4]. As already discussed earlier, the design and application of such devices should be coordinated with the particular test condition. The design by CFD of the top wall shape in Belfast [17] is a good example in this sense.

4.3.4 Changing of the choke trailing edge

A first change on the geometry of the choke comes in order to avoid, or limit, the disturbances generated from the last part which, as presented earlier, finishes quite abruptly with an angle of 45 degrees. Figure 4.13 shows the pressure disturbances for the first wedge choke and a new one with a gentler angle.

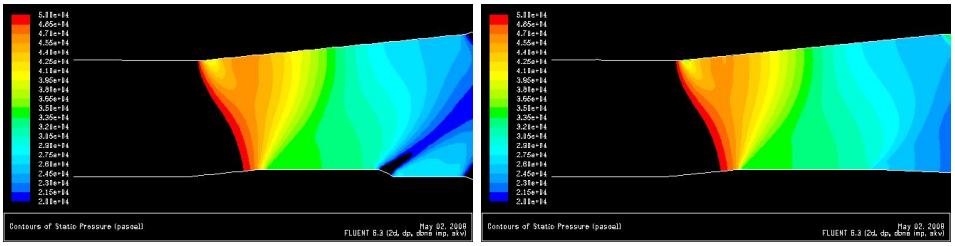

Figure 4.13: Pressure contour for different choke ending shape.

It is clear from these figures how much the ending part of the wedge choke is important to avoid disturbances in expansion waves that would compromise the efforts of the diffusers to keep the slow down of the flow as closer to isentropic as possible.

Therefore a smooth and low slope edge is the best solution and sharp corners in this region have to be avoided.

4.3.5 Shaped walls and choke

Looking at fig. 4.11 it could surprise that the maximum test section Mach number reaches not even 0.9 although the theory claims it should reach the sonic condition. This is again, in another form, the influence of the boundary layer that makes the flow seeing a cross section area smaller then what it really is.

Thus, it is once more explained the need of a combined control of the flow with both the wedge choke and test section wall. Shaping for example the upper wall in order to take into account the thickness of the boundary layer in the test section, is possible to create a constant velocity region with a fixed nearsonic Mach number.

In other words, the shaping of the wall fixes the order and the main distribution of the test section Mach number during the test. The movement

of the choke makes the control finer and gives the possibility of a slow change of the test conditions (see fig. 3.17) or a continuous change during a test.

To emphasize more this aspect, the sonic lines for two cases where the wedge choke is positioned at the same location and the walls in the test section are straight in one case and as in the QUB tests in the other plot, are shown in fig. 4.14.

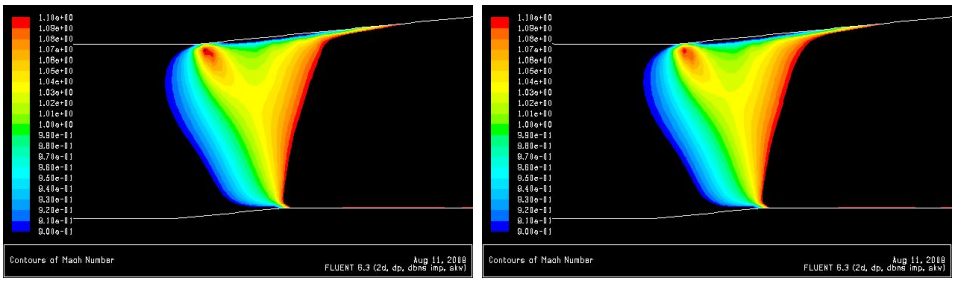

(a) Straight wall. (b) Shaped wall.

Figure 4.14: Sonic lines for $x = 50.8\,\text{mm}$ with different test section upper walls.

It is also reported, in fig. 4.15, the distribution of the Mach number along the test section mean line for the same two cases.

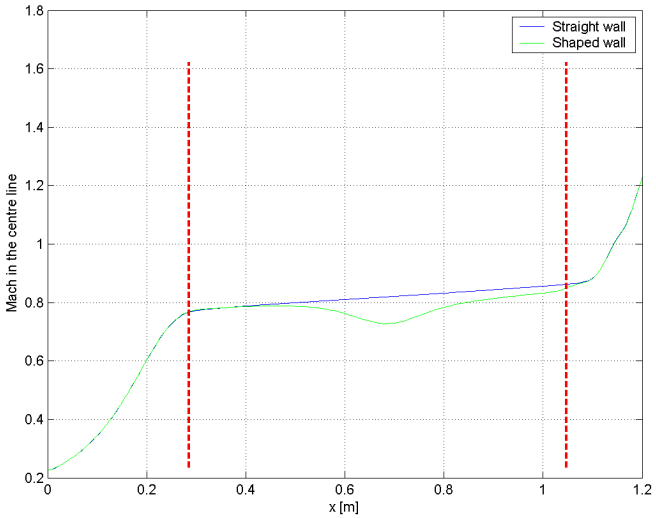

Figure 4.15: Mach number distribution for $x = 50.8\,\text{mm}$ with different test section upper walls.

These figures well visualize how the test section conditions can be strongly changed by the shape of the walls (the upper one in this case) where the

sonic line (that is the choking conditions) is the same (see both the contours and the Mach number distributions at the choke).

The upper wall has therefore the aim to mimic the freestream conditions (i.e. uniform distribution of the velocity) or to set other distributions in conjunction of the particular model and test. It is anyway needed the cross sectional area of the choke to be always the minimum one of the whole wind tunnel.

About the matter on how to design the top wall, what kind of tools are available and which procedures to adopt, it has been already cited the work by Amecke [22] which can be a good starting point. In this Nasa Memorandum, it is illustrated a method for direct calculation of the wall induced interference velocity in two dimensional flows. It applies an one step method that allows shaping the required wall adaptation for interference free flow knowing the wall pressure distribution. Several applications are also reported.

Other references can be found in the bibliography of that article and can be usefully combined with CFD codes in iterative processes with the additional account of boundary layer effects.

Following the simplicity and modularity concept in the design of this facility, the change of the upper wall is a quick task and the need of a new shaped wall each different test is not really a demanding effort.

Chapter 5

Conclusions and future work

The work presented in this thesis has led to an advance stage of the preliminary design of a transonic wind tunnel. Along with a detailed design of the main parts of the wind tunnel, CFD tests have been carried out giving a satisfactory overview of the wind tunnel functioning and a good base for more detailed CFD studies.

A new chocking system for the regulation of the test section Mach number has been proposed and numerical simulations have demonstrated the validity and the accuracy of this design.

A twodimensional numerical model on Fluent have been validated with experimental results leading to the definition of a satisfactory CFD tool to be used for further preliminary analysis. Threedimensionality effects have also been discussed in reference to the experiments on the shock wave/boundary layer interaction on a bump. The limit of the numerical model has been found in a correct detection of the shock Mach number. However, a correct description of the trends of the main features of the flow has been satisfactory achieved.

The validated CFD model has been used for further tests on the new test section Mach number regulation system. Numerical simulations on the particular choke have shown the quality of such arrangement in terms of simplicity and repeatability.

Good agreement with the analytical model has also been achieved by this choke and the not-linear relationship between the test section Mach number and the position of the wedge has been found (see fig. 4.11). The importance of the combination of the wedge and the test section walls has also been highlighted and a test section Mach number range between 0.74 and 0.89 is reached with 110 mm of wedge movement and 6 mm of height.

Further improvements of the proposed wedge choke can be done after experimental results or threedimensional CFD test; a calibration of the chocking system is anyway needed. Moreover, this arrangement gives the possi-

bility to have more then one wedge choke to be used for different purposes (i.e. different Mach ranges or sensitivity changing respectively the height or the angle).

A small wind tunnel (2 m of length and half meter of height and width, excluding the vacuum tank) with a test section area of $4''$ by $4''$ and test section length of 750 mm has been designed.

Pictures of the wind tunnel are reported in the appendix A and some of the sketches are in the appendix B. The main modules have been designed and built when few other parts are still rough sketches and need more work before the possibility to run the wind tunnel: the membrane valve before the tank with the breaking system needs some tests to ensure a good opening; the connection between the choke module and the tank that includes the diffuser/straight tube needs to be assembled; a choice of honeycombs and grids in the settling chamber needs to be done; an accurate choke movement system and control has to be mounted (i.e. step motor).

A visual measurements equipment system and the instrumentation of the test section is also to be designed. The wide windows give visual access on both sides and Schlieren, shadowgraph systems [26] and high speed cameras can be installed. Furthermore the use of pressure tappings, microphones, hot films needs to be thought as part of the particular test and the mounting on the walls or on the model can be easily achieved. The full access of the test section makes all these operations straightforward

Appendix A

Pictures of the wind tunnel

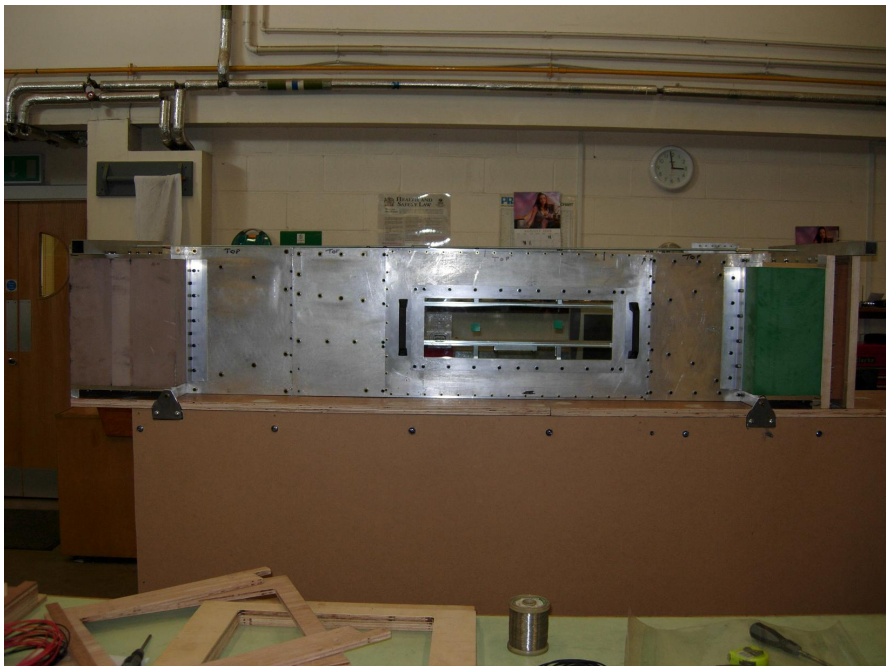

Figure A.1: Wind tunnel assembled (the vacuum tank is missing).

Figure A.2: Wind tunnel from downstream.

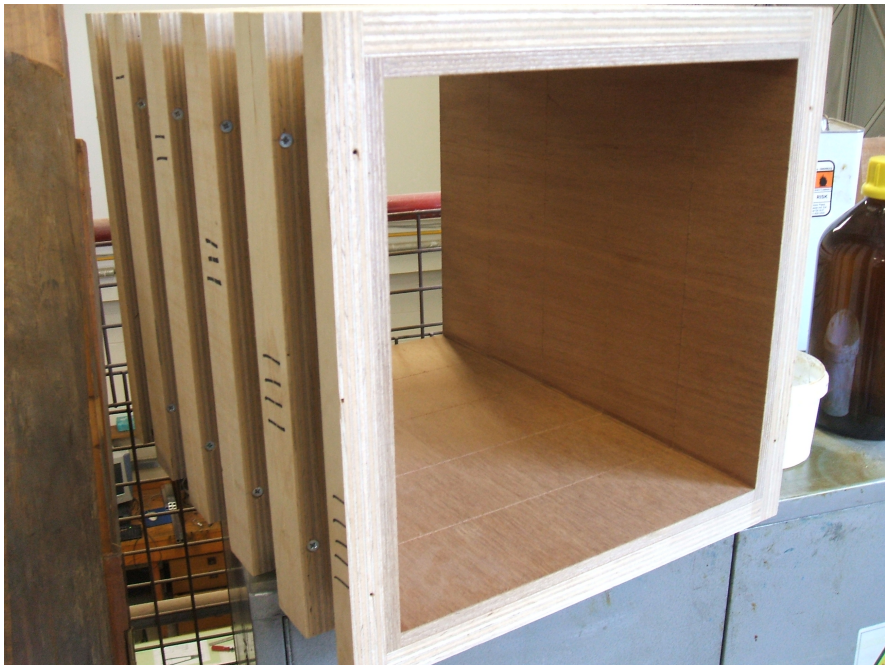

Figure A.3: Settling chamber frames.

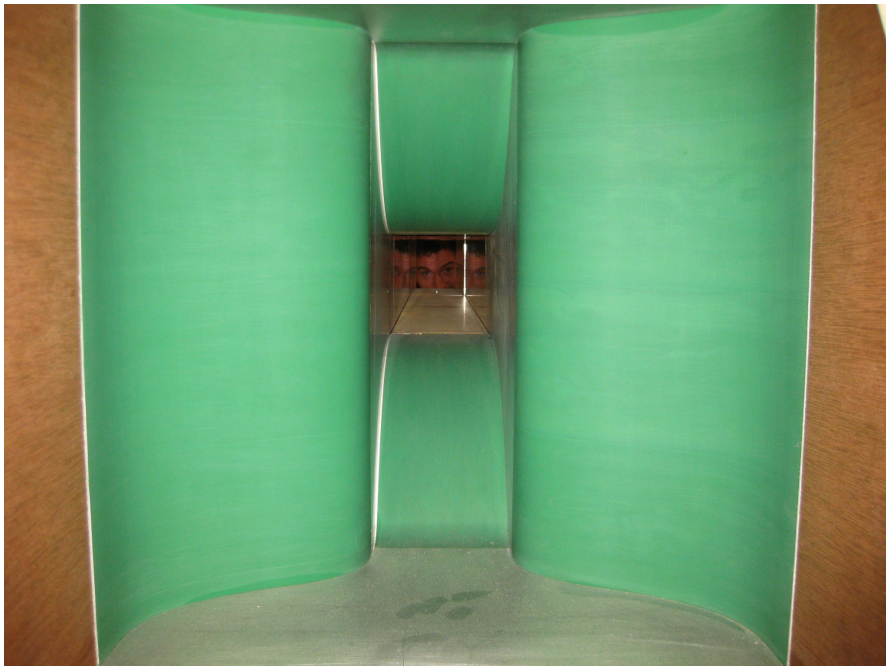

Figure A.4: Contractions.

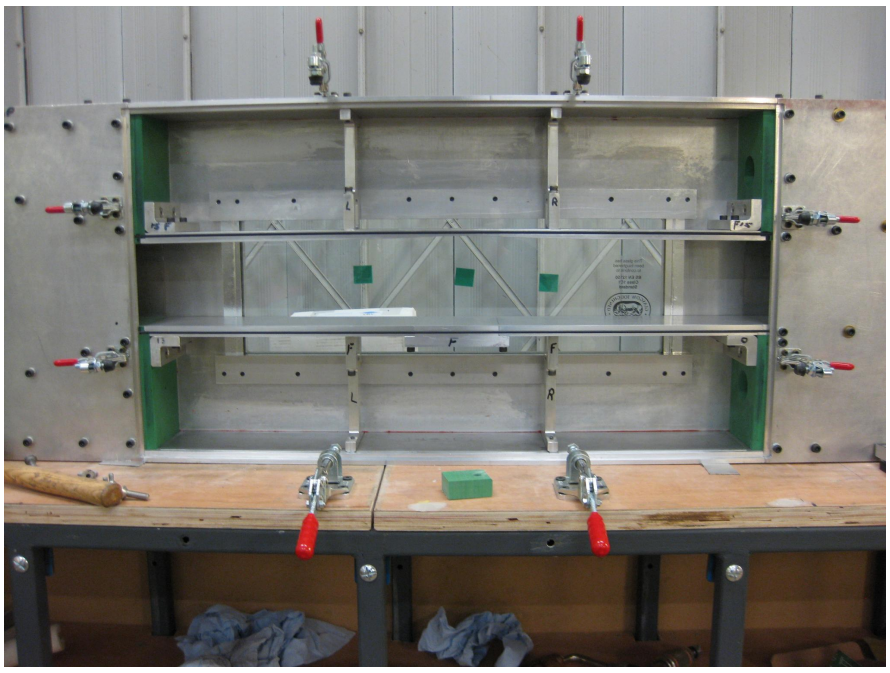

Figure A.5: Test section open 1.

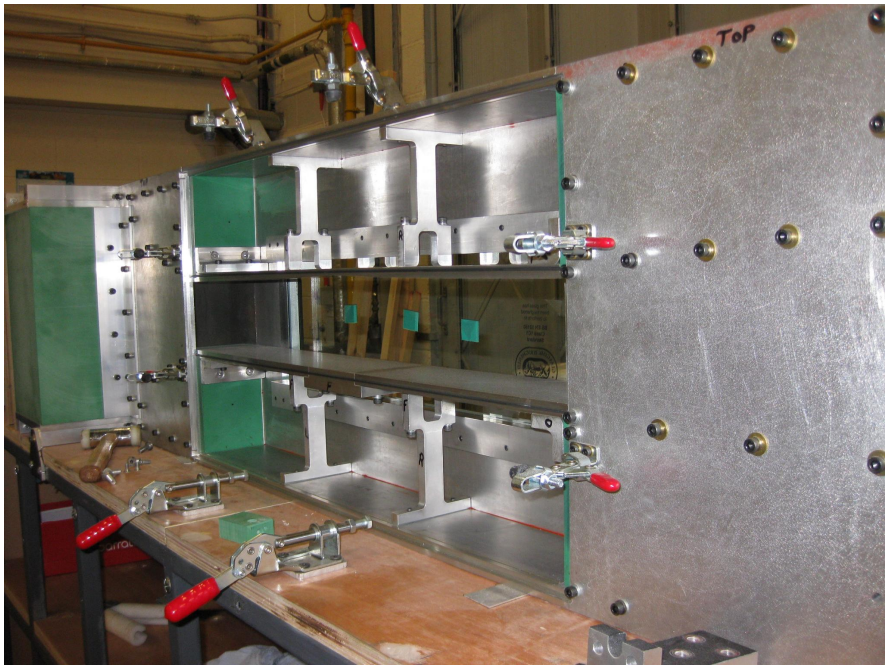

Figure A.6: Test section open 2.

Figure A.7: Choke from below.

Figure A.8: Vacuum tank.

Appendix B

Wind tunnel sketches

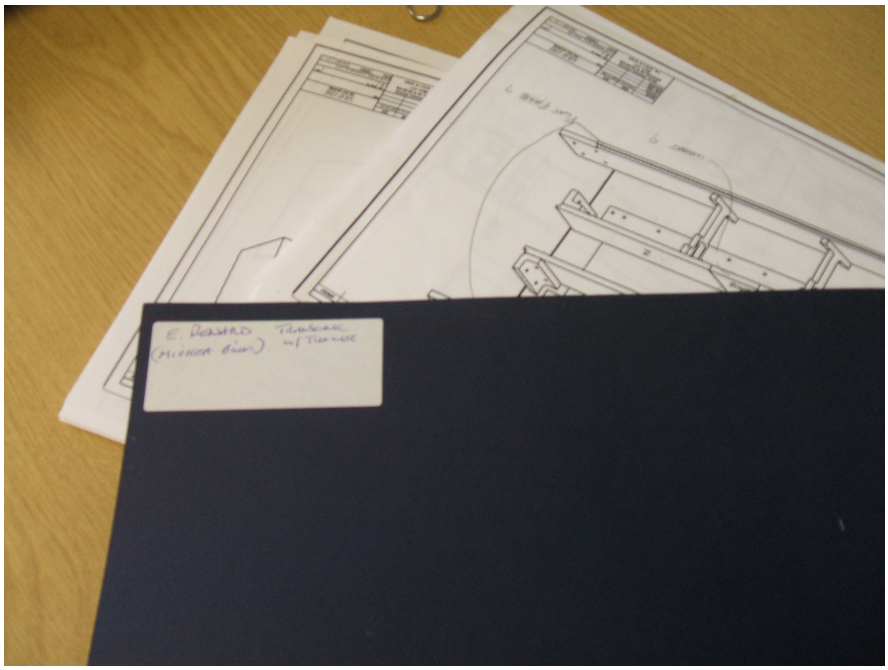

Figure B.1: Sketches folder.

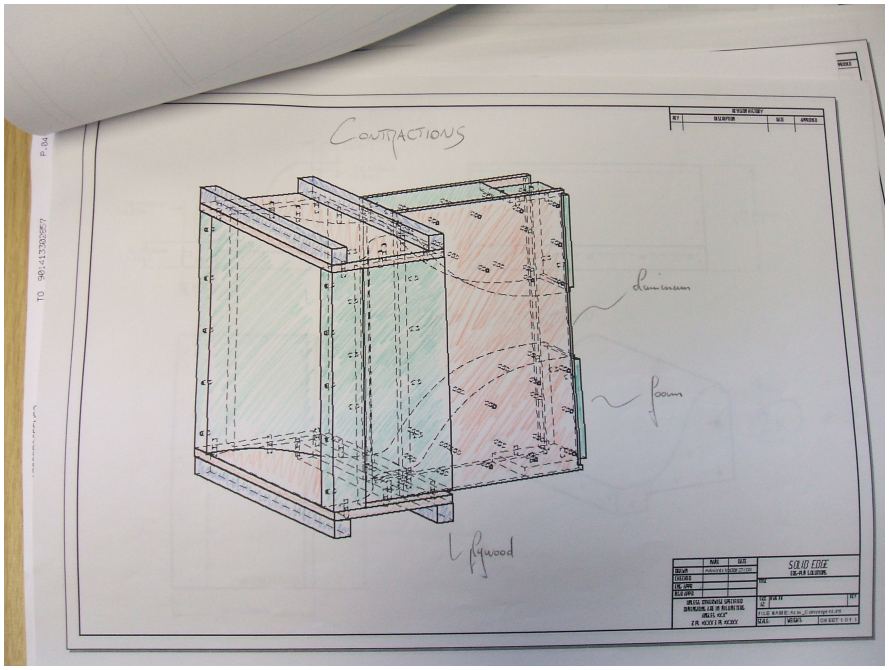

Figure B.2: Sketch of the contractions.

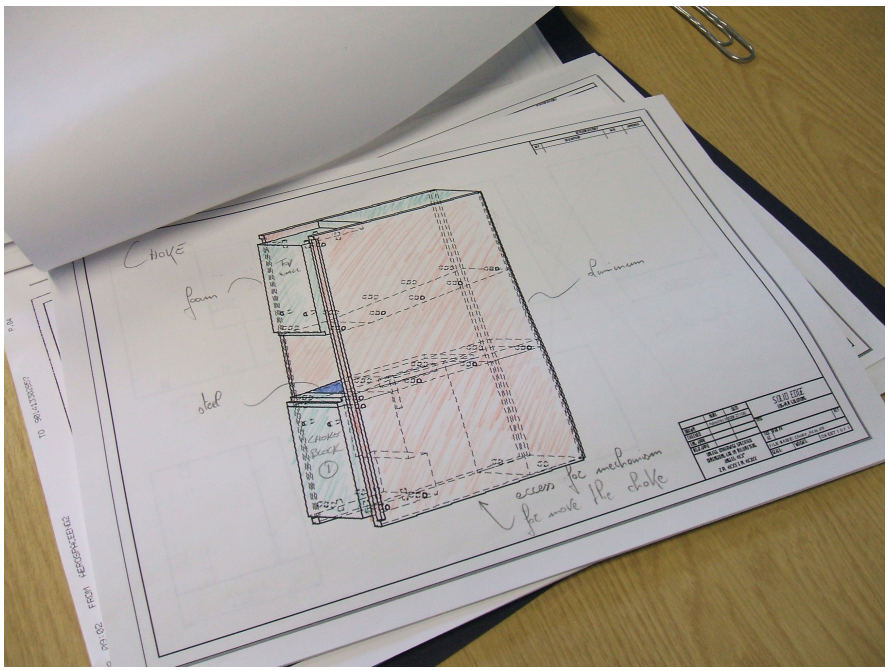

Figure B.3: Sketch of the choke.

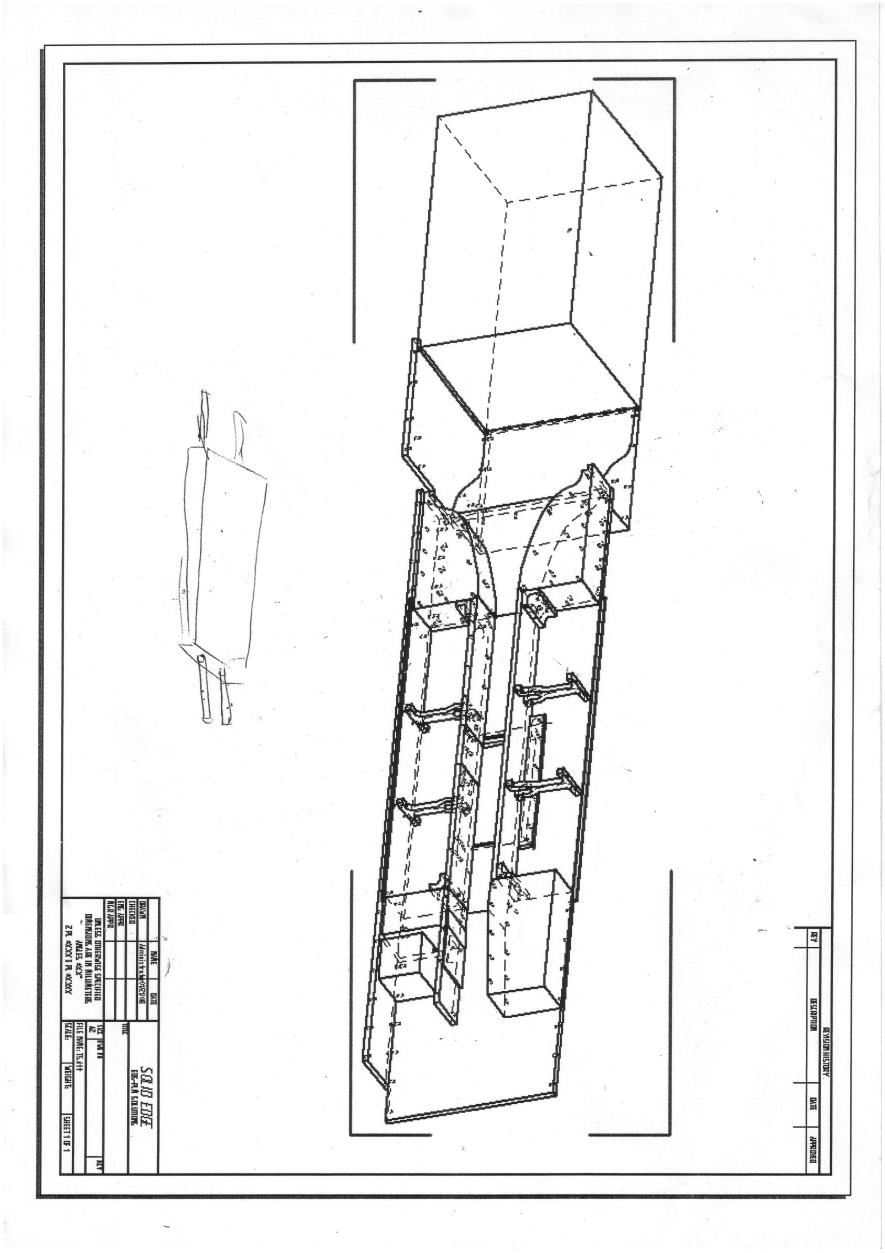

Figure B.4: Sketch of the whole wind tunnel.

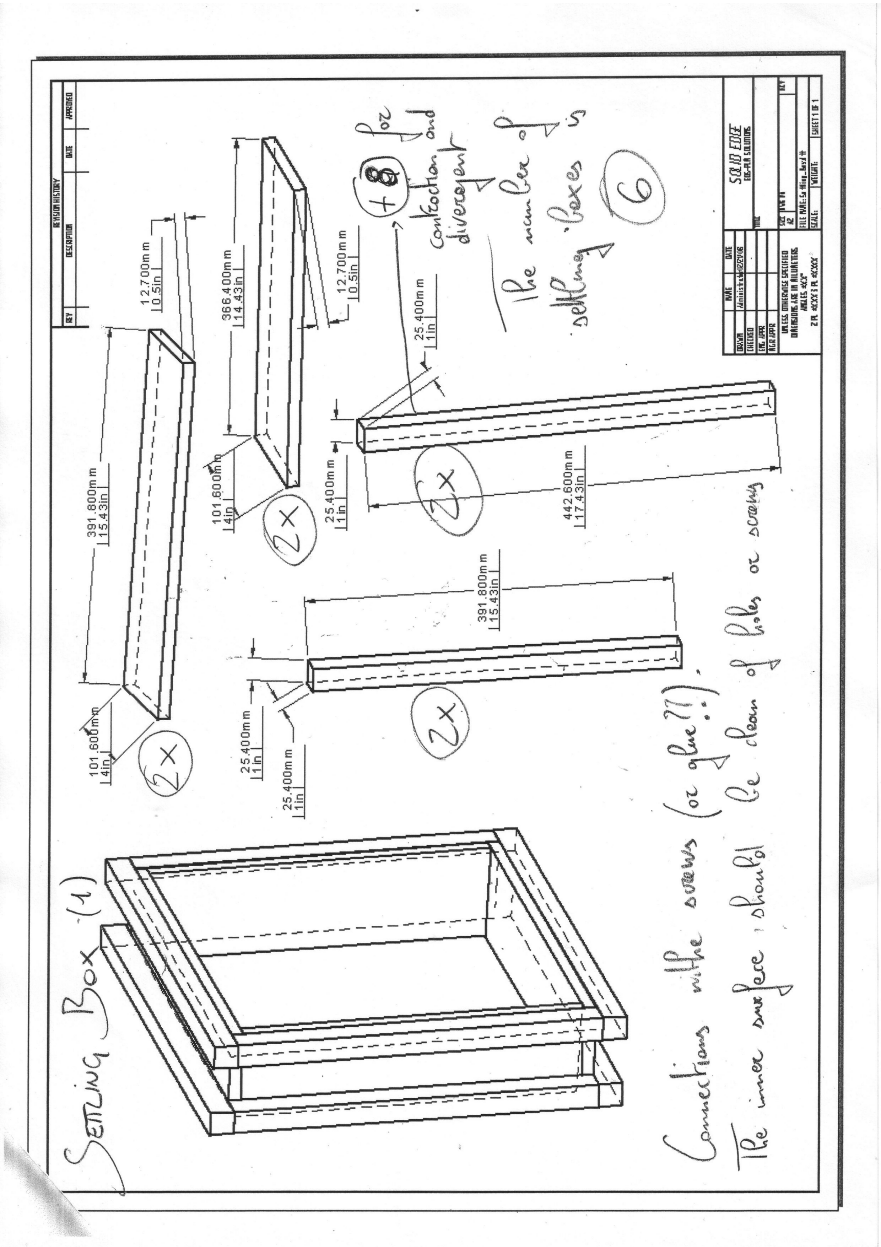

Figure B.5: Sketch of the settling chamber single box.

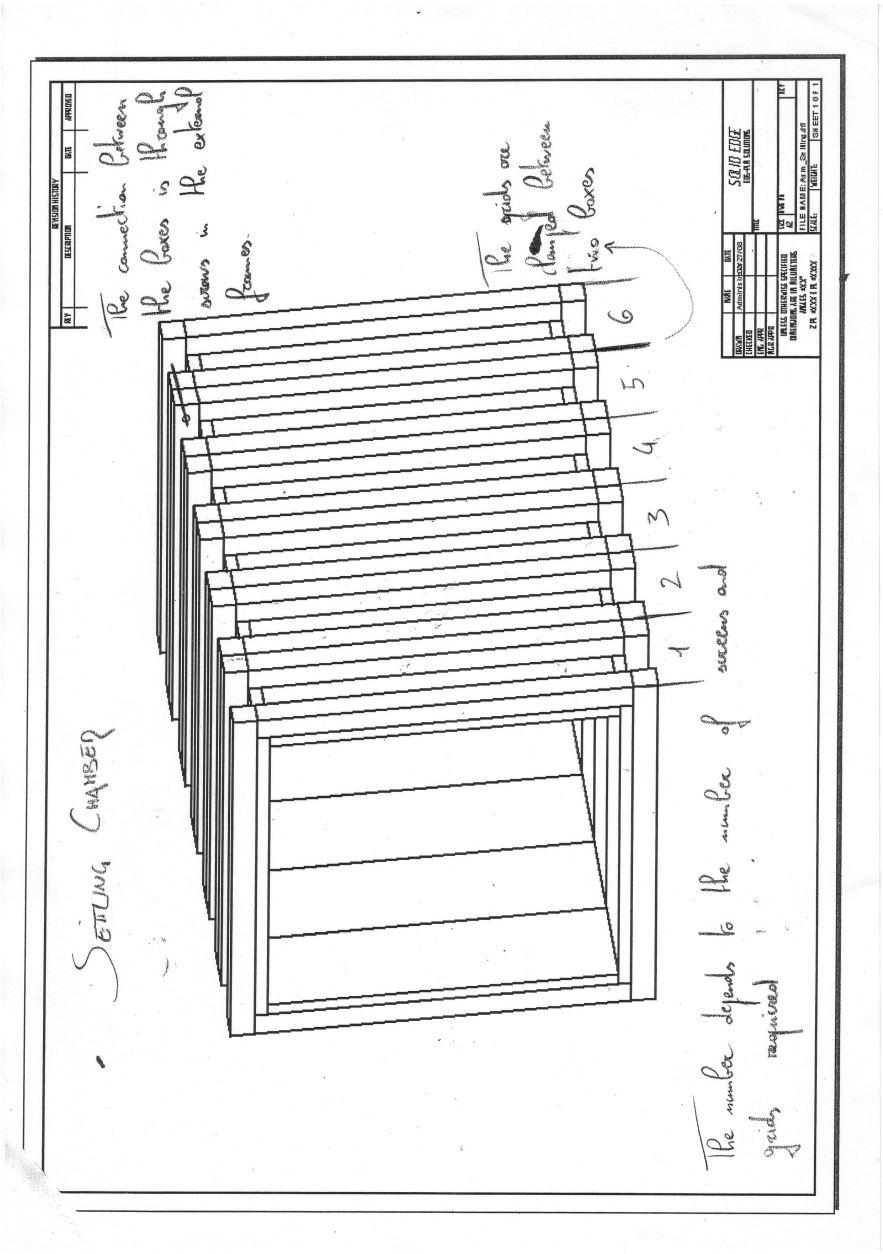

Figure B.6: Sketch of the settling chamber.

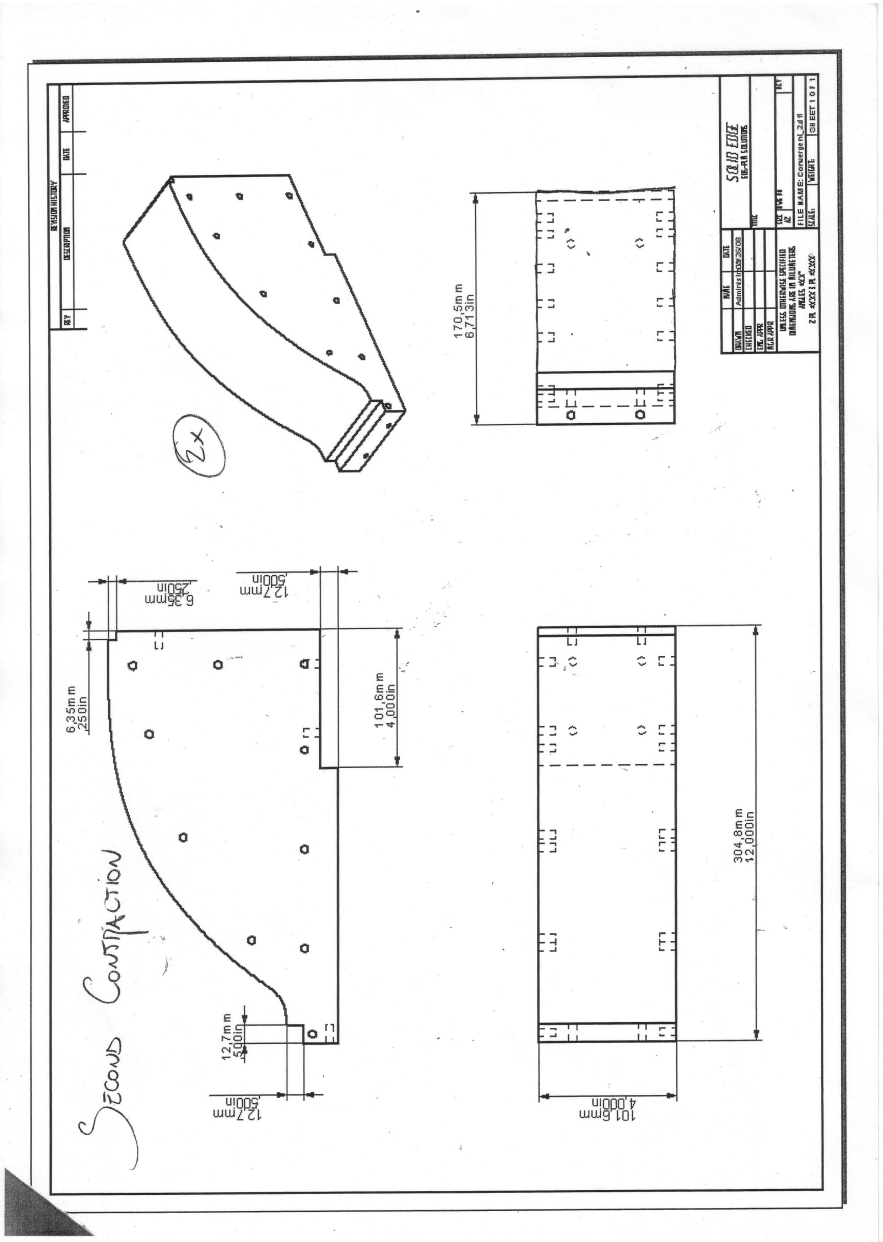

Figure B.7: Sketch of the first part of the convergent.

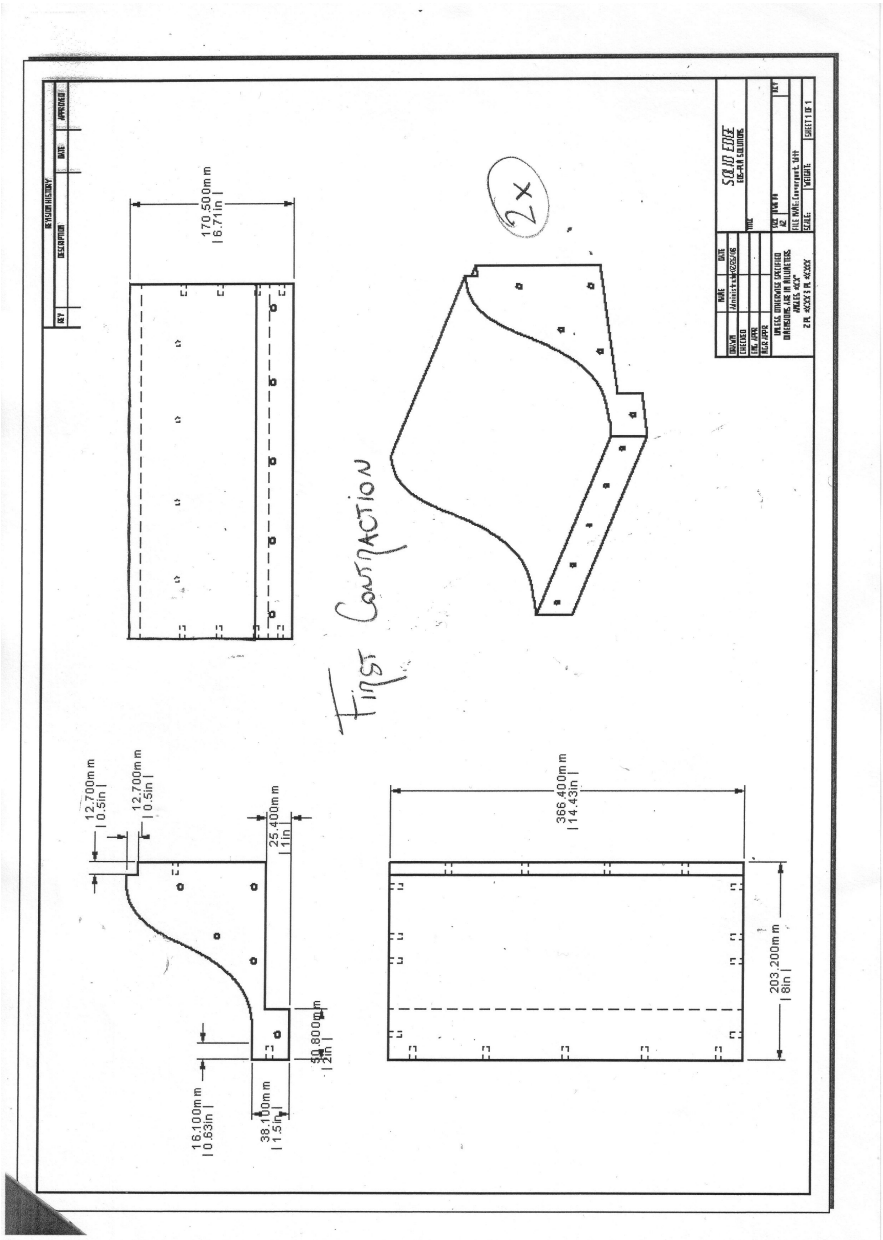

Figure B.8: Sketch of the second part of convergent.

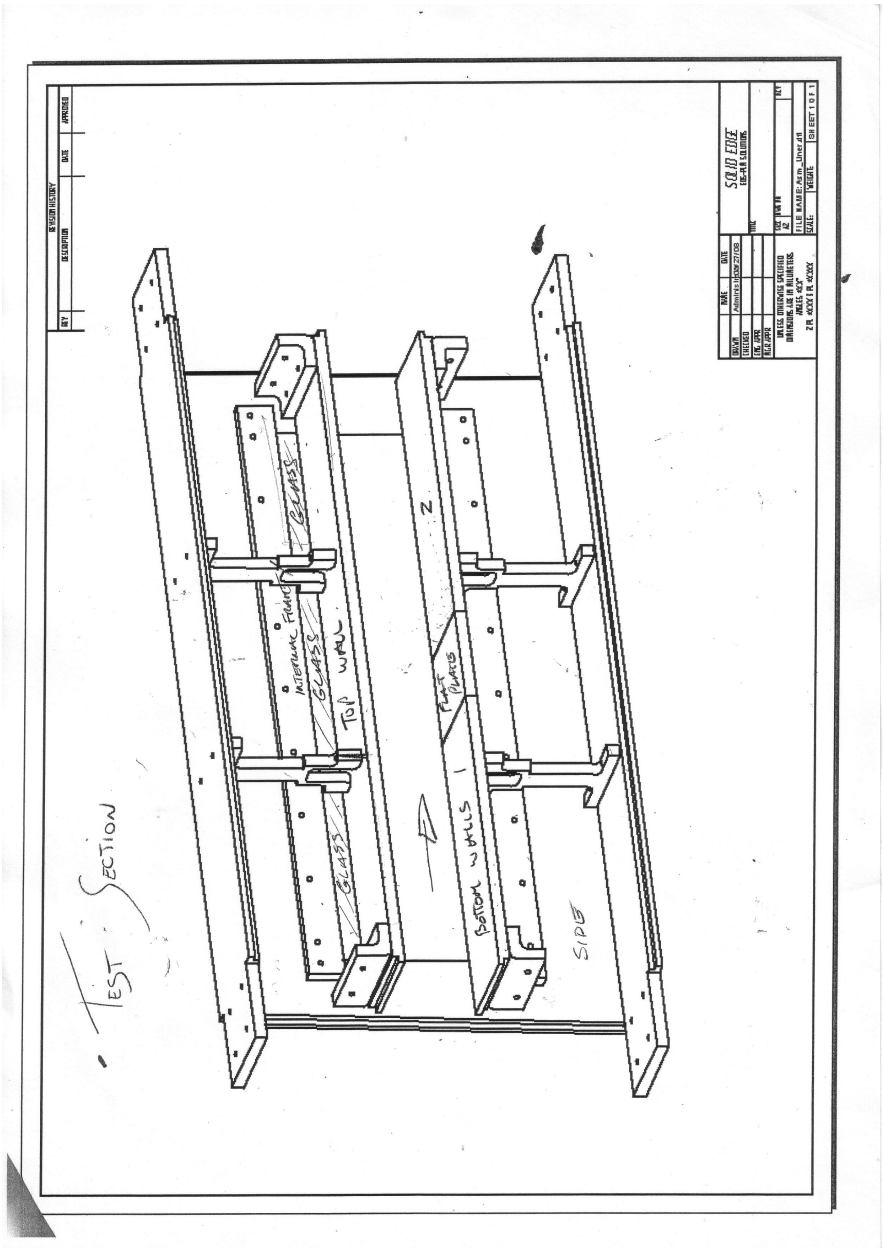

Figure B.9: Sketch of the test section.

Nomenclature

Symbols and abbreviations:

γ	Ratio of specific heats
ν	Kinematic viscosity
ρ	Density
a	Length of the choke
A	Area
BD	Blower and dryer module
c	Speed of sound
C	Convergent module
Ch	Choke module
c_p	Specific heat at constant pressure
c_v	Specific heat at constant volume
d	Diameter
D	Diffuser module
FT	Feeding tank module
h	Height of the wedge choke
L	Length
M	Mach number
$\dot{m}$	Mass flow rate
P	Pressure
q	Dynamic pressure
R	Specific gas constant
SC	Settling chamber module
T	Temperature
TC	Test chamber module
TS	Test section module
U	Velocity
V	Volume of the vacuum tank
Vv	Valve module
VP	Vacuum pump module
VT	Vacuum tank module
x	Coordinate of the choke movement

Subscript:
(the subcripts refer to the location)

$_C$	Choke
$_e$	Exit/Ending
$_i$	Initial
$_m$	Model
$_o$	Initial/Stagnation condition
$_{SC}$	Settling chamber
$_t$	Throat
$_{TS}$	Test section
$_w$	Wall
$_\infty$	Asintotic condition

Superscript:

^{t}	Total/Stagnation condition
*	Sonic condition
$^-$	Average

Bibliography

[1] Sabetta F., *Gasdinamica*, Ingegneria 2000, 2 ed., (2001).

[2] FLUENT, Inc., FLUENT 6.1 Users Guide, 2003, (Lebanon: NH).

[3] Pope A., Goin K. L., *High speed wind tunnel testing*, John Wiley & Sons, Inc., (1965).

[4] A. F. Donovan, R. R. Gilruth, F. E. Goddart, H. R. Lawrence, *High speed aerodynamics and jet propulsion Volume VIII: High speed problems of aircraft and experimental methods*, Oxford university press, (1961).

[5] Kenney J. T., Webb L. M., *A summary of the techniques of variable Mach number supersonic wund tunnel nozzle design*, AGARDograph, (October 1954).

[6] Walter E., Walter E., Pronzato L., *Identification of Parametric Models: from Experimental Data (Communications and Control Engineering)*, Springer, (1997).

[7] Anderson J. D. Jr., *Fundamentals of aerodynamics*, McGraw-Hill international edition, 4th ed., (2007).

[8] Bradshaw P., Mehta R. D., *Technical notes: Design rules for small low speed wind tunnels*, The Aeronautical Journal of the Royal Aeronautical Society, (November 1979).

[9] Jordinson R., B.Sc., D.I.C., M.Sc., *Design of wind tunnel contractions*, Aircraft Engineering, pp. 294-297, (October 1961).

[10] Mikhail M. N., *Optimum design of wind tunnel contractions*, AIAA Journal, vol. 17, no. 5, May 1979, article no. 78-819, pp. 471-477.

[11] Libby P. A., Reiss H. R., *The design of two-dimensional contraction sections*, Quarterly of applied mathematics, vol. IX, no. 1, pp. 95-98, 1951.

[12] Morel T., *Desigh of two-dimensional wind tunnel contractions*, Journal of Fluids Engineering, pp. 371-378, (June 1977).

[13] Hussain A. K. M. F., Ramjee V., *Effect of axisymmetric contraction shape on incompressible turbulent flow*, Journal of Fluids Engineering, trans. ASME, Series I, vol. 98, pp. 58-68, (March 1976).

[14] Stratford B. S., *The prediction of separation of the turbulent boundary layer*, Journal of Fluid Mechanics, vol. 5, pp. 1-16, (1959).

[15] Morel T., *Comprehensive desigh of axisymmetric wind tunnel contractions*, Journal of Fluids Engineering, trans. ASME, series I, vol. 97, pp. 225-233, (1975).

[16] *Discussion of reference "Comprehensive desigh of axisymmetric wind tunnel contractions" by Morel*, Journal of Fluid Engineering, trans. ASME, vol. 98, pp. 131-133, (1976).

[17] Barakos G., Huang J. C., Benard E., Yapalparvi R., Raghunathan S., *Investigation of transonic flow over a bump: base flow and control*, 46th AIAA Aerospace Sciences Meeting and Exhibit, 7-10 January 2008, Reno, Nevada.

[18] Goethert B. H., Nelson W. C., *Transonic wind tunnel testing*, Pergamon press, (1961).

[19] Handa T., Miyazato Y., Masuda M., Matsuo K., *Formation of multiple shocklets in a transonic diffuser flow*, Shock Waves, vol. 11, pp. 423-430, (2002).

[20] Munro S. E., *Effects of elevated driver-tube temperatures on the extent of quiet flow in the purdue Ludwieg tube*, Thesis by Purdue University, (1966).

[21] Konig B., Kramer E., Lutz T., Patzold M., Ritcher K., Rosemann H., Uhlemann H., *Numerical and experimental validation of three-dimensional shock control bumps*, Journal of Aircraft, vol. 46, n. 2, pp. 675-682, (March-April 2009).

[22] Amecke J., *Direct calculation of wall interferences and wall adaption for two-dimensional flow in wind tunnels with closed walls*, NASA Technical Memorandum TM 88523, (1986).

[23] D. C. Wilcox, *Turbulence modeling form CFD*, DCS Industries, Inc., (1993).

[24] Krull H. G., Schmiedlin R. F., Steffen F. W., *Effect of divergence angle on the internal performance characteristics of several conical convergent-divergent nozzles*, NACA Research Memorandum, RM E54H25, National advisory committee for aeronautics, (November 1954).

[25] Krull H. G., Steffen F. W., *Performance characteristics of one convergent and three convergent-divergent nozzles*, NACA Research Memorandum, RM E52H12, National advisory committee for aeronautics, (September 1952).

[26] Settles G. S., *Schlieren and Shadowgraph Techniques*, Springer, (2001).

[27] Holder D. W., Pankhurst R. C., *Wind Tunnel Technique*, Sir Isaac Pitman & Sons, Ltd, (1952).

[28] Bogdonoff S. M., Ferri A., *Design and operation of intermittent supersonic wind tunnel*, AGARDograph, (May 1954).

[29] Gorlin S. M., Slezinger I.I., *Wind tunnels and their instrumentation*, Israel Program for Scientific translations, (1966).